

FACULDADE DE ENGENHARIA DA UNIVERSIDADE DO PORTO



Effect of the birthing position on its evolution from a biomechanical point of view

Margarida Borges Pereira

MSc in Bioengineering

Supervisor: Prof. Dr. Dulce Alves de Oliveira

Co-Supervisor: Prof. Dr. Marco Paulo Lages Parente

July 23, 2020

Effect of the birthing position on its evolution from a biomechanical point of view

Margarida Borges Pereira

MSc in Bioengineering

July 23, 2020

Resumo

Durante o parto vaginal, existem várias posições que podem ser adotadas pela mãe para estar mais confortável e para ajudar no processo do parto. As posições verticais estão associadas a vários benefícios clínicos, apesar da posição supina ser a mais adotada durante o parto na maioria das unidades de saúde. As posições escolhidas são, na realidade, muito influenciadas por fatores relacionados com a monitorização e intervenção durante o segundo estadió do trabalho de parto, uma vez que existe uma evidência científica limitada sobre qual a posição mais favorável. Recentemente, a bioengenharia computacional tem mostrado bastantes avanços nesta área através da aplicação de técnicas computacionais na investigação clínica, substituindo os estudos *in vivo* em animais.

Nesta tese, foi utilizado um modelo de elementos finitos validado composto pelos músculos do pavimento pélvico, pelos ossos da cintura pélvica e pela cabeça do feto para simular partos vaginais. Este modelo foi modificado de forma a imitar duas posições que podem ser adotadas durante o parto: uma que permite o movimento livre do cóccix e outra em que este movimento é mais restrito devido, por exemplo, à presença da cama por baixo da mulher. Para melhor entender os benefícios e riscos destas posturas, foram modeladas as articulações sacroilíacas, sacrococcígea e a sínfise púbica. Foi estudada a abertura da sínfise púbica, o movimento do cóccix e do sacro e o impacto no tecido cortical deste ossos, os efeitos provocados nos músculos do pavimento pélvico da mulher, assim como as forças de reação na cabeça do feto.

Os resultados obtidos mostram que no modelo que imita posições de parto nas quais o movimento do cóccix está restringido ocorre uma abertura da sínfise púbica de 6 mm para permitir a passagem da cabeça do feto, sem ocorrer rutura desta articulação. Por outro lado, no modelo que permite um maior movimento do cóccix ocorre uma menor abertura da sínfise púbica (3 mm), uma vez que o movimento e rotação do cóccix permitem um aumento da área disponível para a passagem da cabeça do feto. Assim, neste trabalho, esta posição mostra ser mais benéfica para os ossos da cintura pélvica da mulher, apesar de ser obtido um campo de tensões um pouco mais elevadas nos músculos do pavimento pélvico.

Globalmente, os resultados obtidos permitem concluir que diferentes posições do parto levam a diferenças no espaço disponível na pelve feminina, pelo que determinadas posições podem ser adotadas durante o segundo estadió do trabalho de parto objetivando reduzir o risco de obstruções durante o parto e de desenvolvimento de diversas disfunções.

Abstract

During a vaginal delivery, there are various positions that the mother can adopt to be more comfortable and to help the process of labor. Upright birthing positions are associated with several clinical benefits, yet supine positions are still most common during delivery in most health centers. The positions chosen are, in fact, very influenced by factors related to the monitoring and intervention during the second stage of labor since there is limited scientific evidence to support an ideal birthing position. More recently, computational bioengineering is experiencing major breakthroughs in this field through the application of computational techniques in the medical research, replacing *in vivo* animal studies.

In this thesis, a validated finite element model composed of the pelvic floor muscles, the pelvic girdle bones, and a fetus head was used to simulate vaginal deliveries. This model was modified to mimic two birthing positions: one that allows the free movement of the coccyx and other in which this movement is more restricted due to, for example, the presence of a bed under the woman. To better understand the benefits and risks of these maternal positions, the pubic symphysis, sacroiliac and sacrococcygeal joints were modeled. The influence of birthing positions on the widening of the pubic symphysis, the movement of coccyx and sacrum, the stress related to the cortical tissue of these bones and the effects induced in the pelvic floor muscles of the woman were analyzed, as well as the reaction forces in the fetus head.

The results obtained show that in the model that mimics birthing positions in which the movement of the coccyx is restricted a 6 mm widening of the pubic symphysis occurs to allow the passage of the fetus head, without occurring rupture of this joint. In contrast, a lower widening of the pubic symphysis (3 mm) occurs in the model that allow the movement of the coccyx, since the movement and rotation obtained for the tip of the coccyx allows an increase in the space for the passage of the fetal head. In this work, this position appears to be more beneficial for the pelvic girdle bones of the mother but slightly higher stresses were detected in the pelvic floor muscles.

Globally, the results obtained allow to conclude that different birthing positions lead to changes in the female pelvic space, so certain positions can be adopted by the mother during the second stage of labor to reduce the risk of obstructed labor and the development of several dysfunctions.

Acknowledgements

I would like to express my sincere gratitude to Professor Dulce Oliveira and Professor Marco Parente for their consistent support, guidance, motivation and flexibility during the development of this work. Without their dedicated involvement, my thesis could not be accomplished. My deepest appreciation extends to Professor Renato Natal for the opportunity and confidence given, and the encouragement to face new challenges.

I gratefully acknowledge the support received from Portuguese FCT under research project UIDB/50022/2020 and from the project NORTE-01-0145-FEDER-030062 (SIM4SafeBirth) cofinanced by NORTE2020, through FEDER.

I would like to express my thanks to all my friends who went through hard times together, cheered me on, and celebrated each accomplishment despite long distances between us, which, in some cases, includes being on another continent.

Most importantly, none of this could have happened without my family. My deepest thank goes to my parents for providing me unfailing support and continuous encouragement throughout the process of researching and writing this thesis. I would like to thank my sister and brother for all their understanding and endless patience. Also, I express my thanks to Cookie and Flash for their company.

“Tell me and I forget, teach me and I may remember, involve me and I learn.”

Benjamin Franklin

Contents

1	Introduction	1
1.1	Context	1
1.2	Motivation and Objectives	2
1.3	Organization	3
2	Anatomy	5
2.1	Female Pelvis and Perineum	5
2.1.1	Pelvic Girdle	6
2.1.2	Pelvic Cavity	8
2.1.3	Perineum	10
2.1.4	Pelvic Floor Dysfunction	11
2.2	Fetus Head	13
3	Labor	15
3.1	Introduction	15
3.2	Fetus	15
3.2.1	Fetal Head Diameters	16
3.3	Maternal Pelvis	17
3.3.1	Maternal Pelvic Diameters	18
3.3.2	Classification of the Pelvis	20
3.3.3	Musculoskeletal System Changes of Pregnancy	21
3.4	Birth Positions	22
3.4.1	Upright (Vertical) Positions	22
3.4.2	Horizontal Positions	24
3.5	Cardinal Movements in Labor	25
4	Computational Solid Mechanics	29
4.1	Introduction	29
4.2	Preliminary Concepts	29
4.2.1	Configuration and Motion of Continuum Bodies	29
4.2.2	Material and Spatial Descriptions	30
4.2.3	Deformation Gradient	30
4.2.4	Strain Measures	31
4.2.5	Stress Measures	32
4.3	Principle of Virtual Work	33
4.4	Constitutive Equations	35
4.4.1	Hyperelasticity	35
4.5	Finite Element Method	41

4.5.1	Discretized Equilibrium Equations	41
4.5.2	Linearization of the Virtual Work Principle	42
4.5.3	ABAQUS® Finite Element Software	43
5	Finite Element Simulations	45
5.1	Introduction	45
5.2	Materials and Methods	46
5.2.1	Finite Element Model	46
5.2.2	Materials	52
5.2.3	Boundary Conditions	55
5.3	Results and Discussion	56
5.3.1	Pubic Symphysis	57
5.3.2	Sacrum and Coccyx	59
5.3.3	Pelvic Floor Muscles	63
5.3.4	Fetus	65
6	Final Remarks and Future Work	67
6.1	Final Remarks	67
6.2	Future Work	68
	References	69
	Appendix A	73
A.1	Article submitted to Computer Methods and Programs in Biomedicine Journal . .	73

List of Figures

2.1	Pelvis and perineum (Moore et al., 2006)	5
2.2	Pelvis (Martini et al., 2012)	7
2.3	Joints and ligaments of the pelvis (Stranding, 2016)	9
2.4	Floor and walls of pelvis (Moore et al., 2006)	10
2.5	Boundary separating pelvis from perineum (Moore et al., 2006)	10
2.6	Superficial and deep layers of perineum viewed from below (Martini et al., 2012)	11
2.7	The fetal skull (adapted from Macdonald et al. (2011))	14
3.1	Examples of fetal lie (Gabbe et al., 2017)	16
3.2	Fetal presentations and positions in labor: left occipit anterior (LOA); left occipito- posterior (LOP); left occipitotransverse (LOT); right occipit anterior (ROA); right occipitotransverse (ROT); right occipitoposterior (ROP) (Gabbe et al., 2017) . . .	17
3.3	Diameters of the fetal skull (adapted from Hacker et al. (2016))	17
3.4	Stations of the fetal head (Gabbe et al., 2017)	18
3.5	Pelvic planes (Posner et al., 2013)	18
3.6	Pelvic inlet diameters (Posner et al., 2013)	19
3.7	Plane of least dimensions (Posner et al., 2013)	20
3.8	Pelvic outlet dimensions (Posner et al., 2013)	20
3.9	Pelvis types (Posner et al., 2013)	20
3.10	Upright Positions: (a) semi-sitting position (Simkin, 2002), (b) sitting on a low stool (Simkin, 2002), (c) kneeling over chair seat (Simkin, 2002), (d) hands-to- knees position (Simkin, 2002), (e) squatting position with bar (Simkin, 2002), (f) standing position (Lowdermilk, 2011)	23
3.11	Horizontal Positions: (a) pure side-lying lateral position (Macdonald et al., 2011), (b) semi-prone lateral position (Macdonald et al., 2011), (c) semi-recumbent po- sition (Lowdermilk, 2011), (d) lithotomy (Perry et al., 2014), (e) supine position (Lowdermilk, 2011), (f) dorsal position (Perry et al., 2014), (g) knee-elbow posi- tion (Perry et al., 2014)	25
3.12	Cardinal movements in labor (Gabbe et al., 2017)	27
4.1	General motion of a deformable body (adapted from Kim (2015))	30
4.2	Positive stress components of the traction vectors \mathbf{t}_e , (adapted from Holzapfel (2002))	33
4.3	ABAQUS [®] /Standard flowchart	44
5.1	Finite element model of the mother showing the pelvic girdle bones in brown, the pelvic floor muscles in light red and the supporting structures in dark red	46
5.2	Dimensions of the levator hiatus	47
5.3	Finite element model of the sacrum and coccyx with cortical bone in black and trabecular bone in brown (lateral view)	47

5.4	Pelvic diameters of the model: A, transverse diameter; B, interspinous diameter; C, obstetric conjugate diameter; D, sagittal outlet diameter; E, intertuberous diameter	48
5.5	Finite element model with the modeled ligaments: 1, sacroiliac ligaments; 2, superior pubic ligament; 3, inferior pubic ligament; 4, sacrospinous ligament; 5, sacrotuberous ligament	49
5.6	Finite element model of the sacrum and coccyx in brown and the sacrococcygeal joint in grey (posterior view)	50
5.7	Diameters of the fetal skull: 1, suboccipitobregmatic diameter; 2, suboccipitofrontal diameter; 3, occipitofrontal diameter; 4, mentovertical diameter; 5, submentobregmatic diameter (adapted from Parente et al. (2010))	50
5.8	Reference line from the inferior border of the pubic symphysis to the inferior border of the sacrum	51
5.9	Curve in black used to evaluate the displacement of the sacrum and coccyx	52
5.10	Model of pelvic floor muscles in red and curve, in black, used to evaluate stress and stretch	52
5.11	3D solid elements used to simulate the interpubic disc of the pubic symphysis and the synovial part of the sacroiliac joints: (a) anterior view of pubic symphysis; (b) lateral view of sacrum	55
5.12	Finite element model of the pelvic floor muscles in red with the identification of the fixed nodes in black	56
5.13	Finite element model of the fetus head with the identification of the reference point used to control its movement (P1)	56
5.14	Widening of pubic symphysis during the vertical descent of the fetus head	57
5.15	Maximum principal stresses in MPa in the superior and inferior pubic ligaments of the non-mob. coccyx model and mob. coccyx model during the vertical descent of the fetus head	58
5.16	Movement of coccyx during the vertical descent of the fetus head	59
5.17	Rotation of coccyx during the vertical descent of the fetus head	60
5.18	Displacement of sacrum and coccyx in x-axis along the normalized path at the sagittal plane of these bones in a vertical descent of the fetus head of 48 mm and 65 mm. The black dashed line corresponds to the beginning of the sacrococcygeal joint	61
5.19	Distribution of the maximum principal stresses in MPa on the sacrum and coccyx, in the cortical bone tissue, in the (a) non-mob. coccyx model and (b) mob. coccyx model, at the moment of maximum movement of the coccyx	62
5.20	Maximum principal stresses in MPa calculated along the normalized path at the most inferior portion of the pelvic floor muscles (figure 5.10) at the peak stresses instant	63
5.21	Distribution of the maximum principal stresses in MPa on the pelvic floor muscles at the peak stresses instant in the (a) non-mob. coccyx model and (b) mob. coccyx model	64
5.22	Stretch ratio calculated along the defined path at the most inferior portion of the pelvic floor muscles (figure 5.10) during the vertical descent of the fetus head	64

List of Tables

5.1	Maternal pelvic diameters considered	47
5.2	Constitutive material parameters for the pelvic floor muscle	53
5.3	Material properties of the sacrum and coccyx	54
5.4	Material properties and cross sectional area of the ligaments	54

Nomenclature

$\{\lambda_{1,2,3}\}$	Principal stretches
$I_{4,5}$	Pseudo-invariants arising directly from anisotropy
:	Double product
α	Activation variable
$\bar{\lambda}_f$	Fiber stretch ratio in the direction \mathbf{N} of the underformed fiber
$\bar{\mathbf{C}}$	Right Cauchy-Green strain tensor with the volume change eliminated
$\bar{\mathbf{F}}$	Deformation gradient with the volume change eliminated
$\bar{I}_1^{\mathbf{C}}$	First invariant of the right Cauchy-Green strain tensor with the volume change eliminated
$\boldsymbol{\lambda}$	Stretch vector
Φ	A configuration of a body B
Ψ	Helmholtz free-energy function
Ψ_f	Fiber part of the strain-energy function
Ψ_m	Ground matrix part of the strain-energy function
Ψ_{PE}	Passive elastic part of the fiber contribution of the strain-energy function
Ψ_{SE}	Active elastic part of the fiber contribution of the strain-energy function
Ψ_{vol}	Volumetric part of the strain-energy function
$\boldsymbol{\sigma}$	Cauchy stress tensor
$\boldsymbol{\tau}$	Kirchhoff stress tensor
\cdot	Scalar product
$\delta\mathbf{D}$	Virtual stretch rate
$\delta\mathbf{L}$	Virtual velocity gradient
$\delta\mathbf{u}$	Virtual displacement field
δW	Virtual work
λ	Stretch

λ_M	Muscle stretch
$\{\hat{\mathbf{N}}_{1,2,3}\}$	Principal stretch directions in the reference configuration
μ	Shear modulus of linear elasticity
\otimes	Tensor product
ρ	Mass density in the deformed configuration
\mathbf{a}_0	Unit vector in the reference configuration
\mathbf{b}	Left Cauchy-Green deformation tensor
\mathbf{C}	Right Cauchy-Green deformation tensor
\mathbf{E}	Lagrangian or Green strain tensor
\mathbf{e}	Eulerian or Almansi strain tensor
\mathbf{F}	Deformation gradient tensor
\mathbf{f}	Force acting on the structure
\mathbf{F}_{ext}	External equivalent nodal forces
\mathbf{F}_{int}	Internal equivalent nodal forces
\mathbf{I}	Unit tensor
\mathbf{K}	Stiffness Matrix
\mathbf{N}	Normal to the surface in the reference configuration
\mathbf{n}	Normal to the surface in the deformed configuration
\mathbf{P}	First Piola-Kirchhoff stress tensor
\mathbf{R}_f	Residual force
\mathbf{S}	Second Piola-Kirchhoff stress tensor
\mathbf{T}	Traction vector in the reference configuration
\mathbf{t}	Traction vector in the deformed configuration
\mathbf{U}	Right stretch tensor
\mathbf{u}	Displacement vector
\mathbf{v}	Velocity field
\mathbf{X}	A particle belonging to the body B
\mathbf{x}	Position of a particle \mathbf{X} of B in the configuration Φ
A, a	Parameters of the fiber part of the Martins constitutive model
B	A body

c, b	Parameters of the ground matrix part of the Martins constitutive model
c_{10}	Parameter of Neo-Hookean constitutive model
D	Derivative operator
$d\mathbf{X}$	Material line element
$d\mathbf{x}$	Spatial line element
D_1	Penalty parameter of the penalty function to ensure incompressibility
dA	Surface element in the reference configuration
da	Surface element in the spatial configuration
dV	Volume element
$I_{1,2,3}$	Invariants of the Cauchy-Green deformation tensor
J	Jacobian
$N_i(\mathbf{X})$	Interpolation or basis functions
t	Time
T_0^M	Maximum muscle tension at resting length
V	Volume of the body
\mathbf{N}	Direction of the undeformed fiber
p	Indeterminate Lagrange multiplier

Chapter 1

Introduction

1.1 Context

Globally, millions of births occur every year. However, maternal morbidity and mortality is unacceptably high. For example, everyday in 2017, approximately 810 women died from preventable causes related to pregnancy and childbirth ([World Health Organization, 2019](#)). One of the main causes are biomechanical complications ([Hemmerich et al., 2019](#)), so several studies have been developed to analyze the mechanisms of labor through computational models, since studies in pregnant women are difficult and involve ethical constraints ([Parente et al., 2008, 2009](#); [Oliveira et al., 2016](#); [Hemmerich et al., 2019](#)).

During pregnancy and labor, there are many hormonal and biomechanical changes in the mother to ensure pelvic girdle stability. The mechanism of labor and the likelihood of safe vaginal delivery depend largely on the bony architecture of the pelvis. The second stage of labor corresponds to the moment when the fetus moves through the birth canal, ending with the birth of the baby. To facilitate the passage of the fetus through the birth canal, pelvic ligament relaxation occurs during pregnancy and, as a consequence, pubic symphysis can be more flexible and wider during labor. Furthermore, during this stage, there are several postures that can be adopted by the mother and the outcomes may vary according to the birthing position assumed.

In the past, the majority of women adopted a wide range of birthing positions, such as squatting, kneeling or sitting positions. Supine position was only used when labor lasted very long or was very difficult and exhausting. Nevertheless, during the second half of the twentieth century, there was a growing awareness among obstetricians and the supine position became popular, although its widespread use was not based on scientific evidence ([Gupta and Nikodem, 2000](#)). In recent years, some birthing positions adopted during the second stage of labor have shown potential benefits in promoting optimal maternal and neonatal outcomes, since maternal positions serve as the non-medical intervention to facilitate the progress of childbirth. Through an analysis of several studies, it was verified that the supine and semi-recumbent positions are the most adopted birthing positions in several countries, such as Australia ([Shorten et al., 2002](#)), United States of America ([Nieuwenhuijze et al., 2012](#)) and Malawi ([Zileni et al., 2017](#)) (56%, 83% and 91%, respectively).

The adoption of other positions is only observed in a small number of women since there is some apprehension of both mother and healthcare professionals (Nieuwenhuijze et al., 2012). Adopting a hostile position, the person giving birth might suffer from several negative outcomes, such as perineal trauma, post-partum urinary incontinence and greater blood loss. The fetus has also a higher probability of complications, such as fetal heart rate abnormalities, brachial plexus injury and clavicle fracture. Unfortunately, there is no evidence to support the most ideal maternal position, so it becomes important to understand the benefits and consequences of assuming different birthing positions.

For this purpose, it is fundamental to consider computational bioengineering, which is a recent field that takes advantage of the latest computational capabilities to deal with biomedical problems. This method aims at replacing the animal research that has been used as a method of study, involving painful procedures that leave animals injured, living impaired or even dead. Through computational modeling, it is possible to simulate biological complex systems, allowing to perform analysis and evaluations of the human performance and, consequently, new surgical concepts can be developed and the postoperative surgical outcomes can be assessed. Therefore, advances in this area contribute to numerous innovations and developments in the medical field and there is an improvement in quality of life. In the particular case of childbirth, it facilitates, for example, the comparison of maternal outcomes, as well as newborn outcomes, aiming to decrease their morbidity and mortality.

1.2 Motivation and Objectives

During the second stage of labor, the fetus passes through the birth canal and, to make the most informed and appropriate decisions, it is fundamental a clear understanding of the dynamic structure of the female pelvis. On one hand, it is crucial to clarify the adaptation that the maternal pelvis may undergo by allowing the widening of the pubic symphysis to facilitate the passage of the fetus. On the other hand, different birthing positions lead to changes in the available space in the pelvis and, although there are some comparative studies in terms of obstetrical, fetal, and maternal outcomes, the most ideal maternal position has been controversial and the biomechanics of birth positioning are not yet fully understood. This study might also help to explain some dysfunctions associated with pregnancy and delivery. To the best of our knowledge, only few studies perform a biomechanical analysis using computational models of the musculoskeletal system changes that occur during pregnancy in the woman's body, and the changes in the pubic symphysis are not considered.

This work aims at contributing to a better knowledge associated with the widening of the pubic symphysis and the biomechanics of different positions that can be adopted during the second stage of labor, as well as their resulting pathophysiological consequences. For this purpose, a modification of a validated computational model is required in order to incorporate the pelvic kinematics under load conditions resulting from selected birthing positions. In this way, it is necessary to include the pelvic joints in the model and to analyze and validate the behavior of

the pubic symphysis and the sacrococcygeal joint. Two birthing positions can be considered: one that allow and other that do not allow the movement of the coccyx, mimicking vertical and horizontal positions, respectively. It is possible to simulate the mechanism of labor during the second stage, assuming these two birthing positions, with the fetus in the vertex presentation and an occipitanterior position. Hence, this work involves the following objectives:

- Model the pelvic joints, such as pubic symphysis, sacroiliac and sacrococcygeal joints;
- Study the influence of birthing positions on the widening of the pubic symphysis;
- Analyze the movement of sacrum and coccyx and the impact on the cortical bone tissue;
- Analyze the effects induced in the pelvic floor muscles of the woman;
- Verify the impact on the fetus head through the reaction forces obtained.

1.3 Organization

To achieve the goals presented, this work is structured in different chapters. Chapter 2 presents a description of the anatomy of female pelvis, perineum, the main pelvic floor dysfunction and fetus head. Chapter 3 focuses on the process of labor, explaining the fetus and the maternal pelvis implications. It also reviews the main birthing positions and the mechanisms of labor. In chapter 4 there are present some solid mechanics preliminary concepts, some constitutive equations and the finite element method since it possibilities to analyze the effects of mechanical stresses and strains and interactions of different components and tissues on clinical outcomes. The overall structure of the ABAQUS® software is outlined to better understand its functioning. Chapter 5 presents the finite element model used in this study, as well as the modifications implemented and the methodology adopted. The results of the numerical simulations performed as well as an analysis and discussion of the results obtained are also included. Finally, the ultimate conclusions and some suggestions for future work are delineated in chapter 6.

Chapter 2

Anatomy

2.1 Female Pelvis and Perineum

The hip bones and the sacrum, which form the skeletal ring, as well as the cavity therein and the region where the trunk and lower limbs meet form the pelvis. Anatomically, the pelvis is the part of the body surrounded by the pelvic girdle (bony pelvis) and also integrates the pelvic cavity, the pelvic floor and the perineum (Standing, 2016).

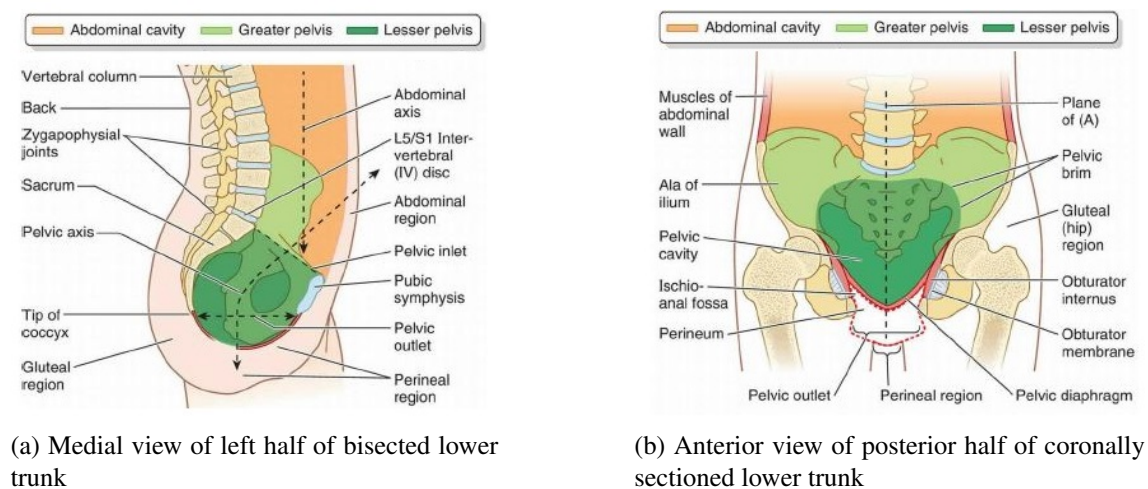


Figure 2.1: Pelvis and perineum (Moore et al., 2006)

The human pelvic can be divided into two compartments: greater (false) and lesser (true) pelvis, as it can be seen in figures 2.1a and 2.1b. The greater pelvis is surrounded by superior pelvic girdle, which includes the ilium and pubis above the lineae terminales (the iliac arcuate line, pectineal line and pubic crest). The lesser pelvis bordered by the inferior pelvic girdle, i.e., it is formed from the pubis, sacrum, ischium, ilium, the ligaments that interconnect these bones, and the muscles that line their inner surfaces. It contains the pelvic organs, including the urinary bladder, the rectum and parts of the reproductive organs. The lesser and greater pelvis are separated by the oblique plane which passes through the sacral promontory posteriorly, the arcuate line on

the ilium, the iliopectineal linea and the posterior surface of the pubic crest; this plane is known as pelvic inlet. The pelvic outlet is formed by the ischiopubic rami, ischial tuberosities, sacrotuberous ligaments and distal sacrum. Therefore, the lesser pelvis is situated between the pelvic inlet and pelvic outlet and the greater pelvis is the part of the pelvis superior to the pelvic inlet (Standring, 2016; Moore et al., 2006).

The perineum corresponds to the perineal compartment that is separated from the pelvic cavity by the fascia covering the inferior aspect of the pelvic diaphragm (formed by the levator ani and coccygeus muscles) and surrounded by the pelvic outlet (Moore et al., 2006).

2.1.1 Pelvic Girdle

The pelvic girdle involves the paired hip bones (each composed of the ilium, ischium and pubis) and the sacrum (figure 2.2a and figure 2.2b). The right and left pubic bones articulate anteriorly at the pubic symphysis (a secondary cartilaginous joint) and the sacrum articulates posteriorly with the two iliac bones at the sacroiliac joint. The pelvic girdle has various functions: serves as a weight-bearing and protective structure, as an attachment for trunk and lower limb muscles, and as the skeletal framework of a birth canal capable of accommodating passage of fetus (Standring, 2016; Moore et al., 2006).

2.1.1.1 Bones of the Pelvic Girdle

With regard to the ilium, it includes the upper acetabulum and expanded area above it; the ischium includes the posteroinferior acetabulum and bone posteroinferior to it; finally, the anteroinferior acetabulum is formed from the pubis (Standring, 2016; Moore et al., 2006).

The ilium has upper and lower parts and three surfaces. The lower part forms a little less than the upper two-fifths of the acetabulum and the upper part has gluteal (an extensive rough area), sacropelvic (posteroinferior part of the medial iliac surface, which is divided into iliac tuberosity and auricular and pelvic surfaces) and iliac (iliac fossa) surfaces. The superior border of the ilium is the iliac crest and it has a curve that follows the contour of the ala between the anterior and posterior superior iliac spines. On its external aspect, the body participates in formation of the acetabulum (Standring, 2016; Moore et al., 2006).

The ischium, the inferoposterior part of the hip bone, has a body, which forms the posteroinferior part of the acetabulum, and ramus, which completes the boundary of the obturator foramen. The ischial tuberosity is formed by the large posteroinferior protuberance of this bone. The ischial spine projects posteromedially near the junction of the ramus and body. The concavity between the ischial spine and the ischial tuberosity is the lesser sciatic notch (Standring, 2016; Moore et al., 2006).

The pubis is the ventral part of the hip bone and forms a median cartilaginous pubic symphysis with its fellow. It also helps to form an inferior ramus, which contributes to the bony borders of the obturator foramen. The pubic crest is a thickening on the anterior part of the body of the pubis and it ends laterally as a prominent swelling, the pubic tubercle. The conjoined inferior rami of

the ischium and pubis forms the pubic arch and the angle at which they converge is known as the subpubic angle. The width of this angle is determined by the distance between the right and the left ischial tuberosities (Standing, 2016; Moore et al., 2006).

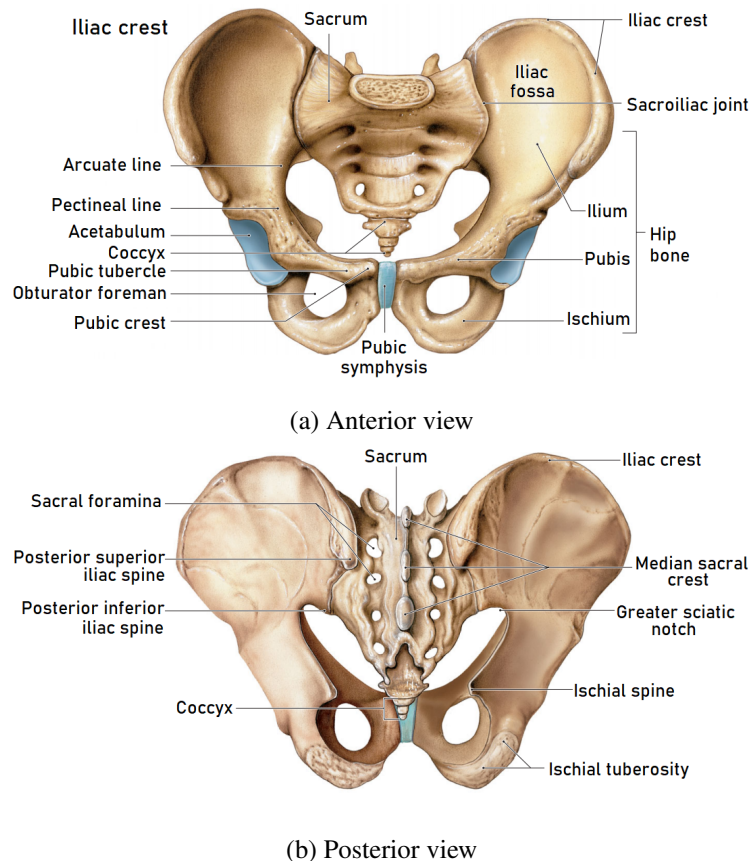


Figure 2.2: Pelvis (Martini et al., 2012)

2.1.1.2 Joints and Ligaments of the Pelvic Girdle

As mentioned before, the medial surfaces of the pubic bones articulate at the pubic symphysis, a secondary cartilaginous joint. They are covered by hyaline cartilage and connected by fibrocartilage, varying in thickness and constituting the interpubic disc. This disc is generally wider in women. The main ligaments joining the bones are the superior pubic ligament, which connects the bones above, extending to the pubic tubercles, and the arcuate pubic ligament, which connects the lower borders of the symphyseal pubic surfaces bounding the pubic arch (Standing, 2016).

The sacroiliac joint occurs between the sacral and iliac auricular surfaces (figure 2.3a). The auricular surfaces have curvatures and irregularities that restrict movements and contribute to the considerable strength of the joint in transmitting weight from the vertebral column to the lower limbs. The ligaments of the sacroiliac joint are the anterior, interosseous and posterior sacroiliac, iliolumbar, sacrotuberous and sacrospinous ligaments (figure 2.3a). The thin anterior sacroiliac ligaments are the anterior part of the fibrous capsule of the synovial part of the joint and it connects

the third sacral segment to the lateral side of the preauricular sulcus. The interosseous sacroiliac ligament is the major bond between the bones and it fills the irregular space posterosuperior to the joint. The posterior sacroiliac ligament overlies the interosseous ligament and it consists of several weak fasciculi connecting the intermediate and lateral sacral crests to the posterior superior iliac spine and posterior end of the internal lip of the iliac crest. The sacrotuberous ligament is attached to the posterior superior iliac spine, the posterior sacroiliac ligaments, lateral sacral crest and the lateral margins of the lower sacrum and upper coccyx. The sacrospinous ligament extends from the ischial spine to the lateral margins of the sacrum and coccyx anterior to the sacrotuberous ligament (Standring, 2016).

In relation to the lumbosacral joints, the anterior intervertebral (IV) joint is where L5 and S2 vertebrae articulate and there is a L5/S1 IV disc between them (figure 2.1a). They also articulate at two posterior zygapophysial joints (facet joints) between the articular processes of these vertebrae. These joints are further strengthened by iliolumbar ligaments radiating from the transverse processes of the L5 vertebra to the ilia (Moore et al., 2006).

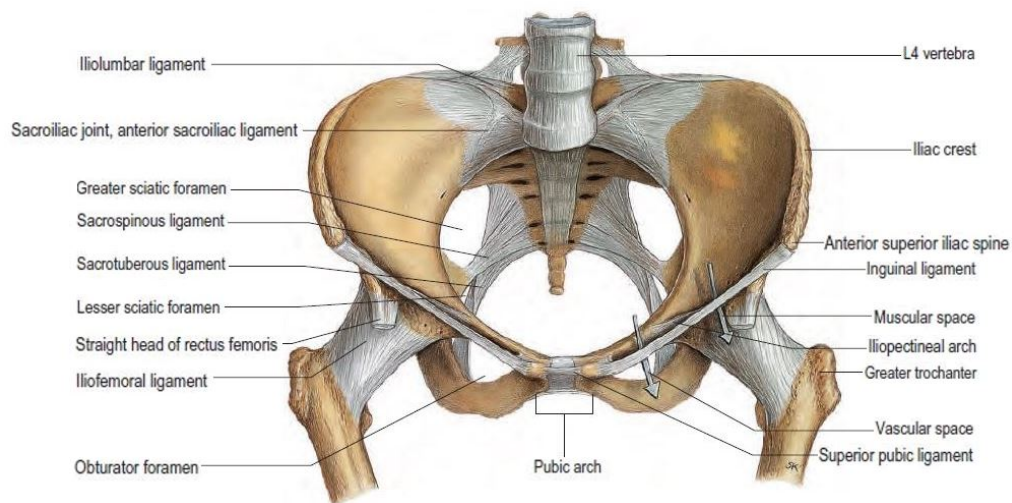
The sacrococcygeal joint is a secondary cartilaginous joint and the anterior and posterior sacrococcygeal ligaments are long strands that reinforce this joint (Moore et al., 2006). The sacrococcygeal joint typically is articulated by a fibrocartilagenous disc, composed of hyaline cartilage. It can also be a synovial joint in some cases and, when this is the case, the joint is more mobile (Hwang, 2015).

2.1.2 Pelvic Cavity

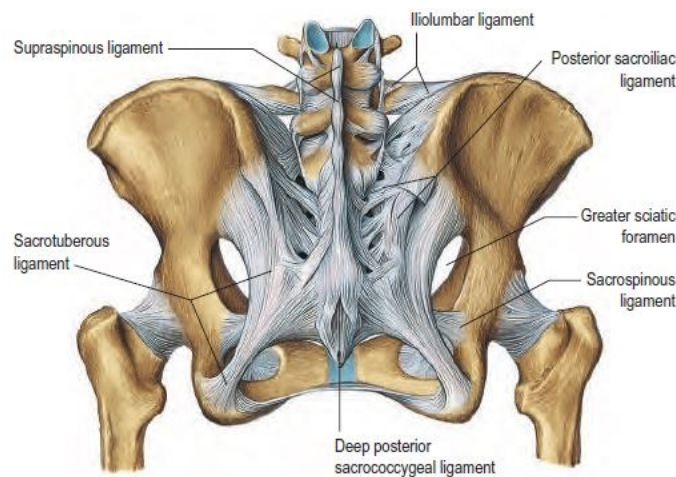
The largest continuous visceral cavity of the human body is formed by the abdomen and pelvis, which is known as the abdominopelvic cavity (figures 2.1a and 2.1b). The pelvic cavity, the inferoposterior part of the abdominopelvic cavity, has a funnel shape and corresponds to the space bounded peripherally by the bony, ligaments, muscular pelvic walls and floor. Inferiorly, the pelvic cavity is limited by the musculo-fascial pelvic diaphragm, which is suspended above (but descends centrally to the level of) the pelvic outlet, forming a bowl-like pelvic floor. Posteriorly, it is bounded by the coccyx and inferiormost sacrum, with the superior part of the sacrum forming a roof over the posterior half of the cavity (Moore et al., 2006).

2.1.2.1 Walls of Pelvic Cavity

The pelvic cavity has an anteroinferior wall, two lateral walls, a posterior wall and a floor (figures 2.4a and 2.4b). The anteroinferior wall is formed by the bodies and rami of the pubic bones and the pubic symphysis. The right and left hip bones, each of which includes an obturator foramen closed by an obturator membrane, form the lateral pelvic walls; the obturator fascia covers the medial surfaces of the obturator internus muscles and it is thickened centrally as a tendinous arch, providing attachment for the pelvic diaphragm. The posterior pelvic wall consists of musculo-ligamentous walls, which are formed by ligaments associated with the sacroiliac joints (anterior sacroiliac, sacrospinous, and sacrotuberous ligaments) and piriformis muscles. The piriformis



(a) Anterior view



(b) Posterior view

Figure 2.3: Joints and ligaments of the pelvis (Stranding, 2016)

muscles, which arise from the superior sacrum, lateral to its pelvic foramina occupy much of the greater sciatic foramen (Moore et al., 2006).

2.1.2.2 Floor of Pelvic Cavity

The pelvic floor (figures 2.4a and 2.4b) is composed by the ligamentous supports of the cervix and the pelvic and urogenital diaphragms and lies within the lesser pelvis, separating the pelvic cavity from the perineum. The pelvic diaphragm is formed by the coccygeus and levator ani muscles. The coccygeus muscles arise from the lateral aspects of the inferior sacrum and coccyx, whereas the levator ani is attached to the bodies of the pubic bones anteriorly, the ischial spines posteriorly and a thickening in the obturator fascia (the tendinous arch of the levator ani) between the two bony sites on each side. The levator ani muscles are composed by three parts (puborectalis, pubococcygeus and iliococcygeus), noting that an anterior gap between the medial borders of them

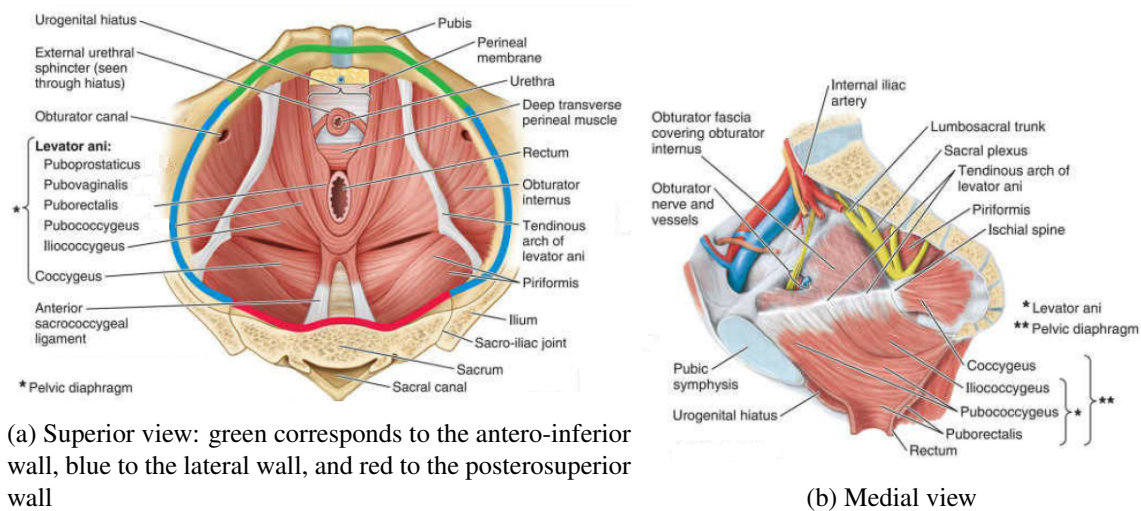


Figure 2.4: Floor and walls of pelvis (Moore et al., 2006)

of each side (urogenital hiatus) gives passage to the urethra and vagina (Standing, 2016; Moore et al., 2006). The urogenital diaphragm is formed by two muscles: the deep transverse perineal and the sphincter urethrae (figure 2.6).

2.1.3 Perineum

The perineum includes external genitalia, perineal muscles, and anal canal, and it is separated from the pelvis by the inferior fascia of the pelvic diaphragm (levator ani muscle), as can be seen in figure 2.5. Considering the anatomical position, the perineal region, which corresponds to the surface of the perineum, is the narrow region between the proximal parts of the thighs.

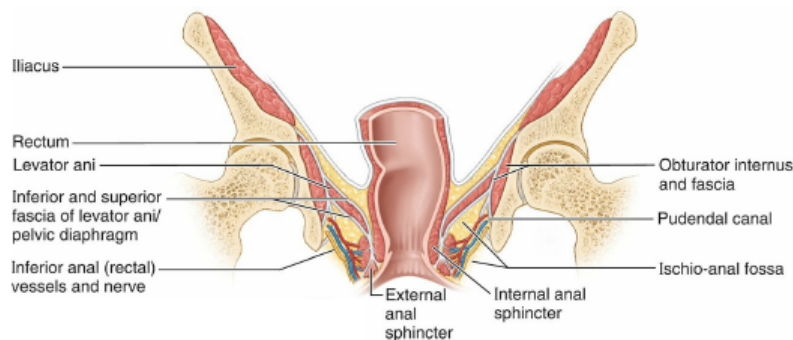


Figure 2.5: Boundary separating pelvis from perineum (Moore et al., 2006)

Concerning the osseofibrous structures forming the boundaries of the perineum (Moore et al., 2006), anteriorly there is the pubic symphysis, anterolaterally the ischiopubic rami, laterally the ischial tuberosities, posterolaterally the sacrotuberous and posteriorly the inferiormost sacrum and coccyx.

The perineum, when the lower limbs are abducted, corresponds to a diamond-shaped area and it is divided by an imaginary transverse line joining the anterior ends of the ischial tuberosities into

two triangles. The urogenital triangle, anterior to this line, is closed by the perineal membrane, which stretches between the two sides of the pubic arch, covering the anterior part of the pelvic outlet. The anal triangle lies posterior to this line and the major features of it are the anal canal and its orifice, the anus, lying centrally surrounded by ischio-anal fat. The perineal membrane fills the anterior gap in the pelvic diaphragm (the urogenital hiatus) but is perforated by the urethra and by the vagina. The membrane and the ischiopubic rami to which it attaches provide a foundation for the vulva, which is the superficial feature of the triangle (Moore et al., 2006).

The central point of the perineum corresponds to the midpoint of the line joining the ischial tuberosities and is the location of the perineal body, which is the central tendon of the perineum. It contains collagenous and elastic fibers and both skeletal and smooth muscle. The perineal body lies deep to the skin, with relatively little overlying subcutaneous tissue, posterior to the vestibule of the vagina and anterior to the anus and anal canal. It is the site of convergence and interlacing of fibers of several muscles, as it can be seen in figure 2.6, including: bulbospongiosus; external anal sphincter; superficial and deep transverse perineal muscles; and smooth and voluntary slips of muscle from the external urethral sphincter, levator ani, and muscular coats of the rectum. Superiorly, the perineal body blends with the rectovesical or rectovaginal septum and anteriorly with the posterior border of the perineal membrane (Moore et al., 2006).

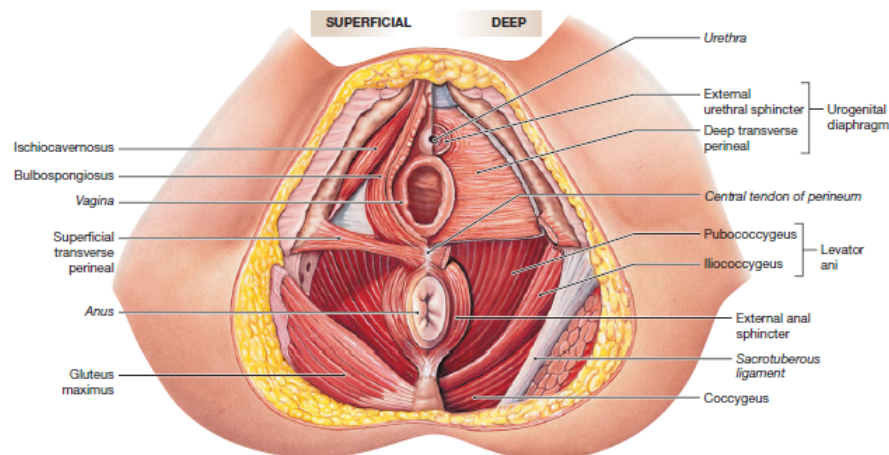


Figure 2.6: Superficial and deep layers of perineum viewed from below (Martini et al., 2012)

2.1.4 Pelvic Floor Dysfunction

Pelvic floor function and continence can be damaged by direct anatomical injury (as in vaginal delivery, which results in dilatation and stretching of the pelvic floor). The principal types of female pelvic floor dysfunction can manifest as urinary and/or fecal incontinence and as prolapse of the female reproductive organs (Donelson and Minocha, 2002).

Female urinary incontinence is often attributed to the consequences of pregnancy and childbirth since it is more common among pregnant women compared with other groups of women. A link between urinary incontinence and parity has already been demonstrated. Childbirth may

have pelvic floor laxity as a consequence of weakening and stretching of the muscles and connective tissue during delivery. As a result of spontaneous lacerations and episiotomies, damage may occur. The stretching of the pelvic tissues during vaginal delivery may damage the pudendal and pelvic nerves and also the muscles and connective tissue of the pelvic floor (Donelson and Minocha, 2002).

Bowel dysfunctions include different clinical problems such as fecal incontinence and constipation. Pelvic outlet obstruction is a common cause of constipation and is attributed to muscular dysfunction of the pelvic floor. For example, a rectocele is a herniation or protrusion the anterior rectal wall into the vagina and is associated with pelvic laxity and, during vaginal delivery or chronic straining, damage to the rectovaginal septum, pelvic floor muscles, and the pudendal nerves may occur. Also, the descending perineum syndrome occurs as a result of the injury of the sacral or pudendal nerves or damage to the pelvic floor muscles and it occurs consequent to childbirth or chronic straining at stool (Donelson and Minocha, 2002).

The most common factor of fecal incontinence in women is obstetric trauma. Concerning the effects of pregnancy, when parturition occurs, there is stretching of the levators and the vaginal wall, stretching and tearing of the rectovaginal septum and compression of the pudendal nerves against the pelvis sidewall. The incidence of sphincter injury is higher in patients with perineal tears and, after a third degree tear (involving the sphincter muscle), some patients developed fecal incontinence symptoms. Similar to tears, episiotomies are associated with incontinence and it can be also associated with an increased risk of sphincter injury (Donelson and Minocha, 2002).

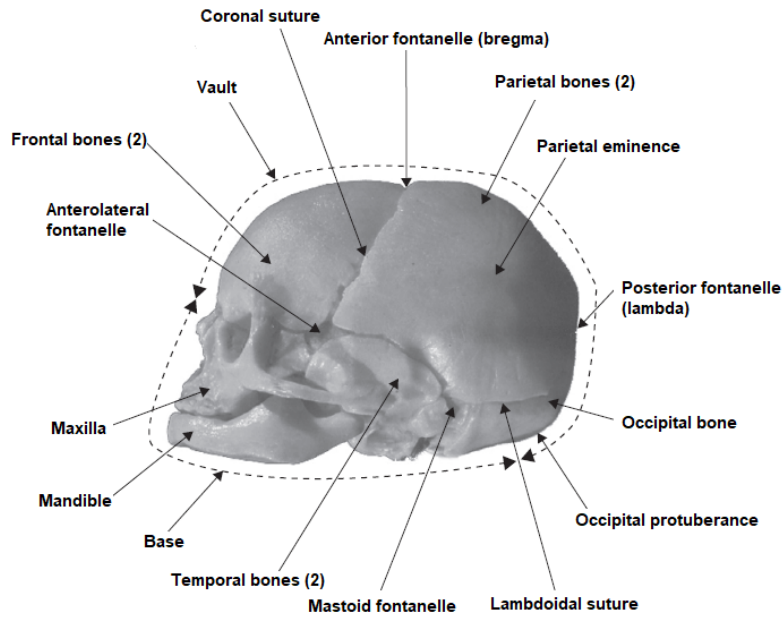
Genital prolapse refers to weakening or loss of support to the pelvic organs (bladder, vagina, uterus, and rectum), which results in a herniation of those pelvic organs. There are several types of genital prolapse (Donelson and Minocha, 2002), including:

- vaginal vault prolapse, which corresponds to herniation of the vaginal vault (the expanded region of the vaginal canal at the internal end of the vagina) caused by many factors, such as loss of support or weakening of specific ligaments; uterine prolapse (herniation of the uterus caused by the loss of support of some ligaments);
- cystocele, which is the herniation of the anterior vaginal wall and bladder;
- enterocele, which corresponds to the herniation of the superior portion of the posterior vaginal wall caused by tearing, stretching, or a combination of the two, of the posterior vaginal wall endopelvic fascia;
- rectocele, corresponding to the herniation of the inferior portion of the posterior vaginal wall and rectum also caused by tearing, stretching, or a combination of the two, of the posterior vaginal wall endopelvic fascia.

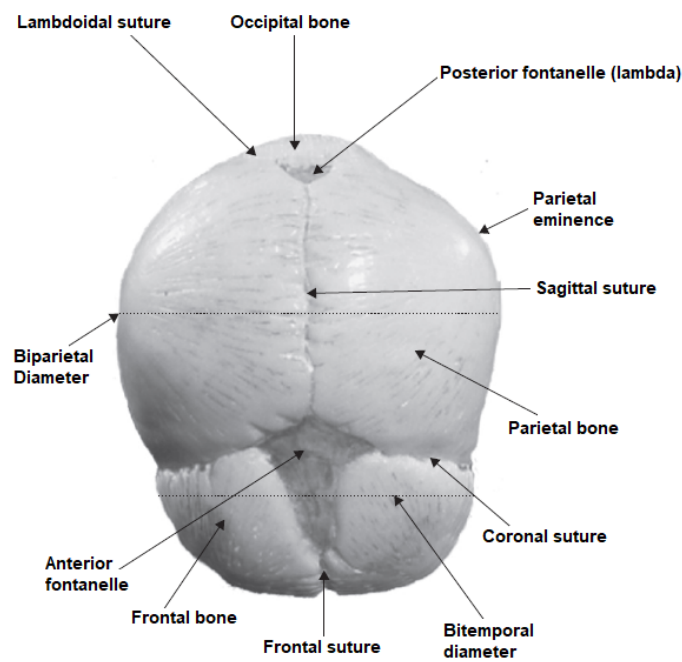
2.2 Fetus Head

The skull (figures 2.7a and 2.7b) consists of the cranium, facial skeleton, and mandible. The cranium may be subdivided into the calvaria, also known as cranial vault, and the basicranium (cranial base) (Standring, 2016). It protects the brain, which is subjected to pressure during labor, and has an ability to change shape to adapt to the process of labor in response to uterine contractions and the size and shape of the pelvis. It is divided into three main regions: vault, base and face (figures 2.7a and 2.7b). The vault comprises two frontal bones, two parietal bones, two temporal bones and one occipital bone. The soft fibrous tissues that link some bones of the skull are known as sutures and there are four: frontal, sagittal, lambdoidal and coronal. A fontanelle is a membranous, non-ossified area of the skull where three or more sutures meet and the most significant are: anterior fontanelle or bregma, posterior fontanelle, anterolateral or temporal fontanelles, posterolateral or mastoid fontanelles (Macdonald et al., 2011).

Since the fetal skull presents an incomplete ossification and many bones are still in various elements that are united by fibrous tissue or cartilage, it has a unique capacity to flex during birth. This enables the adaptation to prolonged compression to enhance its passage through the birth canal. The adaption process described, which enables the bones of the skull override each other as a result of pelvic girdle pressures, is known as molding (Macdonald et al., 2011). Consequently, the diameters of the skull can increase or decrease. The flexion or extension degree of the fetus head is influenced by its presentation and position in relation to the pelvic brim and this also determines the precise realignment of the skull bones during labor and delivery (Macdonald et al., 2011).



(a) Lateral view



(b) Superior view

Figure 2.7: The fetal skull (adapted from [Macdonald et al. \(2011\)](#))

Chapter 3

Labor

3.1 Introduction

During a normal labor, painful regular uterine contractions occur in order to stimulate progressive effacement and dilatation of the cervix with descent of the fetus, through the pelvis. Then, the spontaneous vaginal birth of the fetus occurs as well as the expulsion of the placenta and membranes. This sequential pattern can be divided into three stages: the first stage, which consists of latent phase, during which cervical effacement and early dilation occur, and active phase, during which more rapid cervical dilatation occurs; the second stage, which also consists of two phases, the passive stage (during which the cervix is fully dilated, but there are no voluntary or involuntary expulsive efforts) and the active stage (during which the woman begins to push either voluntarily or involuntarily); the third stage is from the birth of the baby to the expulsion of the placenta and membranes ([Macdonald et al., 2011](#); [Hacker et al., 2016](#); [Posner et al., 2013](#)).

Concerning the second stage, as labor progresses, the fetus is moved through the birth canal and, due to the forces that occur, various twists and turns of it are induced, which causes it to respond to the contours and planes of the maternal pelvis. It is important to note that it is necessary to take advantage of the available space and, to do so, the widest presenting diameter of the fetal head should enter the pelvis in the widest diameter. Nevertheless, specific physiology of individual women, different maternal birthing positions and fetal pairs can require different mechanisms ([Macdonald et al., 2011](#)).

3.2 Fetus

There are several fetal variables that influence the process of labor ([Gabbe et al., 2017](#)):

- the **fetal size** that can be estimated clinically, but it is a method subject to a large degree of error;
- the **fetal lie**, which refers to the longitudinal axis of the fetus relative to the longitudinal axis of the uterus. It can be classified as longitudinal, transverse, or oblique (see figure 3.1), noting that only fetuses in the longitudinal lie can be safely delivered vaginally;

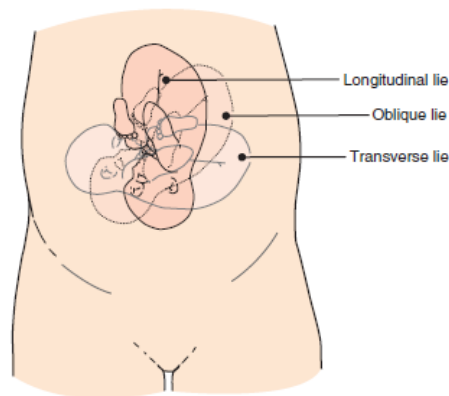


Figure 3.1: Examples of fetal lie (Gabbe et al., 2017)

- **presentation**, associated with the fetal part that directly overlies the pelvic inlet, and, in a fetus presenting in the longitudinal lie, the presentation can be cephalic (vertex) or breech;
- **attitude**, which refers to the position of the head with regard to the fetal spine (the degree of flexion and/or extension of the fetal head) and it is fundamental to note that the flexion of the head is important to facilitate engagement of the head in the maternal pelvis.
- **position of the fetus**, which is associated with the relationship of the fetal presenting part to the maternal pelvis (see figure 3.2). At onset of labor, the left occipit anterior position is considered as optimum when compared with other fetal positions for initiating the normal mechanism of labor (Gabbe et al., 2017; Webb et al., 2011; Ahmad et al., 2014).

3.2.1 Fetal Head Diameters

Concerning the dimensions of the fetal skull, there are several important diameters, as it is shown in figure 3.3, since the anteroposterior diameter presenting to the maternal pelvis depends on the degree of flexion or extension of the head. Thus, it is important to know the various diameters as they can differ in length. When the fetal chin is optimally flexed onto the chest, the suboccipitobregmatic diameter, which extends from the undersurface of the occipital bone at the junction with the neck to the center of the anterior fontanelle, presents at the pelvic inlet. The occipitofrontal diameter, which extends from the external occipital protuberance to the glabella, corresponds to the presenting anteroposterior diameter when the head is deflexed, as in an occipitoposterior presentation. The supraoccipitomenal diameter extends from the vertex to the chin and in a brow presentation it is the presenting anteroposterior diameter. In face presentations, the presenting anteroposterior diameter is the submentobregmatic and it extends from the junction of the neck and lower jaw to the center of the anterior fontanelle. Regarding the transverse diameters of the fetal skull, there are two: the biparietal, which is the largest transverse diameter and extends between the parietal bones, and the bitemporal, which is the shortest transverse diameter and extends between the temporal bones (Hacker et al., 2016).

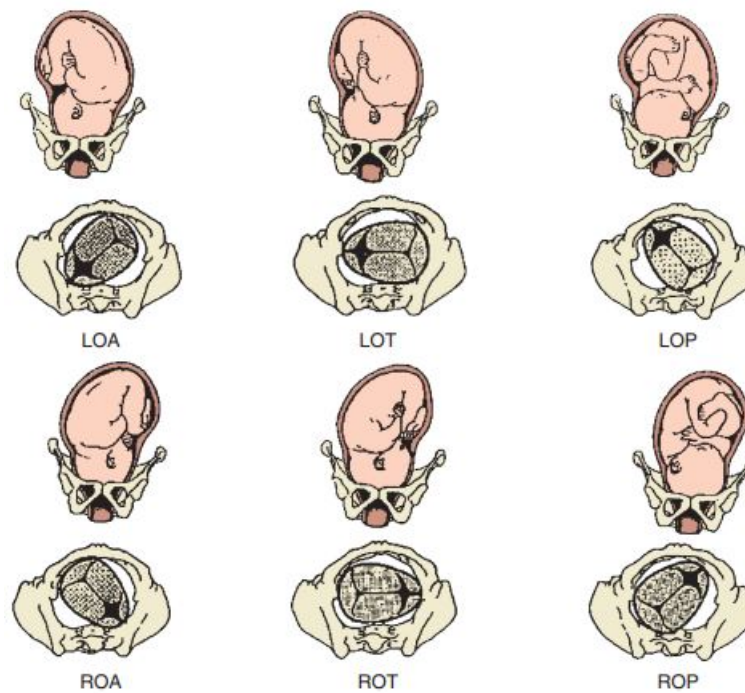


Figure 3.2: Fetal presentations and positions in labor: left occipit anterior (LOA); left occipitoposterior (LOP); left occipitotransverse (LOT); right occipit anterior (ROA); right occipitotransverse (ROT); right occipitoposterior (ROP) (Gabbe et al., 2017)

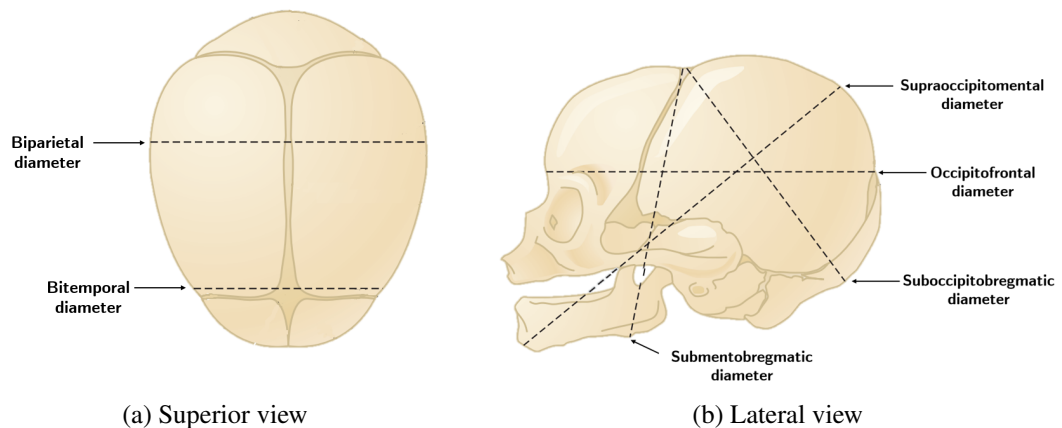


Figure 3.3: Diameters of the fetal skull (adapted from Hacker et al. (2016))

3.3 Maternal Pelvis

During parturition, the fetus will pass through the birth canal and, therefore, the bony pelvis as well as the resistance provided by the soft tissues have to be taken into consideration.

Thus, engagement occurs when the widest diameter of the fetal presenting part has passed through the pelvic inlet. Moreover, a measure of descent of the fetus through the birth canal is known as station and the current standard classification (-5 to +5) is based on the distance (in centimeters) of the leading bony edge from the ischial spines and the midpoint (0 station)

corresponds to the plane of the maternal ischial spines, as it can be seen in figure 3.4 (Gabbe et al., 2017).

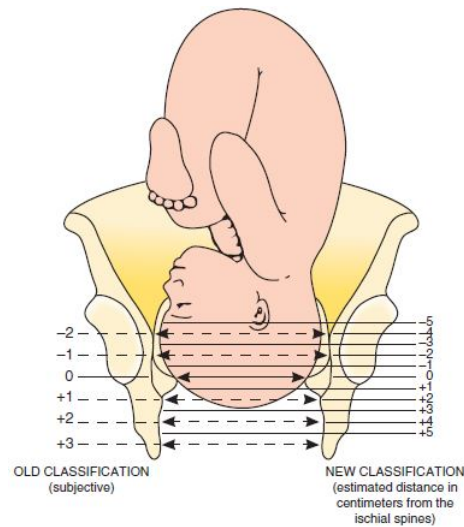


Figure 3.4: Stations of the fetal head (Gabbe et al., 2017)

3.3.1 Maternal Pelvic Diameters

In obstetrics, to determine the female pelvis capacity for childbearing, it is important to analyze the diameters of the pelvis, which correspond to the main measurements for assessing the capacity of the maternal pelvis (Gabbe et al., 2017). The pelvic planes are imaginary flat surfaces passing across the pelvis at different levels and they are used for the purposes of description (figures 3.5a and 3.5b).

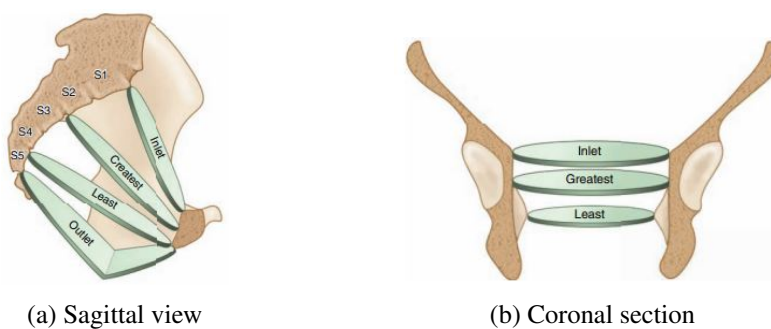


Figure 3.5: Pelvic planes (Posner et al., 2013)

3.3.1.1 Pelvic inlet

Concerning the pelvic inlet (figures 3.6a and 3.6b), the transverse diameter corresponds to the maximum distance between similar points on opposite sides of the pelvic inlet and this is its largest measurement. The diagonal conjugate diameter corresponds to the distance from the sacral

promontory to the inferior margin of the pubic symphysis. The distance of the middle of the sacral promontory to the superior aspect of the pubic symphysis is known as the true or anatomic conjugate diameter, whereas the obstetric conjugate represents the actual space available to the fetus and extends from the middle of the sacral promontory to the closest point on the convex posterior surface of the symphysis pubic. The distance from the iliopubic ramus to the opposite sacroiliac joint is known as the oblique diameter. The posterior sagittal diameter extends from the anteroposterior and transverse diameters to the middle of the sacral promontory (Hacker et al., 2016; Gabbe et al., 2017).

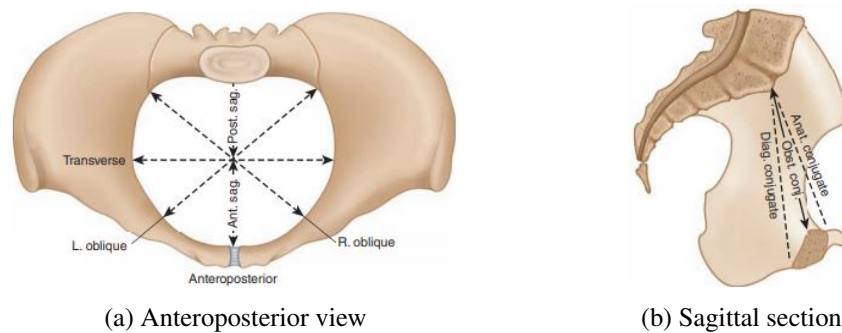


Figure 3.6: Pelvic inlet diameters (Posner et al., 2013)

3.3.1.2 Plane of Greatest Diameter

The anteroposterior diameter extends from the midpoint of the posterior surface of the pubis to the junction of the second and third sacral vertebrae. The transverse diameter is the widest distance between the lateral borders of the plane (Hacker et al., 2016; Gabbe et al., 2017).

3.3.1.3 Plane of Least Diameter (Midplane)

This is the most important plane of the pelvis (figures 3.7a and 3.7b). The anteroposterior diameter extends from the lower border of the pubis to the junction of the fourth and fifth sacral vertebrae. The limiting factor of the midpelvis is the interspinous (or transverse) diameter, which corresponds to the measurement between the ischial spines. The posterior sagittal diameter extends from the midpoint of the bispinous diameter to the junction of the fourth and fifth sacral vertebrae (Hacker et al., 2016; Gabbe et al., 2017).

3.3.1.4 Pelvic Outlet

Concerning the pelvic outlet, although being rarely of clinical significance, there are four measurements that can be made (figures 3.8a and 3.8b). The anatomic anteroposterior diameter is measured from the apex of the coccyx to the midpoint of the lower rim of the pubic symphysis, whereas the obstetric anteroposterior diameter extends from the inferior margin of the pubis to the sacrococcygeal joint. The distance between the ischial tuberosities at the lower borders of their

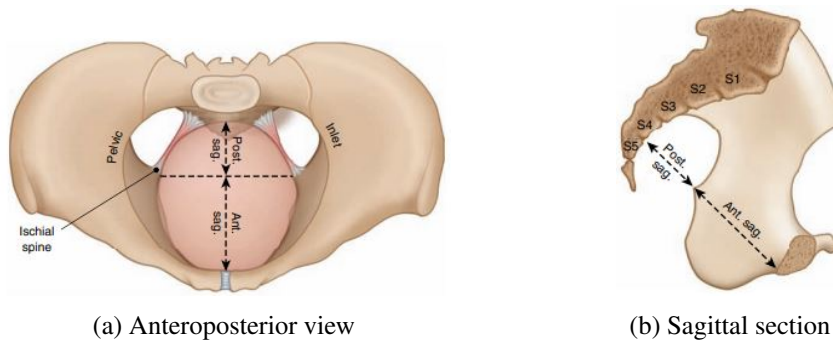


Figure 3.7: Plane of least dimensions (Posner et al., 2013)

medial surfaces is known as the transverse or bituberous diameter. The posterior sagittal diameter extends from the middle of the transverse diameter to the sacrococcygeal joint (Hacker et al., 2016; Gabbe et al., 2017).

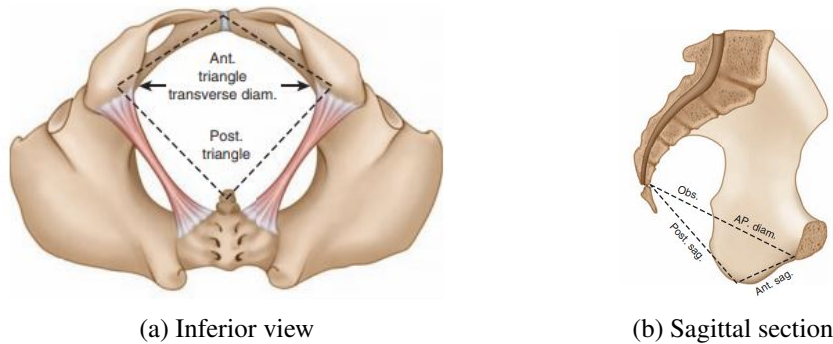


Figure 3.8: Pelvic outlet dimensions (Posner et al., 2013)

3.3.2 Classification of the Pelvis

There is a wide variation in the female pelvis and, based on the general bony architecture, the pelvis may be classified into four basic types, as can be seen in figure 3.9, according to the classification of Caldwell and Moloy: gynecoid, which is found in approximately 50% of women; android, found in less than 30% of women; anthropoid, which is found in approximately 20% of women; and platypelloid, found in only 3% of women (Hacker et al., 2016).

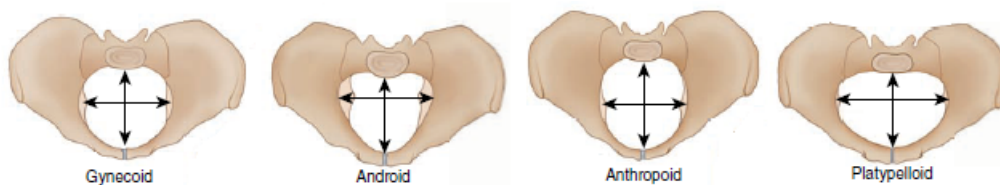


Figure 3.9: Pelvis types (Posner et al., 2013)

Concerning the gynecoid pelvis, it is round at the inlet, with straight sidewalls, far-spaced ischial spines and well-curved sacrum. The android pelvis has a triangular inlet, with convergent

sidewalls with prominent spines and with a shallow sacral curve. The anthropoid pelvis is much larger anteroposterior than transverse diameter, with sidewalls that do not converge and ischial spines that are not prominent but are close. This pelvis type is more often associated with delivery in the occipitoposterior position. Finally, the platypelloid pelvis has an oval-shaped inlet (short anteroposterior and wide transverse diameter), with straight or divergent sidewalls, a posterior inclination of a flat sacrum and a wide bispinous diameter (Hacker et al., 2016).

This classification separates female pelvis with favorable characteristics for vaginal delivery (gynecoid, anthropoid) from those that are less favorable (android, platypelloid), in order to determine whether a given fetus will be able to safely negotiate a given pelvis (Hacker et al., 2016).

3.3.3 Musculoskeletal System Changes of Pregnancy

During pregnancy, the female body undergoes many hormonal and anatomic changes that affect the musculoskeletal system. These changes occur naturally during pregnancy and often cause pain on the pelvic region, ranging in intensity from mild to severe pain. The pain starts during pregnancy and often disappears soon after childbirth. Pregnancy-related pelvic pain includes pain from the posterior pelvis and/or from the pubic symphysis.

A progressively increasing anterior convexity of the lumbar spine (lordosis) is often observed. This corresponds to a compensatory mechanism that allows the woman's center of gravity to be kept over her legs and also prevents the enlarging uterus from moving the center of gravity anteriorly. However, this modification as low back pain as a consequence (Gabbe et al., 2017).

Ligamentous laxity is another physiologic change of pregnancy and it is often associated with the production of the hormone relaxin, which levels increase in the third trimester. Due to the relaxation of the pelvic ligaments, it allows the joints of the pelvis to become more flexible to the fetus to pass. Weight gain combined with ligamentous laxity increase joint discomfort and there is an increasing mechanical strain on the sacroiliac and pelvis (Borg-Stein et al., 2005). This is consistent with what was found in several studies where the pelvic area was compared between pregnant and nonpregnant women: the former had a larger area than the latter (Hemmerich et al., 2019; Reitter et al., 2014).

The sacroiliac joint takes part in the flexion and extension of the lumbar spine and, in female joints, in terms of mobility, it facilitates the demands of pregnancy and parturition. The sacroiliac joints oppose this rotation and, consequently, cause an increase of mechanical tension of the pelvic ligaments. It is important to note that, to observe a small amount of motion in the sacroiliac joints, it is required a significant force, as it occurs during the pregnancy (Sipko et al., 2010; McGrath, 2004; Aldabe et al., 2012).

Concerning the pubic symphyseal region, there are several disorders during pregnancy and parturition. As mentioned before, the symphysis pubis is a fibrocartilaginous structure and there are some ligaments enveloping the joint. It is believed that relaxin increases pelvic laxity and predisposes separation of the pubic symphysis, by altering the structure of collagen (Aldabe et al., 2012). Therefore, the nonpregnant woman's symphysis pubis gap is, approximately, 4-5 mm and it is normal to widen 2-3 mm, without discomfort, during the third trimester of pregnancy.

Consequently, there is an increase in the diameters of the pelvic brim and cavity outlet to facilitate delivery of the fetus (Jain et al., 2006). However, widening of 10 mm or greater can occur and it is considered pubic symphysis separation, or pubic symphysis diastasis. Several factors have been associated with this condition, such as rapid labor, larger birth weight of the infant, delivery using instrumentation, cephalopelvic disproportion, abnormal presentation of the infant, and excessive forceful abduction of the thighs during delivery (Hwang, 2015).

The sacrococcygeal joint enables a small amount of flexion and extension of the coccyx. Flexion is produced by contraction of levator ani muscle whilst extension is mostly passive. It is considered that coccyx can be extended by approximately 5-15 degrees and flexed by approximately 5-22 degrees (Woon and Stringer, 2012). Nonetheless, coccydynia can occur, which is defined as pain in the coccyx region and it is typically the result of traumatic etiology. Postpartum coccydynia is an example and it has been estimated that approximately 7% of women suffer from this condition. Two characteristic lesions have been described in postpartum coccydynia, both of which are thought to be the result of the coccyx being pushed rearwards by the child's head (Hwang, 2015).

3.4 Birthing Positions

There is a wide range of positions for giving birth that can be adopted, but the most widely used is based on the work of François Mauriceau, which is called the semi-recumbent or the French birthing position (Gupta and Nikodem, 2000). Maternal positions can be classified into two main groups, depending on the angle made by the horizontal plane and the line linking the midpoints of the third and fifth lumbar vertebrae: when the angle is greater than 45 degrees it is considered upright or vertical, otherwise it is labeled horizontal. It is important to note that this definition can vary, since there are some studies that define upright position by an angle greater than 30 degrees (Desseauve et al., 2017). In relation to the upright positions, they include the sitting, kneeling, squatting and standing positions, with their variations. On the other hand, the lateral, semi-recumbent, lithotomy, supine, knee-elbow and dorsal positions, as well as their variants, are considered horizontal (Atwood, 1976).

3.4.1 Upright (Vertical) Positions

3.4.1.1 Sitting Position

In the sitting position, a woman rests mostly on her buttocks, although she may rely on some support (Atwood, 1976). This type of position includes semi-sitting and sitting upright. In semi-sitting, figure 3.10a, a woman sits with her trunk at an angle greater than 45 degrees to the bed and she can be supported by pillows or bedrest. In sitting upright position, figure 3.10b, a woman sits in bed supported by a person or on a birthing stool or similar birthing aid (Huang et al., 2019).

3.4.1.2 Kneeling Position

Kneeling positions include upright kneeling and all fours' position. Upright kneeling position, figure 3.10c, a woman rests mainly on her knees and may place her arms in different positions to distribute the weight between knees and her feet. Consequently, all fours' position, also known as hands-to-knees position, a woman supports herself on either the palms of her first (figure 3.10d) (Huang et al., 2019; Atwood, 1976).

3.4.1.3 Squatting Position

In the squatting position, a woman's weight rests essentially on her feet, but her knees are considerably bent and she may lean or pull on some support (figure 3.10e). The squatting position is often regarded as the most natural position (Huang et al., 2019).

3.4.1.4 Standing Position

In the standing or erect position, a woman's weight is essentially on her feet and her knees may be bent slightly or not at all (Atwood, 1976), as can be seen in figure 3.10f.

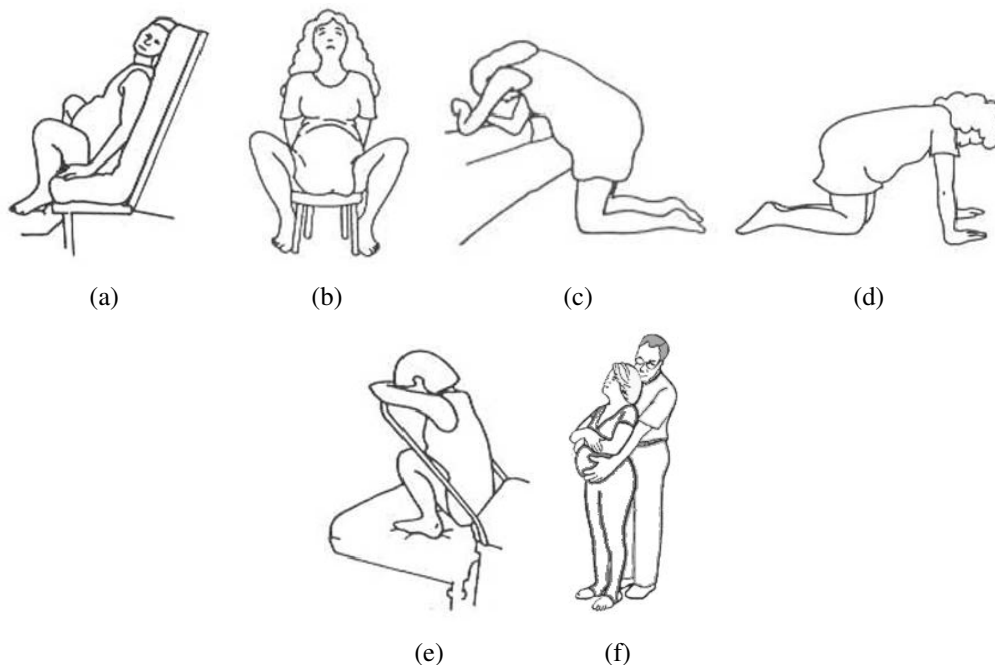


Figure 3.10: Upright Positions: (a) semi-sitting position (Simkin, 2002), (b) sitting on a low stool (Simkin, 2002), (c) kneeling over chair seat (Simkin, 2002), (d) hands-to-knees position (Simkin, 2002), (e) squatting position with bar (Simkin, 2002), (f) standing position (Lowdermilk, 2011)

3.4.2 Horizontal Positions

3.4.2.1 Lateral Position

Lateral positions, also known as side-lying positions, include pure side-lying position and exaggerated Sims positions (semi-prone). In pure side-lying position, figure 3.11a, a woman rests on either side of her body with her legs either bent at right angles with her upper legs raised and supported. In lateral-prone, lateral Sims or exaggerated Sims positions, figure 3.11b, a woman lies on her side with lower arm behind (or in front of) her trunk, her lower leg extended, and her upper hip and knee flexed 90° or more, she rolls partly toward her front (Huang et al., 2019; Atwood, 1976).

3.4.2.2 Semi-recumbent Position

In the semi-recumbent position, figure 3.11c, a woman rests on her back which is supported at an angle. Her feet may either be drawn up to her buttocks or be fully extended (Atwood, 1976).

3.4.2.3 Lithotomy Position

In the lithotomy position, figure 3.11d, the woman rests on back, her legs are neither bent with her feet flat on the surface, placed in stirrups, straight leg supports or held by attendants (Huang et al., 2019).

3.4.2.4 Supine Position

In the supine position, figure 3.11e, the woman lies flat on her back or with her trunk slightly raised ($< 45^\circ$ to the horizontal), her legs may be out straight, bent with her feet flat on the bed, in the leg rests or drawn up and back toward her shoulders (Huang et al., 2019).

3.4.2.5 Dorsal Position

In the dorsal position, figure 3.11f, the weight of the woman rests mainly on her back and her legs are fully extended (Atwood, 1976).

3.4.2.6 Knee-elbow

In the knee-elbow, also known as knee-chest, figure 3.11g, the woman either squats or kneels with a large part of her weight supported by her hands or elbows (Atwood, 1976).

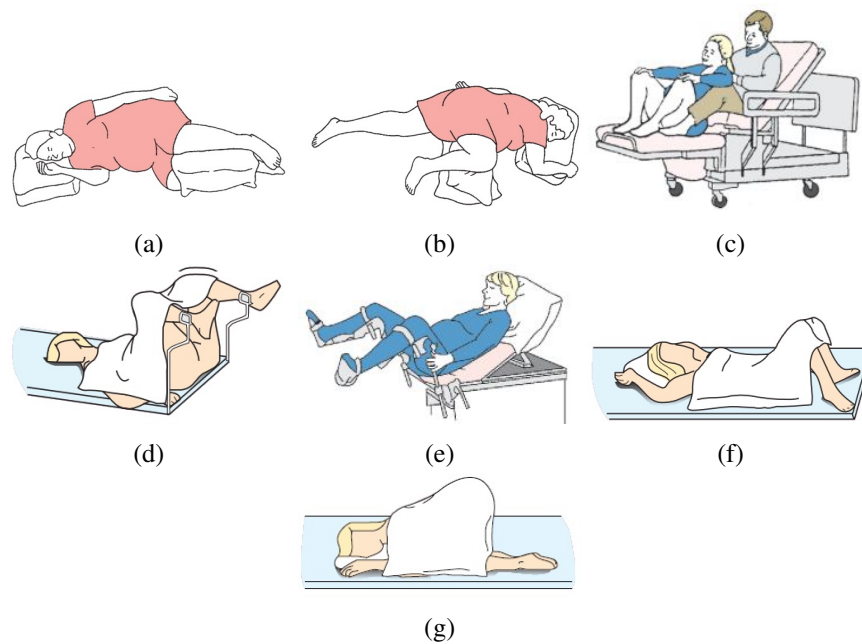


Figure 3.11: Horizontal Positions: (a) pure side-lying lateral position (Macdonald et al., 2011), (b) semi-prone lateral position (Macdonald et al., 2011), (c) semi-recumbent position (Lowdermilk, 2011), (d) lithotomy (Perry et al., 2014), (e) supine position (Lowdermilk, 2011), (f) dorsal position (Perry et al., 2014), (g) knee-elbow position (Perry et al., 2014)

3.5 Cardinal Movements in Labor

The changes in the position of the fetal head during its passage through the birth canal correspond to the cardinal movements. A rotation of the fetal head is required to successfully negotiate the birth canal due to the asymmetry of the shape of the birth canal. As it can be seen in figure 3.12, there are seven movements (Gabbe et al., 2017; Hacker et al., 2016):

1. **Engagement** - This movement refers to the passage of the widest diameter of the presenting part to a level below of the pelvic inlet. It is an important clinic prognostic sign because it demonstrated that, at least at the level of the pelvic inlet, the maternal bony pelvis is sufficiently large to allow descent of the fetal head.
2. **Descent** - Descent corresponds to the downward passage of the presenting part through the pelvis, but it is not continuous.
3. **Flexion** - As the fetal head descends owing to the shape of the bony pelvis and the resistance offered by the soft tissues of the pelvic floor, its flexion occurs passively. Complete flexion usually occurs only during the course of labor and corresponds to present the smallest diameter of the fetal head (the suboccipitobregmatic diameter) for optimal passage through the pelvis.

4. **Internal Rotation** - This movement refers to rotation of the presenting part from its original position as it enters the pelvic inlet to the anteroposterior position as it passes through the pelvis. It is a movement that results from the shape of the pelvis and the pelvic floor musculature. As the head descends, the occiput of the fetus rotates toward the pubic symphysis or, less commonly, toward the hollow of the sacrum, allowing the widest portion of the fetus to negotiate the pelvis at its widest dimension.
5. **Extention** - Extension occurs once the fetus has descended to the level of the introitus. The base of the occiput is in contact with the inferior margin at the symphysis pubis and, at this point, the birth canal curves upward. The fetal head is delivered by extension and rotates around the pubic symphysis.
6. **External Rotation** - This movement is also known as restitution and it refers to the return of the fetal head to the correct anatomic position in relation to the fetal torso. Further head rotation may occur as the shoulders undergo an internal rotation to align themselves anteroposteriorly within the pelvis.
7. **Expulsion** - The anterior shoulder delivers under the symphysis pubis, followed by the posterior shoulder over the perineal body. After the shoulder, the rest of the body is usually delivered without difficulty.

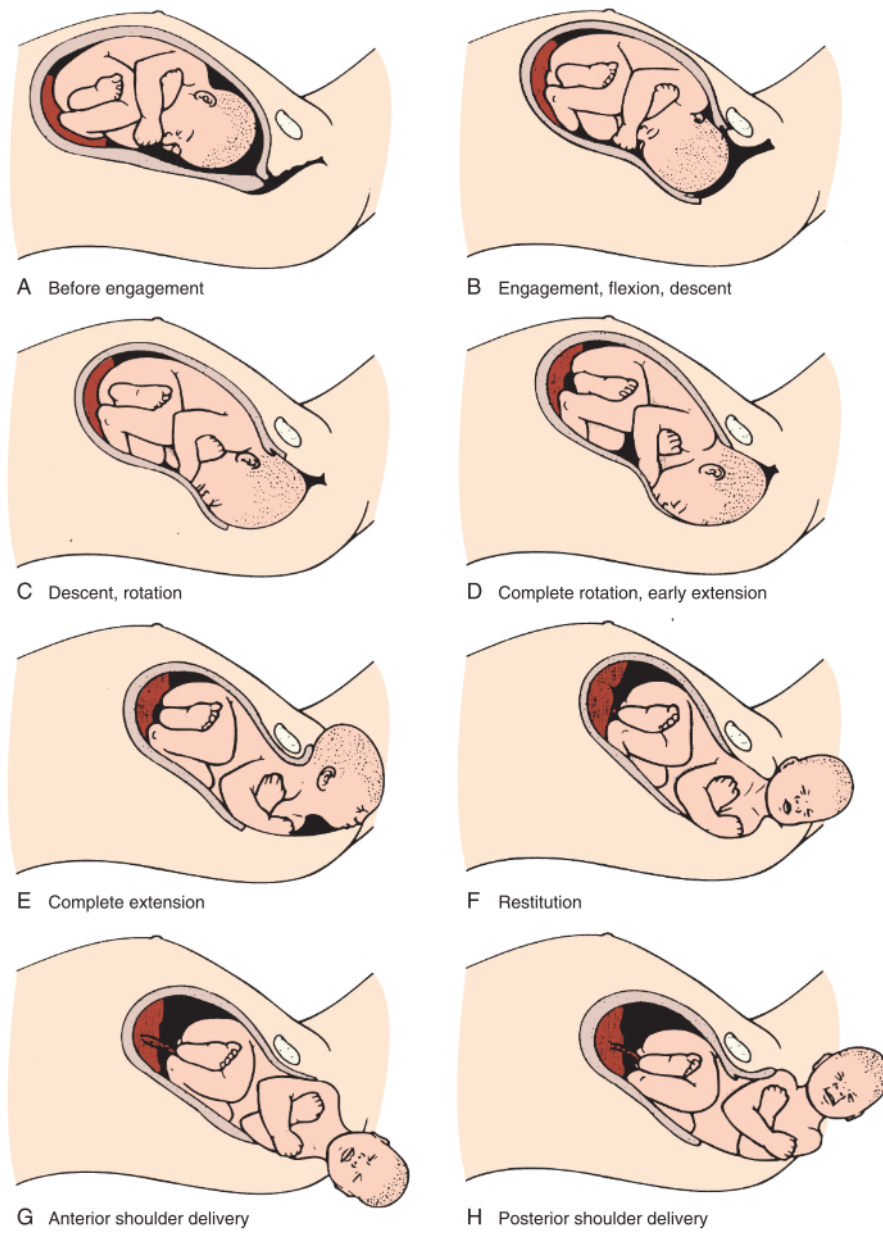


Figure 3.12: Cardinal movements in labor (Gabbe et al., 2017)

Chapter 4

Computational Solid Mechanics

4.1 Introduction

Computational bioengineering takes advantage of the latest computational capabilities to deal with biomedical problems. Through computational modeling, it is possible to assess new surgical concepts and postoperative surgical outcomes. Since it is not restricted to ethical constraints, it is a powerful and valuable tool that contributes to numerous innovations and developments in the medical field.

For this purpose, and from a mechanical perspective, it is important to consider the principles of continuum mechanics since they provide mathematical frameworks for modeling the behavior of matter. This continuum mechanics approach has been widely adopted for the analysis of biological tissues.

Furthermore, it is fundamental to consider the finite element method possibilities the analysis and determination of the effects of mechanical stresses, strains and interactions of different components in complex geometries by reducing them into a finite number of elements with simple geometries. Consequently, this method is often used to model and simulate biological components.

4.2 Preliminary Concepts

4.2.1 Configuration and Motion of Continuum Bodies

A continuum approach is usually used to describe macroscopic systems, which leads to the continuum theory. A fundamental assumption therein states that a body, denoted by B , may be viewed as having a continuous distribution of matter in space and time and it is considered to have a composition of a (continuous) set of particles, represented by $P \in B$. Hence, in a macroscopic study of a body, mass and volume are continuous functions of continuum particles and it is known as a continuum body (Holzapfel, 2002).

In figure 4.1, it is represented a continuum body B with particle $P \in B$ embedded in the three-dimensional Euclidean space at a given instant of time t . The continuum body B moves in space

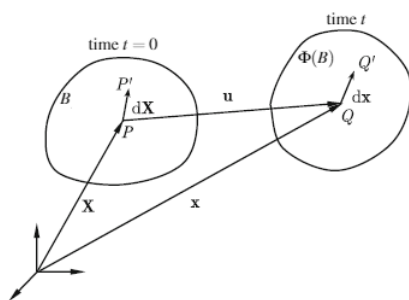


Figure 4.1: General motion of a deformable body (adapted from Kim (2015))

from one instant of time to another, and the placement of the body B is denoted as configuration $\Phi(B)$ of body B (Holzapfel, 2002).

A configuration of the body B is a one-to-one mapping which places all the particles of B in the Euclidean space. The motion of the body B is associated with the vector field Φ that defines the new location \mathbf{x} of a particle \mathbf{X} for a fixed t :

$$\mathbf{x} = \Phi(\mathbf{X}) \quad (4.1)$$

Considering a given particle \mathbf{X} that occupies the position (\mathbf{x}, t) , in a given instance, its position, which is associated with the place \mathbf{x} at time t , is given by:

$$\mathbf{X} = \Phi^{-1}(\mathbf{x}) \quad (4.2)$$

4.2.2 Material and Spatial Descriptions

In finite deformation analysis, it is necessary to have a careful distinction between the coordinate systems that can be chosen to describe the behavior of the body whose motion is under consideration. The so-called material (or referential) description is a characterization of the motion, or any other quantity, with respect to the material coordinates X_1, X_2, X_3 and time t , given by equation 4.1. In the material description, also referred to as Lagrangian description or Lagrangian form, attention is paid to a particle, so it is observed what happens to the particle as it moves. The so-called Eulerian (or spatial) description, or Eulerian form, corresponds to a characterization of the motion, or any other quantity, with respect to the spatial coordinates x_1, x_2, x_3 and time t , given by equation 4.2. In the spatial description, attention is paid to a point in space, and it is study what happens at the point as time changes (Holzapfel, 2002).

4.2.3 Deformation Gradient

A motion of a body will generally change its shape, position and orientation. A continuum body which is able to change its shape is said to be deformable (Kim, 2015). Taking into consideration the equation 4.1, it is said that, for a given point P in the undeformed configuration, a unique

point Q exists in the deformed configuration and this mapping relation can be written as:

$$\mathbf{x} = \Phi(\mathbf{X}, t) = \mathbf{X} + \mathbf{u}(\mathbf{X}, t) \quad (4.3)$$

where $\mathbf{u}(\mathbf{X}, t)$ is the displacement of point P .

In figure 4.1, neighboring points P' and Q' at infinitesimal distances from P and Q are denoted by vectors $d\mathbf{X}$ and $d\mathbf{x}$, respectively, in the two geometries. Note that the vector $d\mathbf{X}$ deforms to $d\mathbf{x}$. Assuming continuous mapping, the relationship between differential elements $d\mathbf{X}$ and $d\mathbf{x}$ can be expressed as follows:

$$d\mathbf{x} = \frac{\partial \mathbf{x}}{\partial \mathbf{X}} d\mathbf{X} \Rightarrow d\mathbf{x} = \mathbf{F} d\mathbf{X} \quad (4.4)$$

where \mathbf{F} is known as the deformation gradient that maps elemental vectors of the reference configuration to elemental vectors in the spatial configuration. It is a tensor which associates a material line element $d\mathbf{X}$ in B to the spatial line element $d\mathbf{x}$ in $\Phi(B)$. If $\mathbf{F} = \mathbf{1}$, then $d\mathbf{X} = d\mathbf{x}$, which means that there is no deformation. Even if an infinitesimal volume in the undeformed geometry can increase or decrease its size, it cannot shrink to a point, i.e., a zero volume. Mathematically, this means that the determinant of deformation gradient must be positive:

$$\det \mathbf{F} \equiv J > 0 \quad (4.5)$$

This property is important to make a valid mapping of $\Phi(\mathbf{X}, t)$ during large deformation (Kim, 2015).

4.2.4 Strain Measures

At this stage, it is necessary to determine the material elements changes in terms of (second-order) strain tensors associated with both reference or current configuration (Bonet and Wood, 2008).

Taking into account the change in the scalar product of two elemental vectors $d\mathbf{X}_1$ and $d\mathbf{X}_2$, since they deform to $d\mathbf{x}_1$ and $d\mathbf{x}_2$, the stretching (change in length) and changes in the enclosed angle between the two vectors will be involved. Therefore, considering the equation 4.4, the spatial scalar product $d\mathbf{x}_1 \cdot d\mathbf{x}_2$ can be written in terms of the material vectors $d\mathbf{X}_1$ and $d\mathbf{X}_2$:

$$d\mathbf{x}_1 \cdot d\mathbf{x}_2 = d\mathbf{X}_1 \cdot \mathbf{C} d\mathbf{X}_2 \quad (4.6)$$

where \mathbf{C} corresponds to the right Cauchy-Green deformation tensor, which is known as material tensor quantity and it is given in terms of the deformation gradient as \mathbf{F} as:

$$\mathbf{C} = \mathbf{F}^T \mathbf{F} \quad (4.7)$$

On the other hand, the initial material scalar product $d\mathbf{X}_1 \cdot d\mathbf{X}_2$ can be written in terms of the

spatial vectors $d\mathbf{x}_1$ and $d\mathbf{x}_2$:

$$d\mathbf{X}_1 \cdot d\mathbf{X}_2 = d\mathbf{x}_1 \cdot \mathbf{b}^{-1} d\mathbf{x}_2 \quad (4.8)$$

where \mathbf{b} is the left Cauchy-Green or Finger tensor and it is a spatial tensor quantity:

$$\mathbf{b} = \mathbf{F}\mathbf{F}^T \quad (4.9)$$

The change in scalar product can be found in terms of the material vectors $d\mathbf{X}_1$ and $d\mathbf{X}_2$ and the Lagrangian or Green strain tensor \mathbf{E} as:

$$\frac{1}{2}(d\mathbf{x}_1 \cdot d\mathbf{x}_2 - d\mathbf{X}_1 \cdot d\mathbf{X}_2) = d\mathbf{X}_1 \cdot \mathbf{E}d\mathbf{X}_2 \quad (4.10)$$

where the material tensor \mathbf{E} is

$$\mathbf{E} = \frac{1}{2}(\mathbf{C} - \mathbf{I}) \quad (4.11)$$

Alternatively, the same change in scalar product can be expressed with reference to the spatial elemental vectors dx_1 and dx_2 and the Eulerian or Almansi strain tensor \mathbf{e} as:

$$\frac{1}{2}(dx_1 \cdot dx_2 - d\mathbf{X}_1 \cdot d\mathbf{X}_2) = d\mathbf{x}_1 \cdot \mathbf{e}d\mathbf{x}_2 \quad (4.12)$$

where the material tensor \mathbf{e} corresponds to

$$\mathbf{e} = \frac{1}{2}(\mathbf{I} - \mathbf{b}^{-1}) \quad (4.13)$$

4.2.5 Stress Measures

Motion and deformation give rise to interactions between the material and neighboring material in the inferior part of the body. This leads to stress, which has a physical dimension force per unit of area, and it is responsible for the deformation of material. However, depending on the area used, the definition of stress changes, so, when a large deformation occurs, it is important to clarify what area is used (Bonet and Wood, 2008).

A deformable body is considered during a finite motion and, for that body, a traction vector \mathbf{t} can be defined using the area of the differential element da , the force $d\mathbf{f}$ acting on it, and the unit normal vector \mathbf{n} of the area as:

$$\mathbf{t} = \lim_{da \rightarrow 0} \frac{d\mathbf{f}}{da} = \boldsymbol{\sigma} \mathbf{n} \quad (4.14)$$

where $\boldsymbol{\sigma}$ is the Cauchy stress tensor, which refers to the deformed geometry as a reference for both force and area. It is often known as true stress and it is always symmetric. Therefore, there are six independent stress components acting at a certain point of a body, with $\sigma_{12} = \sigma_{21}$, $\sigma_{13} = \sigma_{31}$, $\sigma_{23} = \sigma_{32}$. For each stress component σ_{ij} , it adopts the mathematically logical convention that the first index characterizes the component of the vector \mathbf{t} at a certain point in the direction of the associated base vector \mathbf{e}_i , and the second index characterizes the plane that \mathbf{t} is acting on, which is described by the direction of the base vector \mathbf{e}_j , as can be seen in figure 4.2.

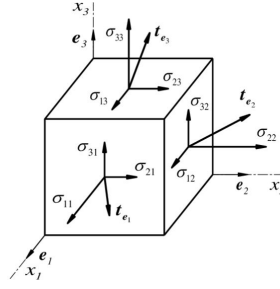


Figure 4.2: Positive stress components of the traction vectors $\mathbf{t}_{\mathbf{e}_i}$ (adapted from [Holzapfel \(2002\)](#))

It is important to note that, to define stress tensors based on the undeformed geometry, it is necessary to know both configurations and, therefore, it is possible to define the Kirchhoff stress from the Cauchy stress as follows:

$$\boldsymbol{\tau} = J\boldsymbol{\sigma} \quad (4.15)$$

where J represents its Jacobian defined by $J = \det \mathbf{F}$.

Considering the same force $d\mathbf{f}$, the differential area dA and the unit normal \mathbf{N} in the undeformed geometry, another traction vector \mathbf{T} can be defined as:

$$\mathbf{T} = \lim_{dA \rightarrow 0} \frac{d\mathbf{f}}{dA} = \mathbf{P}^T \mathbf{N} \quad (4.16)$$

where \mathbf{P} is known as the first Piola-Kirchhoff stress tensor and the force is associated with the deformed geometry and the area with the undeformed geometry.

Moreover, it is possible to obtain a relationship between the Cauchy stress tensor and the first Piola-Kirchhoff stress tensor:

$$\mathbf{P} = J\boldsymbol{\sigma}\mathbf{F}^{-T} \quad (4.17)$$

The Cauchy stress is symmetric, but since the deformation gradient is not, the first Piola-Kirchhoff stress tensor will also not be symmetric. This particularity restricts its use and it actually led to the definition of the material or Second Piola-Kirchhoff stress tensor and it can be defined as it follows:

$$\mathbf{S} = \mathbf{P}\mathbf{F}^{-T} = J\mathbf{F}^{-1}\boldsymbol{\sigma}\mathbf{F}^{-T} \quad (4.18)$$

The second Piola-Kirchhoff stress tensor is symmetric and can be visualized as force per unit undeformed, except that forces that are regarded as acting within the undeformed solid rather than on the deformed solid.

4.3 Principle of Virtual Work

Various problems in computational mechanics want to find an approximate (finite element) solution for deformations, displacements, forces, stresses, or other variables in a solid body subjected to some series of events. The force and moment equilibrium have to be maintained at all times over an arbitrary volume of the body to find the exact solution ([Bonet et al., 2017](#)).

The principle of conservation of linear momentum states that the rate of change of the total linear momentum of a continuum medium equals the vector sum of all external forces acting on the body. Therefore, it can be written the following equation of motion:

$$\frac{\partial \boldsymbol{\sigma}}{\partial \mathbf{x}} + \mathbf{f} = \rho \frac{\partial^2 \mathbf{u}}{\partial t^2} \quad (4.19)$$

where ρ represents the mass density of the deformed solid, \mathbf{f} is the body force vector (per unit volume) and $\boldsymbol{\sigma}$ the Cauchy stress distribution. These equations must be satisfied for any continuum in motion and are also called Cauchy's Equations of Motion. If the acceleration vanishes, the following static equilibrium equation is obtained:

$$\frac{\partial \boldsymbol{\sigma}}{\partial \mathbf{x}} + \mathbf{f} = 0 \quad (4.20)$$

The principle of virtual work (Bower, 2010) is a different way of rewriting partial differential equation for linear moment balance in an equivalent integral form. Therefore, it forms the basis for the finite element method and corresponds to the equilibrium of the work done by both internal and external forces with small, arbitrary, virtual displacements that satisfy kinematic constraints.

Supposing that a deformable solid is subject to the loading that induces a displacement field $\mathbf{u}(x)$ and a velocity field $\mathbf{v}(x)$, the loading consists of a prescribed displacement on a part of the boundary (S_1), together with a traction \mathbf{t} applied to the rest of the boundary (S_2). The loading induces a Cauchy stress and its distribution within the solid is denoted by σ_{ij} .

It is necessary to define a kinematically admissible velocity field $\delta \mathbf{v}(\mathbf{x})$, satisfying $\delta \mathbf{v} = 0$ on S_1 , which corresponds to an arbitrary differentiable vector field. As a consequence, the virtual velocity gradient and virtual stretch rate are denoted, respectively, as:

$$\delta \mathbf{L} = \frac{\partial \delta \mathbf{v}}{\partial \mathbf{x}} \quad (4.21)$$

$$\delta \mathbf{D} = \frac{1}{2} \left(\frac{\partial \delta \mathbf{v}}{\partial \mathbf{x}} + \left(\frac{\partial \delta \mathbf{v}}{\partial \mathbf{x}} \right)^T \right) \quad (4.22)$$

Consequently, the principle of virtual work can be stated, noting that the stress, body force and traction are in equilibrium if, and only if, the rate of the work done by Cauchy stresses on the rate of deformation of any virtual velocity field are equal to the rate of work done by the traction and body forces acting on the body (external forces). Therefore, the principle of virtual work can be written as:

$$\int_V \boldsymbol{\sigma} : \delta \mathbf{D} dV + \int_V \rho \frac{d\mathbf{v}}{dt} \delta \mathbf{v} dV = \int_V \mathbf{f} \delta \mathbf{v} dV + \int_{S_2} \mathbf{t} \delta \mathbf{v} dA \quad (4.23)$$

The Gauss's theorem can be applied as well as some statements regarding the properties of the Cauchy Stress to prove this result. Thus, concerning the Gauss's theorem, it defines the theorem

as an equality relationship between surface integrals and volume integrals:

$$\int_S \mathbf{n} \cdot () dS = \int_V \frac{\partial}{\partial \mathbf{x}} \cdot () dV \quad (4.24)$$

where () is any continuous function-scalar, vector or tensor. Also, some statements regarding the properties of the Cauchy Stress can be used:

$$\sigma_{ij} \delta D_{ij} = \frac{1}{2} \sigma_{ij} \left(\frac{\partial \delta v_i}{\partial x_j} + \frac{\partial \delta v_j}{\partial x_i} \right) = \frac{1}{2} \left(\sigma_{ji} \frac{\partial \delta v_i}{\partial x_j} + \sigma_{ij} \frac{\partial \delta v_j}{\partial x_i} \right) = \sigma_{ji} \frac{\partial \delta v_i}{\partial x_j} = \frac{\partial}{\partial x_j} (\sigma_{ji} \delta v_i) - \frac{\partial \sigma_{ji}}{\partial x_j} \delta v_i \quad (4.25)$$

Applying these to the first term on the right-hand side of the principle of virtual work, it becomes:

$$\int_V \boldsymbol{\sigma} : \delta \mathbf{D} dV = \int_V \frac{\partial \boldsymbol{\sigma} \delta \mathbf{v}}{\partial \mathbf{x}} dV - \int_V \frac{\partial \boldsymbol{\sigma}}{\partial \mathbf{x}} \delta \mathbf{v} dV \quad (4.26)$$

Applying the Gauss theorem to same term and replacing it in equation 4.23, it becomes:

$$\int_{S_2} (\boldsymbol{\sigma} \cdot \mathbf{n}) \delta \mathbf{v} dA - \int_V \frac{\partial \boldsymbol{\sigma}}{\partial \mathbf{x}} \delta \mathbf{v} dV + \int_V \rho \frac{d\mathbf{v}}{dt} \delta \mathbf{v} dV = \int_V \mathbf{f} \delta \mathbf{v} dV + \int_{S_2} \mathbf{t} \delta \mathbf{v} dA \quad (4.27)$$

Concerning the equation 4.14, it is obtained:

$$\int_V \mathbf{f} \delta \mathbf{v} dV + \int_V \frac{\partial \boldsymbol{\sigma}}{\partial \mathbf{x}} \delta \mathbf{v} dV = \int_V \rho \frac{d\mathbf{v}}{dt} \delta \mathbf{v} dV \quad (4.28)$$

4.4 Constitutive Equations

The stresses produced in a body, which result from the deformation of the material, are related to material straining. Constitutive models aim to develop mathematical models for representing the real behavior of matter, and, consequently, they depend on the type of material under consideration and can be dependent or independent of time. They may also satisfy certain physical principles, but they are generally fit to experimental measurements since they cannot be calculated using fundamental physical laws.

4.4.1 Hyperelasticity

Materials for which the constitutive behavior is only a function of the current state of deformation are generally known as elastic. Under such conditions, any stress measure at a particle is a function of the current deformation gradient \mathbf{F} associated with that particle. In the particular case when the work done by the stresses during a deformation process is dependent only on the initial state at time t_0 and the final configuration at time t , the behavior of a material is said to be path-independent and it is called hyperelastic (Bonet and Wood, 2008).

A hyperelastic material assumes the existence of a Helmholtz free-energy function Ψ , which is defined per unit undeformed volume. In the particular case in which $\Psi = \Psi(\mathbf{F})$ is a function of \mathbf{F} or some strain tensor, the Helmholtz free-energy function is referred to as the strain-energy

function or stored-energy function and the first Piola-Kirchhoff stress tensor can be calculated as (Holzapfel, 2002):

$$\mathbf{P} = \frac{\partial \Psi(\mathbf{F})}{\partial \mathbf{F}} \quad (4.29)$$

Taking into account the symmetric Cauchy stress tensor, i.e. $\boldsymbol{\sigma} = J^{-1} \mathbf{P} \mathbf{F}^T = \boldsymbol{\sigma}^T$:

$$\boldsymbol{\sigma} = J^{-1} \mathbf{F} \left(\frac{\partial \Psi(\mathbf{F})}{\partial \mathbf{F}} \right)^T \quad (4.30)$$

It is presumed that Ψ can be obtained from physical experiments, which defines a given material.

The strain-energy function can be represented in equivalent forms. It is known that Ψ must remain invariant under rigid body rotations, which means that it is independent of the rotational part of $\mathbf{F} = \mathbf{R}\mathbf{U}$. Consequently, it can be concluded that a hyperelastic material depends on the stretching part of \mathbf{F} , i.e. the symmetric right stretch tensor \mathbf{U} .

Since the right Cauchy-Green tensor and the Green-Lagrange strain tensor are given by $\mathbf{C} = \mathbf{U}^2$ and $\mathbf{E} = (\mathbf{U}^2 - \mathbf{I})/2$, Ψ can be expressed as a function of the six components of the symmetric material tensors \mathbf{C} , \mathbf{E} , respectively:

$$\Psi(\mathbf{F}) = \Psi(\mathbf{C}) = \Psi(\mathbf{E}) \quad (4.31)$$

and it is possible to reduce the constitutive equations for hyperelastic materials at finite strains. Thus, it can be deduced that:

$$\left(\frac{\partial \Psi(\mathbf{F})}{\partial \mathbf{F}} \right)^T = 2 \frac{\partial \Psi(\mathbf{C})}{\partial \mathbf{C}} \mathbf{F}^T \quad (4.32)$$

which gives an important reduced form of the constitutive equation for hyperelastic materials, namely:

$$\boldsymbol{\sigma} = J^{-1} \mathbf{F} \left(\frac{\partial \Psi(\mathbf{F})}{\partial \mathbf{F}} \right)^T = 2J^{-1} \mathbf{F} \frac{\partial \Psi(\mathbf{C})}{\partial \mathbf{C}} \mathbf{F}^T \quad (4.33)$$

Alternative expressions may be obtained for the Piola-Kirchhoff stress tensors \mathbf{P} (which is not symmetric) and \mathbf{S} (which is symmetric):

$$\mathbf{P} = 2\mathbf{F} \frac{\partial \Psi(\mathbf{C})}{\partial \mathbf{C}} \quad (4.34)$$

$$\mathbf{S} = 2 \frac{\partial \Psi(\mathbf{C})}{\partial \mathbf{C}} = \frac{\partial \Psi(\mathbf{E})}{\partial \mathbf{E}} \quad (4.35)$$

4.4.1.1 Isotropic Hyperelastic Materials

Isotropy is a property based on the physical idea that the response of the material, when studied in a stress-strain experiment, is the same in all directions. Thus, the strain-energy function can

be restricted by a particular property that the material may possess. One example of an (approximately) isotropic material with a wide range of applications is rubber (Holzapfel, 2002).

Taking into account the Material or Lagrangian description, the constitutive relation has to be independent of the coordinate frame selected, since the material has the same property for all directions (Holzapfel, 2002; Bonet and Wood, 2008). Therefore, Ψ must be only a function of the invariants of \mathbf{C} :

$$\Psi(\mathbf{C}, \mathbf{X}) = \Psi(I_1, I_2, I_3, \mathbf{X}) \quad (4.36)$$

The invariants of \mathbf{C} can be defined as:

$$I_1(\mathbf{C}) = \text{tr}(\mathbf{C}) \quad (4.37)$$

$$I_2(\mathbf{C}) = \frac{1}{2}(I_1^2 - \mathbf{C} : \mathbf{C}) \quad (4.38)$$

$$I_3(\mathbf{C}) = \det(\mathbf{C}) = J^2 \quad (4.39)$$

By means of the chain rule of differentiation, it is found:

$$\frac{\partial \Psi(\mathbf{C})}{\partial \mathbf{C}} = \frac{\partial \Psi}{\partial I_1} \frac{\partial I_1}{\partial \mathbf{C}} + \frac{\partial \Psi}{\partial I_2} \frac{\partial I_2}{\partial \mathbf{C}} + \frac{\partial \Psi}{\partial I_3} \frac{\partial I_3}{\partial \mathbf{C}} \quad (4.40)$$

The derivatives of the invariants with respect to \mathbf{C} can be obtained after some algebra. Recalling the constitutive equation 4.35 and substituting these derivatives into equation 4.40, the second Piola-Kirchhoff stress can be obtained:

$$\mathbf{S} = 2 \left[\left(\frac{\partial \Psi}{\partial I_1} + I_1 \frac{\partial \Psi}{\partial I_2} \right) \mathbf{I} - \frac{\partial \Psi}{\partial I_2} \mathbf{C} + I_3 \frac{\partial \Psi}{\partial I_3} \mathbf{C}^{-1} \right] \quad (4.41)$$

For isotropic hyperelastic materials, the spatial counterpart of the constitutive equation can be obtained from the previous equation. The relationship between the Cauchy stress and the second Piola-Kirchhoff stress is given by equation 4.18. Thus, replacing \mathbf{S} in this relation by equation 4.41 and multiplying the tensor variables \mathbf{I} , \mathbf{C} , \mathbf{C}^{-1} and \mathbf{F}^T from the right hand side and \mathbf{F} from the left hand side, it is possible to obtain the following equation in terms of the left cauchy-green tensor \mathbf{B} :

$$\boldsymbol{\sigma} = 2J^{-1} \left[\left(\frac{\partial \Psi}{\partial I_1} + I_1 \frac{\partial \Psi}{\partial I_2} \right) \mathbf{b} - \frac{\partial \Psi}{\partial I_2} \mathbf{b}^2 + I_3 \frac{\partial \Psi}{\partial I_3} \mathbf{I} \right] \quad (4.42)$$

However, this expression still involves derivatives with respect to the invariants of the material tensor \mathbf{C} . Since \mathbf{b} and \mathbf{C} have the same eigenvalues, their invariants are identical, so:

$$I_1(\mathbf{b}) = \text{tr}(\mathbf{b}) = \text{tr}(\mathbf{C}) = I_1(\mathbf{C}) \quad (4.43)$$

$$I_2(\mathbf{b}) = \frac{1}{2}(I_1^2 - \mathbf{b} : \mathbf{b}) = \frac{1}{2}(I_1^2 - \mathbf{C} : \mathbf{C}) = I_2(\mathbf{C}) \quad (4.44)$$

$$I_3(\mathbf{b}) = \det(\mathbf{b}) = J^2 = \det(\mathbf{C}) = I_3(\mathbf{C}) \quad (4.45)$$

Consequently, the derivatives that appear on equation 4.42 are also with respect to the invariants of \mathbf{b} .

If the strain-energy function Ψ is an invariant, Ψ is also a function of the principal stretches $\{\lambda_a\}_{a=1,2,3}$. Therefore, Ψ can be represented in the form:

$$\Psi = \Psi(\mathbf{C}) = \Psi(\lambda_1, \lambda_2, \lambda_3) \quad (4.46)$$

It is necessary to note that:

$$\mathbf{I} = \sum_{a=1}^3 \hat{\mathbf{N}}_a \otimes \hat{\mathbf{N}}_a \quad (4.47)$$

$$\mathbf{C}^{-1} = \sum_{a=1}^3 \lambda_a^{-2} \hat{\mathbf{N}}_a \otimes \hat{\mathbf{N}}_a \quad (4.48)$$

Substituting these equations into equation 4.41, the second Piola-Kirchhoff stress tensor can be obtained:

$$\mathbf{S} = \sum_{a=1}^3 \left(2 \frac{\partial \Psi}{\partial I_1} + 4 \frac{\partial \Psi}{\partial I_2} \lambda_a^2 + 2 I_3 \frac{\partial \Psi}{\partial I_3} \lambda_a^{-2} \right) \hat{\mathbf{N}}_a \otimes \hat{\mathbf{N}}_a \quad (4.49)$$

Since λ_a^2 are the eigenvalues of \mathbf{C} , the invariants can also be obtained by:

$$I_1 = \lambda_1^2 + \lambda_2^2 + \lambda_3^2 \quad (4.50)$$

$$I_2 = \lambda_1^2 \lambda_2^2 + \lambda_1^2 \lambda_3^2 + \lambda_2^2 \lambda_3^2 \quad (4.51)$$

$$I_3 = \lambda_1^2 \lambda_2^2 \lambda_3^2 \quad (4.52)$$

Differentiating these equations and substituting them into equation 4.49, the following expression can be reached using the chain rule:

$$\mathbf{S} = \sum_{a=1}^3 S_{aa} \hat{\mathbf{N}}_a \otimes \hat{\mathbf{N}}_a; \quad S_{aa} = 2 \frac{\partial \Psi}{\partial \lambda_a^2} \quad (4.53)$$

Considering the relationship with the second Piola-Kirchhoff stress tensor, the Cauchy stress can be obtained once again:

$$\boldsymbol{\sigma} = J^{-1} \mathbf{F} \mathbf{S} \mathbf{F}^T = \sum_{a=1}^3 \frac{2}{J} \frac{\partial \Psi}{\partial \lambda_a^2} (\mathbf{F} \hat{\mathbf{N}}_a) \otimes (\mathbf{F} \hat{\mathbf{N}}_a) \quad (4.54)$$

4.4.1.2 Incompressible Hyperelastic Materials

Incompressible materials (Holzapfel, 2002; Bonet and Wood, 2008) can sustain finite strains without noticeable volume changes. They keep the volume constant throughout a motion and are characterized by the incompressibility constraint:

$$J = 1 \quad (4.55)$$

To obtain general constitutive equations for incompressible hyperelastic materials, the strain-energy function is given by:

$$\Psi = \Psi(\mathbf{F}) - p(J - 1) \quad (4.56)$$

where the strain-energy Ψ is defined for $J = \det \mathbf{F} = 1$ and the scalar p serves as an indeterminate Lagrange multiplier which can be identified as a hydrostatic pressure and it may only be determined from the equilibrium equations and the boundary conditions.

Differentiating equation 4.56 with respect to \mathbf{F} and taking into account that:

$$\frac{\partial J}{\partial \mathbf{F}} = J \mathbf{F}^T \quad (4.57)$$

a constitutive equation for the first Piola-Kirchhoff stress tensor \mathbf{P} can be obtained:

$$\mathbf{P} = -p \mathbf{F}^T + \frac{\partial \Psi(\mathbf{F})}{\partial \mathbf{F}} \quad (4.58)$$

Multiplying the previous equation by \mathbf{F}^{-1} on the left hand side, it is possible to obtain the second Piola-Kirchhoff stress \mathbf{S} :

$$\mathbf{S} = -p \mathbf{F}^{-1} \mathbf{F}^T + \mathbf{F}^{-1} \frac{\partial \Psi(\mathbf{F})}{\partial \mathbf{F}} = -p \mathbf{C}^{-1} \frac{\partial \Psi(\mathbf{C})}{\partial \mathbf{C}} \quad (4.59)$$

Nevertheless, if we multiply instead equation 4.58 by \mathbf{F}^{-T} from the right hand side, the Cauchy stress is obtained:

$$\boldsymbol{\sigma} = -p \mathbf{I} + \frac{\partial \Psi(\mathbf{F})}{\partial \mathbf{F}} \mathbf{F}^T = -p \mathbf{I} + \mathbf{F} e \frac{\partial(\mathbf{F})^T}{\partial \mathbf{F}} \quad (4.60)$$

4.4.1.3 Transversely Isotropic Hyperelastic Materials

Materials composed of a matrix material and one or more families of fibers and are known as composite materials or fiber-reinforced composite (Holzapfel, 2002). This type of material is heterogenous since it has different compositions throughout the body. In the bioengineering field, biological tissues are heterogenous composite materials made of cells and molecules of the extracellular matrix. In the case of muscle tissue, it is composed by collagen fibers that are coated by an extracellular matrix, which is composed of collagens, laminins, fibronectin and proteoglycans (Grzelkowska-Kowalczyk, 2016).

A material reinforced with one family of fibers has a single preferred direction and the stiffness of the material in that direction is much higher than in the direction orthogonal to the fibers. It is possible to consider that the material response along direction orthogonal to this preferred direction is isotropic. This corresponds to the simplest representation of material anisotropy, which is called transversely isotropic with respect to this preferred direction.

Considering transversely isotropic materials with an incompressible isotropic matrix material, the embedded fibers can be extensible or inextensible. In order to describe the properties of the fiber family and its interaction with the other material constituents, two pseudo-invariants I_4 and I_5 arises directly from the anisotropy and are defined by:

$$I_4 = \lambda^2 = \mathbf{a}_0 \cdot \mathbf{C} \mathbf{a}_0, \quad I_5 = \mathbf{a}_0 \cdot \mathbf{C}^2 \mathbf{a}_0 \quad (4.61)$$

where λ is the stretch in the fiber in the direction defined in the reference configuration by a unit vector field \mathbf{a}_0 .

When the embedded fibers are extensible, and assuming incompressibility of the isotropic matrix material ($I_3 = 1$), the strain-energy function Ψ can be represented in terms of the remaining four independent invariants:

$$\Psi = \Psi[I_1(\mathbf{C}), I_2(\mathbf{C}), I_4(\mathbf{C}, \mathbf{a}_0), I_5(\mathbf{C}, \mathbf{a}_0)] - \frac{1}{2} p(I_3 - 1) \quad (4.62)$$

When the embedded fibers are inextensible, which means that $\lambda = 1$ and $I_4 = 1$. Assuming incompressibility of the isotropic matrix material ($I_3 = 1$), the strain-energy function Ψ can be written as:

$$\Psi = \Psi[I_1(\mathbf{C}), I_2(\mathbf{C}), I_5(\mathbf{C}, \mathbf{a}_0)] - \frac{1}{2} p(I_3 - 1) - \frac{1}{2} p(I_4 - 1) \quad (4.63)$$

where I_1 and I_2 are responsible for the hyperelastic isotropic matrix material and I_5 is responsible for the fibers.

Applying the chain rule, the second Piola-Kirchhoff stress tensor \mathbf{S} can be obtained from equation 4.35:

$$\mathbf{S} = 2 \frac{\partial \Psi(\mathbf{C}, \mathbf{a}_0 \otimes \mathbf{a}_0)}{\partial \mathbf{C}} = 2 \sum_{a=1}^5 \frac{\partial \Psi(\mathbf{C}, \mathbf{a}_0 \otimes \mathbf{a}_0)}{\partial I_a} \frac{\partial I_a}{\partial \mathbf{C}} \quad (4.64)$$

Obtaining the derivates $\partial I_a / \partial \mathbf{C}$ from 4.61, it is possible to reach the following expression:

$$\mathbf{S} = 2 \left[\left(\frac{\partial \Psi}{\partial I_1} + I_1 \frac{\partial \Psi}{\partial I_2} \right) \mathbf{I} - \frac{\partial \Psi}{\partial I_2} \mathbf{C} + I_3 \frac{\partial \Psi}{\partial I_3} \mathbf{C}^{-1} + \frac{\partial \Psi}{\partial I_4} \mathbf{a}_0 \otimes \mathbf{a}_0 + \frac{\partial \Psi}{\partial I_5} (\mathbf{a}_0 \otimes \mathbf{C} \mathbf{a}_0 + \mathbf{a}_0 \mathbf{C} \otimes \mathbf{a}_0) \right] \quad (4.65)$$

which extends the constitutive equation 4.41. Due to the relation between the stress tensors, the expression for the Cauchy stress is obtained:

$$\boldsymbol{\sigma} = 2J^{-1} \left[\left(\frac{\partial \Psi}{\partial I_1} + I_1 \frac{\partial \Psi}{\partial I_2} \right) \mathbf{B} - \frac{\partial \Psi}{\partial I_2} \mathbf{B}^2 + I_3 \frac{\partial \Psi}{\partial I_3} \mathbf{I} + I_4 \frac{\partial \Psi}{\partial I_4} \mathbf{a}_0 \otimes \mathbf{a}_0 + I_4 \frac{\partial \Psi}{\partial I_5} (\mathbf{a}_0 \otimes \mathbf{B} \mathbf{a}_0 + \mathbf{a}_0 \mathbf{B} \otimes \mathbf{a}_0) \right] \quad (4.66)$$

4.5 Finite Element Method

One of the numerical methods used for solving differential equations that describe many engineering problems is the finite element method. Therefore, to solve these problems, in finite element method the domain of the body is divided into small regions known as elements. Each element has a set of nodes that are used to connect this element with other elements used in the discretization of the body. The displacement of the material points of an element is approximated using a set of shape functions and the displacements of the nodes and possibly their derivatives with respect to the spatial coordinates. Taking into account the principle of virtual work, the finite element formulation establishes the equilibrium equations. For a given material and loading conditions, its solution is given by a deformed configuration in a state of equilibrium. To obtain this new equilibrium position, the Newton-Raphson iterative solution is applied, which requires the linearization of the virtual work (Kim, 2015; Bonet et al., 2017).

4.5.1 Discretized Equilibrium Equations

The displacement field can be approximated by interpolation functions (shape functions), where n denotes the number of nodes per element, (Bonet et al., 2017) and it is given as:

$$\mathbf{u}(\mathbf{x}) \approx \sum_{i=1}^n N_i(\mathbf{X}) \mathbf{u}_i \quad (4.67)$$

where the position vector at the beginning of each iteration is represented by \mathbf{X} , the shape functions defined within the finite element correspond to $N_i(\mathbf{X})$ and \mathbf{u}_i represents the unknown nodal displacement. Considering the interpolation of equation 4.67 and that the virtual field $\delta \mathbf{u}$ must be compatible with all kinematics constraints, it can be written as:

$$\delta \mathbf{u} \approx \sum_{i=1}^n N_i(\mathbf{X}) \delta \mathbf{u}_i \quad (4.68)$$

Moreover, the virtual work equation 4.23 can be rewritten in terms of the virtual displacement:

$$\delta W = \int_V \boldsymbol{\sigma} : \delta \mathbf{e} dV - \int_V \mathbf{f} \cdot \delta \mathbf{u} dV - \int_{S_2} \mathbf{t} \cdot \delta \mathbf{u} dA \quad (4.69)$$

Equation 4.69 can be approximated by a variation over the finite set of $\delta \mathbf{u}_i$, from the discretization process. Thus, for an arbitrary node (a) of the element (e), it may be written by:

$$\delta W^{(e)} = \int_{V^{(e)}} \boldsymbol{\sigma} : (\delta \mathbf{u}_a \otimes N_a) dV - \int_{V^{(e)}} \mathbf{f} \cdot (N_a \delta \mathbf{u}_a) dV - \int_{S_2^{(e)}} \mathbf{t} \cdot (N_a \delta \mathbf{u}_a) dA \quad (4.70)$$

Consequently, equation 4.70 can be rearranged, since the virtual nodal displacement are independent of the integration. Also, the virtual work per element (e) per node (a) can be expressed in

terms of internal and external equivalent nodal forces, $\mathbf{F}_{int a}^{(e)}$ and $\mathbf{F}_{ext a}^{(e)}$, respectively:

$$\delta W^{(e)} = \delta \mathbf{u}_a \cdot \left(\int_{V^{(e)}} \boldsymbol{\sigma} N_a dV - \int_{V^{(e)}} N_a \mathbf{f} dV - \int_{S_2^{(e)}} N_a \mathbf{t} dA \right) = \delta \mathbf{u}_a \cdot (\mathbf{F}_{int a}^{(e)} - \mathbf{F}_{ext a}^{(e)}) \quad (4.71)$$

where $\mathbf{F}_{int a}^{(e)} = \int_{V^{(e)}} \boldsymbol{\sigma} N_a dV$ and $\mathbf{F}_{ext a}^{(e)} = \int_{V^{(e)}} N_a \mathbf{f} dV - \int_{S_2^{(e)}} N_a \mathbf{t} dA$.

Since the virtual work equation must be satisfied for any arbitrary virtual displacement and the equilibrium conditions require that $\delta W^e = 0$, the discretized equilibrium equations, in terms of nodal residual force $\mathbf{R}_{fa}^{(e)}$, emerge as:

$$\mathbf{R}_{fa}^{(e)} = (\mathbf{F}_{int a}^{(e)} - \mathbf{F}_{ext a}^{(e)}) = 0 \quad (4.72)$$

After summing the contribution of every nodes and elements, which corresponds to the assembling process, the global equilibrium equation in the discretized form can be written as:

$$\mathbf{R}_f = (\mathbf{F}_{int} - \mathbf{F}_{ext}) = 0 \quad (4.73)$$

4.5.2 Linearization of the Virtual Work Principle

The principle of virtual work has been presented in section 4.3 and, considering a trial solution $\boldsymbol{\varphi}_k$, it can be linearized in the direction of an increment $\Delta \mathbf{u}$ in Φ_k as (Bonet et al., 2017):

$$\delta W(\boldsymbol{\varphi}_k, \delta \mathbf{u}) + D_{\Delta \mathbf{u}} \delta W(\boldsymbol{\varphi}_k, \delta \mathbf{u}) = 0 \quad (4.74)$$

where the operator D denotes directional derivative of the virtual work equation at $\boldsymbol{\varphi}_k$ in the direction of $\Delta \mathbf{u}$ and finding it is fundamental, noting that it corresponds to the change in δW due to $\boldsymbol{\varphi}_k$ changing to $\boldsymbol{\varphi}_k + \Delta \mathbf{u}$. Thus, to bring the internal forces into equilibrium with the external forces, this is necessary in the Newton-Raphson procedure to adjust the configuration $\boldsymbol{\varphi}_k$. The linearization of the equilibrium equation (Bonet et al., 2017) will be considered in terms of internal and external work components as:

$$D_{\Delta \mathbf{u}} \delta W(\boldsymbol{\varphi}_k, \delta \mathbf{u}) = D_{\Delta \mathbf{u}} \delta W_{int}(\boldsymbol{\varphi}_k, \delta \mathbf{u}) - D_{\Delta \mathbf{u}} \delta W_{ext}(\boldsymbol{\varphi}_k, \delta \mathbf{u}) = 0 \quad (4.75)$$

Although the definition of the directional derivative is complex, the final expression can be state in the discretized form as:

$$D_{\Delta \mathbf{u}} \delta W(\boldsymbol{\varphi}_k, \delta \mathbf{u}) = \delta \mathbf{u}^T \mathbf{K} \mathbf{u} \quad (4.76)$$

where $\mathbf{K} = \frac{\partial \Delta \boldsymbol{\sigma}}{\partial \Delta \boldsymbol{\varepsilon}}$ corresponds to the stiffness matrix.

Taking into account equation 4.73, and substituting equation 4.76 into equation 4.74, it can be obtained:

$$\mathbf{R}_f + \mathbf{K} \mathbf{u} = 0 \quad (4.77)$$

which provides the basis of the iterative Newton-Raphson scheme, that can be formulated as:

$$\mathbf{K}\mathbf{u} = -\mathbf{R}_f(x_k); \quad x_{k+1} = x_k + \mathbf{u} \quad (4.78)$$

4.5.3 ABAQUS[®] Finite Element Software

ABAQUS[®] is a software for finite element analysis and computer-aided engineering. It is based on the finite element method and can solve problems ranging from simple linear analysis to the most challenging nonlinear simulations. It consists in a vast product set, which includes, for example: ABAQUS/CAE[®] (Complete ABAQUS[®] Environment) that is used for the modeling and analysis of mechanical components and assemblies, as well as to visualize the finite element analysis result; and ABAQUS/Standard[®] that is a general-purpose analysis product that can solve a wide range of linear and nonlinear problems.

The software contains an extensive library of elements and the most common materials already defined, but, for complex problems, it enables the development of an user subroutine, known as UMAT, to consider specific constitutive equations to calculate the stiffness matrix and the stresses.

To better understand the overall structure and functioning of the software, figure 4.3 shows a basic flow chart of data and actions from the start of an ABAQUS[®]/Standard analysis to the end of a step.

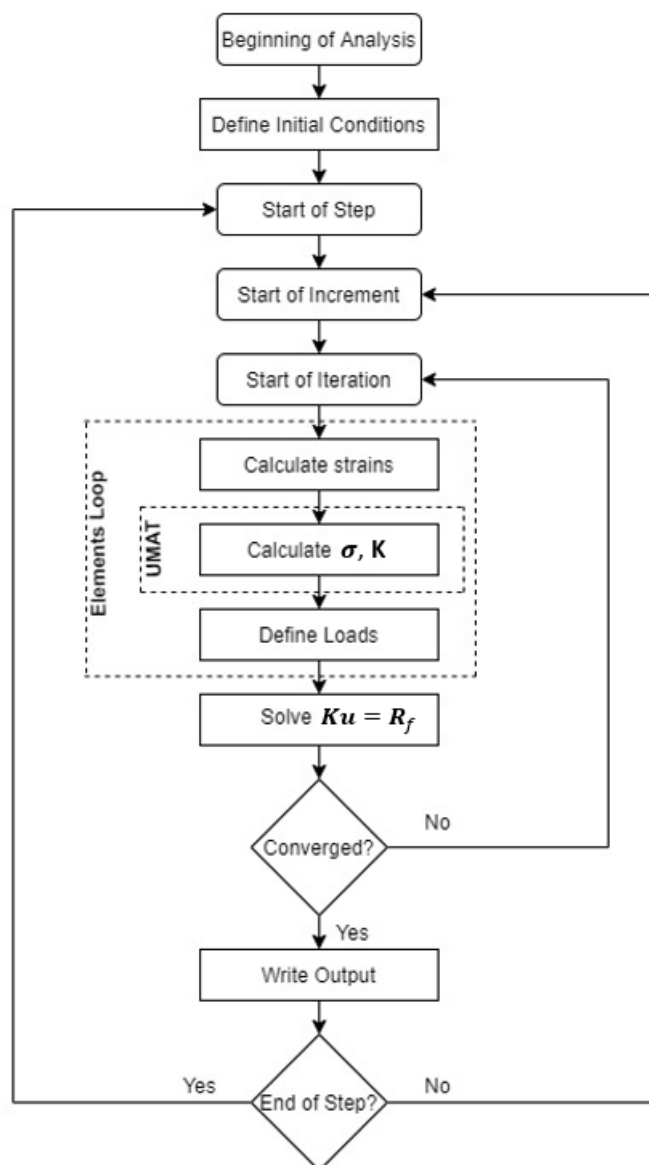


Figure 4.3: ABAQUS®/Standard flowchart

Chapter 5

Finite Element Simulations

5.1 Introduction

Childbirth can be both psychologically and mechanically traumatic for the mother. Despite being a natural process, it involves extensive physiologic changes in the mother to allow the passage of the fetus through the birth canal. Vaginal birth is not a passive process implying uterine contractions to push a rigid body through a fixed aperture. This leads to a significant stretching of the levator musculatures and of the pudendal nerves, being responsible for several dysfunctions (Donelson and Minocha, 2002) and requiring a successful negotiation of the pelvis. Therefore, it is important to take into account the position that the mother assume during the second stage of labor and the associated maternal outcomes.

In this work, a validated finite element model of the pelvic bones, pelvic floor muscles, and the fetus was modified in order to mimic two birthing positions: one that allows free movement of the coccyx and the other in which it is more restricted. It is important to note that, taking into account section 3.4, in the majority of horizontal birthing positions sacrum and coccyx movement is restricted due to the presence of the bed under them, unlike to what happens in most of vertical birthing positions. This is the main difference that distinguish the two positions considered.

Ligament laxity is a physiological change that occurs during pregnancy, therefore some musculoskeletal changes that are observed during labor were also considered in the biomechanical model, such as the widening of the pubic symphysis that may occur to facilitate the passage of the fetus. In this way, the movements of the fetal head during the second stage of labor in the vertex presentation and an occipitanterior position were simulated. Hence, it is intended to be study the biomechanical changes caused by different childbirth positions. Knowing the risk and benefits of each position, pregnant women may decide on the birthing position adopted during the second stage of labor. The prediction of the childbirth outcomes may help to prevent mother and/or fetus complications.

5.2 Materials and Methods

5.2.1 Finite Element Model

The three-dimensional (3D) finite element model presented in figure 5.1 was constructed using a geometrical data point-set obtained from an embalmed 72 years old female cadaver [Janda et al. \(2003\)](#) as it is fully explained in [Parente et al. \(2008\)](#).

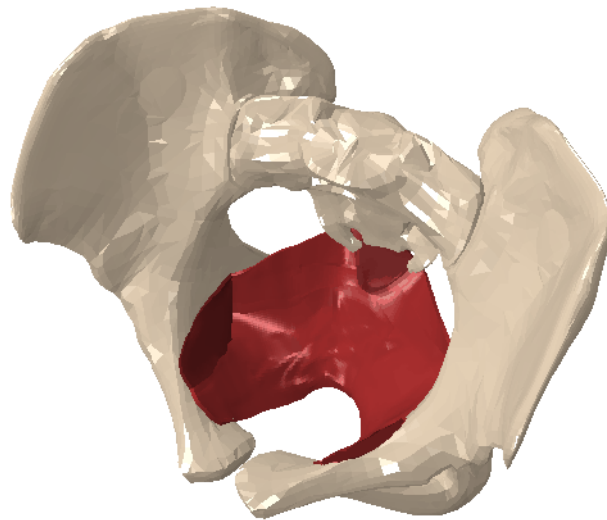


Figure 5.1: Finite element model of the mother showing the pelvic girdle bones in brown, the pelvic floor muscles in light red and the supporting structures in dark red

Regarding the mother, the biomechanical model includes the pelvic floor muscles and the supporting structures. Figure 5.1 illustrates the pelvic floor muscles in light red and the supporting structures in dark red. The latter is divided into three structures, as it can be seen in figure 5.2: the two lateral meshes represent the arcus tendineus, obturator fascia and the obturator internus, and the posterior mesh represents the different connections between muscles of the pelvic floor and the sacrum. All these structures were modeled using hexahedral elements with hybrid formulation (C3D8H).

The finite element model of the mother also includes the pelvic girdle, which consists of paired hip bones, each composed of the ilium, ischium and pubis, sacrum and coccyx. These bones were modeled using triangular shell elements with reduced integration (S3R). Taking into account the birthing positions that were simulated, the sacrum and coccyx are important bones in terms of the space available for the passage of the fetus. These bones were modeled considering the existing two types of bone tissue and using FEMAP[®] 2020.1 software. Thus, the bone tissue that forms the hard exterior (cortex) of bones, known as cortical bone, was modeled using triangular shell elements with reduced integration (S3R) and with a thickness of 2 mm ([Zhao et al., 2012](#)). The internal tissue of the skeletal bone, known as trabecular bone, was modeled using tetrahedral elements with hybrid formulation (C3D4H). Figure 5.3 illustrates the finite element model of the

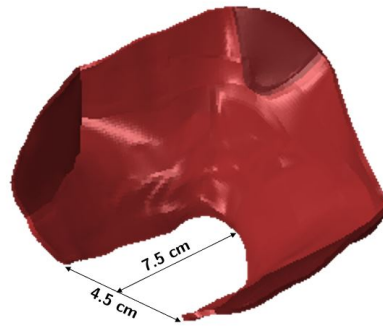


Figure 5.2: Dimensions of the levator hiatus

sacrum and coccyx, considering its cortical bone tissue in black and its trabecular bone tissue in brown.

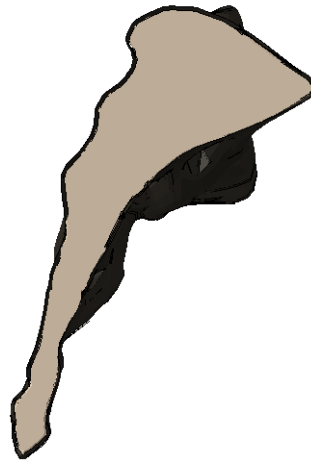


Figure 5.3: Finite element model of the sacrum and coccyx with cortical bone in black and trabecular bone in brown (lateral view)

The maternal pelvic diameters presented in figure 5.4 were modified according to the measures on pelvimetry obtained by Michel et al. (2002), which are listed in table 5.1. The initial pubic symphysis gap is 4.05 mm, which is in accordance with Jain et al. (2006).

Table 5.1: Maternal pelvic diameters considered

Diameters [mm]	
Transverse	129
Interspinous	110
Obstetric conjugate	124
Sagittal outlet	115
Intertuberous	124

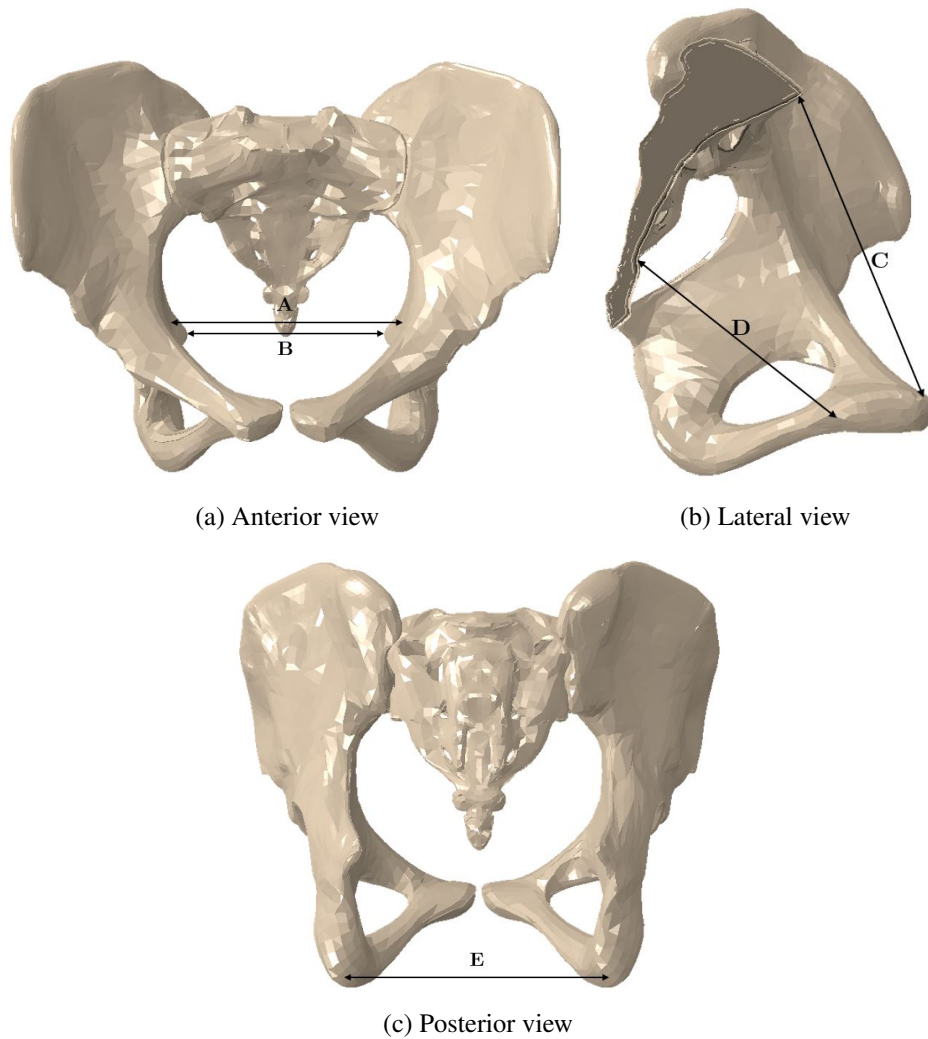
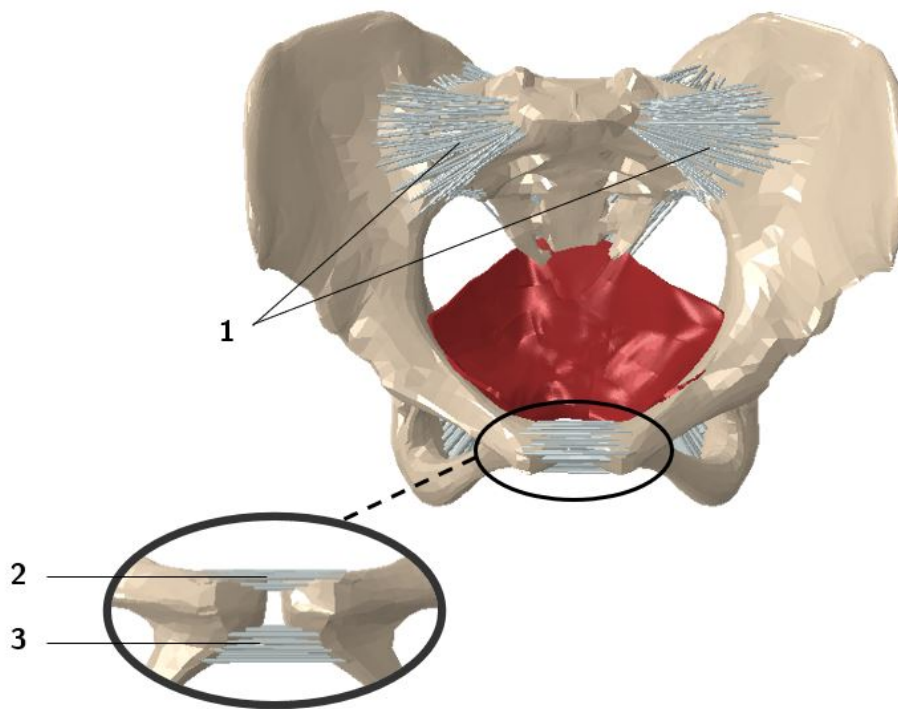


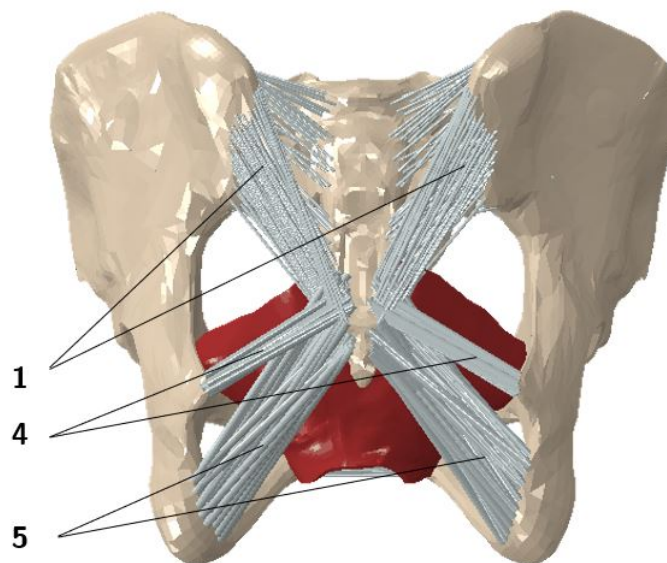
Figure 5.4: Pelvic diameters of the model: A, transverse diameter; B, interspinous diameter; C, obstetric conjugate diameter; D, sagittal outlet diameter; E, intertuberous diameter

In the pubic symphysis and sacroiliac joints, the main ligaments were modeled, based on anatomic data available in the literature ([Strandring, 2016](#)). The anterior, interosseous and posterior sacroiliac ligaments were simulated using several linear truss elements (T3D2), as well as the sacrospinous and sacrotuberous ligaments. In order to give numerical stability to the simulation, linear beam elements (B31), using a low Young modulus, were superimposed to the truss elements mesh of the sacrospinous and sacrotuberous ligaments, providing a residual bending stiffness. In the pubic symphysis, the superior and inferior pubic ligaments were also modeled using linear truss elements (T3D2). Figure 5.5 illustrates the biomechanical model of the mother with the mentioned ligaments modeled.

To ensure a correct simulation of the motion of the pelvis joints and to provide some stability to the simulation, 3D solid elements were added in the joints area. In the sacroiliac joint, a group of wedge elements with hybrid formulation (C3D6H) were added in the auricular surfaces of the



(a) Anterior view



(b) Posterior view

Figure 5.5: Finite element model with the modeled ligaments: 1, sacroiliac ligaments; 2, superior pubic ligament; 3, inferior pubic ligament; 4, sacrospinous ligament; 5, sacrotuberous ligament

ilium and sacrum in each sacroiliac joint to mimic the synovial part of this joint. In the pubic symphysis, another group of 3D solid elements was added to mimic the interpubic disc.

In this study, two different birthing positions were mimicked: one in which the coccyx is mobile and another in which its movement is restricted. The sacrococcygeal joint corresponds to a symphysis between the sacrum and coccyx and its mobility aims to increase the anteroposterior diameter of the pelvis during labor. The movement of the coccyx is only possible when there is no surface (for example, a bed) under the woman. In the majority of vertical birthing positions, the sacrum and coccyx are free to move and, in the majority of horizontal birthing positions, the movement of these bones is more restricted due to the presence of the bed under them. Thus, in the mob. coccyx model, the sacrococcygeal joint was considered. The biomechanical model of the sacrum, coccyx and sacrococcygeal joint is shown in figure 5.6.



Figure 5.6: Finite element model of the sacrum and coccyx in brown and the sacrococcygeal joint in grey (posterior view)

Regarding the fetus, the head was modeled using tetrahedral elements (C3D4) and the principal diameters presented in figure 5.7 are the following, according to [Parente et al. \(2010\)](#): biparietal diameter 9.0 cm; bitemporal diameter, 7.5 cm; suboccipitobregmatic diameter, 9.5 cm; suboccipitofrontal diameter, 10.5 cm; occipitofrontal diameter, 11.5 cm; mentovertical diameter, 13.0 cm; submentobregmatic diameter, 9.5 cm.

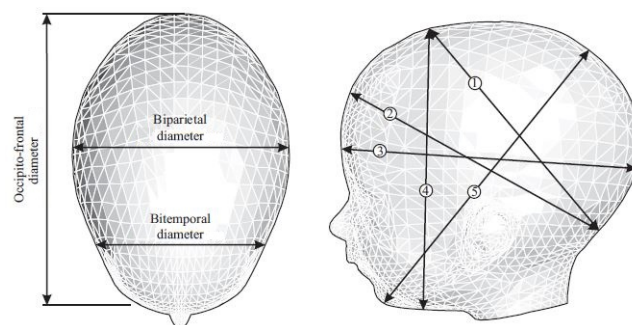


Figure 5.7: Diameters of the fetal skull: 1, suboccipitobregmatic diameter; 2, suboccipitofrontal diameter; 3, occipitofrontal diameter; 4, mentovertical diameter; 5, submentobregmatic diameter (adapted from [Parente et al. \(2010\)](#))

To verify the influence of the birthing position on the pubic symphysis gap, sacrum, coccyx and pelvic floor muscles, the second stage of a birth in vertex presentation and occipit anterior position was simulated assuming the two mentioned maternal positions. The model in which the coccyx has a restricted movement will be designated as non-mobile coccyx model (non-mob. coccyx model) and the other model in which the coccyx is free to move will be designated as mobile coccyx model (mob. coccyx model). Abaqus[®] software 2018 (Dassault Systèmes Simulia Corp., Providence, RI, USA) was used to perform the numerical simulations. For this purpose, the widening of the pubic symphysis gap, the stress related to the pubic ligaments, the movement and rotation of coccyx, the stress related to the cortical bone of sacrum and coccyx, the stretch and stress related to the pelvic floor muscles and the reaction forces on the fetus head were evaluated.

Concerning to the pubic symphysis, the distance between the narrowest points of the symphyseal gap was measured and, knowing that the initial gap is 4.05 mm, the widening of this joint was calculated. The movement of coccyx was measured using a reference line that was drawn from the inferior border of the symphysis to the inferior border of the sacrum, as shown in figure 5.8. The

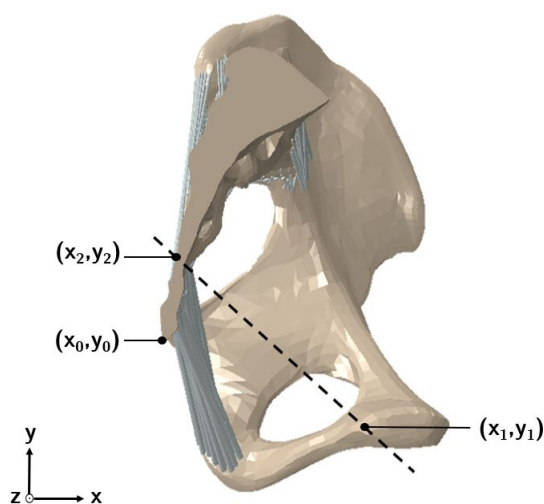


Figure 5.8: Reference line from the inferior border of the pubic symphysis to the inferior border of the sacrum

distance from the tip of the coccyx to this reference line was calculated based on equation 5.1 and the difference in movement was obtained. The rotation of the tip of the coccyx around the z-axis was also obtained.

$$dist((x_1, y_1), (x_2, y_2), (x_0, y_0)) = \frac{|(y_2 - y_1)x_0 - (x_2 - x_1)y_0 + x_2y_1 - y_2x_1|}{\sqrt{(y_2 - y_1)^2 + (x_2 - x_1)^2}} \quad (5.1)$$

To evaluate the displacement along the x-axis of both sacrum and coccyx, a curve was defined along the sagittal plane of these bones, as it is shown in figure 5.9.

Concerning the pelvic floor muscles, a curve was defined on the most inferior part of the pelvic floor mesh, as shown in figure 5.10. The length of this curve during the simulation was measured and, knowing its initial value, the evolution of the stretch values for the curve was obtained. Note

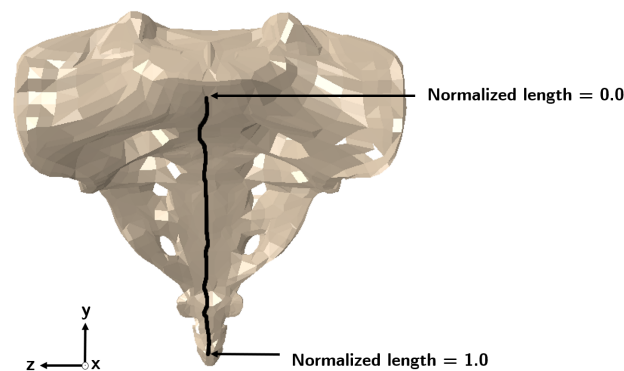


Figure 5.9: Curve in black used to evaluate the displacement of the sacrum and coccyx

that the stretch ratio is defined as the ratio between the current tissue length to the original tissue length. The stress of the pelvic floor muscles were also measured along this curve, considering the position of the fetus head causing the maximum stress value. At this moment, the stress distribution throughout all the pelvic floor muscles were analyzed. Lastly, the reaction forces on the fetus head, in the medial-lateral direction, were obtained.

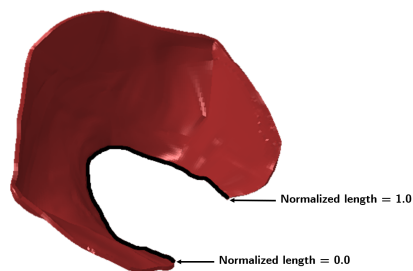


Figure 5.10: Model of pelvic floor muscles in red and curve, in black, used to evaluate stress and stretch

5.2.2 Materials

To govern the deformation of the pelvic floor muscles, the theory of continuum mechanics was considered, allowing to analyze several mechanical properties. As mentioned before, soft tissues have material and geometric nonlinear characteristics. In the case of muscle tissues, they are heterogenous composite materials composed by collagen fibers that are coated by an extracellular matrix. To account for the muscle behavior, it was necessary to simulate both passive and active finite strain responses of the muscle, where contributions of different parts of the tissue microstructure were taken into account, such as the contribution of: the extracellular matrix that endows the tissue strength and resilience (Ψ_m); the fibers (Ψ_f), both passive elastic part (Ψ_{PE}) and active part (Ψ_{SE}), responsible for muscle contraction and with an initial direction that corresponds to the direction of the maximum principal stress in the element when applying pressure to the muscle; and the volumetric contribution to enforce the incompressibility condition (Ψ_{vol}). For this purpose, the

constitutive model used to represent these physical properties was the quasi-incompressible transversely isotropic hyperelastic model proposed by [Martins et al. \(1998\)](#) and already successfully used by [Parente et al. \(2008\)](#), as follows:

$$\Psi = \Psi_m(\bar{I}_1^C) + \Psi_f(\bar{\lambda}_f, \alpha) + \Psi_{vol}(J) \quad (5.2)$$

where

$$\Psi_m = c \left[e^{b(\bar{I}_1^C - 3)} - 1 \right] \quad (5.3)$$

$$\Psi_f = A \left[\overbrace{e^{a(\bar{\lambda}_f - 1)^2} - 1}^{\Psi_{PE}} \right] + T_0^M \int_1^{\bar{\lambda}_f} \overbrace{f_{SE}(\lambda^M, \alpha) d\lambda^M}^{\Psi_{SE}} \quad (5.4)$$

$$\Psi_{vol} = \frac{1}{D_1} (J - 1)^2 \quad (5.5)$$

In these definitions, c , b , A , a , D_1 and T_0^M are constants, \bar{I}_1^C is the first invariant of the right Cauchy-Green strain tensor, \mathbf{C} , with the volume change eliminated, i.e:

$$\bar{I}_1^C = tr(\bar{\mathbf{C}}) = tr(\bar{\mathbf{F}}^T \bar{\mathbf{F}}) = J^{-2/3} tr(\mathbf{C}) \quad (5.6)$$

$\bar{\lambda}_f$ represents the fiber stretch ratio in the direction \mathbf{N} of the undeformed fiber:

$$\bar{\lambda}_f = \sqrt{\mathbf{N}^T \bar{\mathbf{C}} \mathbf{N}} = \sqrt{\bar{\mathbf{C}} : (\mathbf{N} \otimes \mathbf{N})} \quad (5.7)$$

In equation 5.6, $\bar{\mathbf{F}}$ is the deformation gradient with the volume change eliminated and J the volume change. Regarding equation 5.4, for the function $f_{SE}(\lambda^M, \alpha)$, the following expression was used:

$$f_{SE} = \alpha \begin{cases} 1 - 4(\lambda^M - 1)^2 & \text{for } 0.5 < \lambda^M < 1.5 \\ 0 & \text{otherwise} \end{cases} \quad (5.8)$$

which means that for $0.5 \geq \lambda^M \geq 1.5$ the muscle produces no energy. The level of activation is controlled by the internal variable $\alpha \in [0, 1]$.

The constitutive parameters considered in [Parente et al. \(2009\)](#) were applied and they are listed in table 5.2.

Table 5.2: Constitutive material parameters for the pelvic floor muscle

Material Parameters
$c = 0.00185$ MPa
$b = 1.173$
$A = 0.0280$ MPa
$a = 0.6215$
$D_1 = 1.0 \times 10^{-4}$ MPa ⁻¹
$T_0^M = 0.682$ MPa

For the supporting structures, the Neo-Hookean constitutive model, used in several other biomechanical studies, was considered (Peña et al., 2006). The Neo-Hookean model (Kim, 2015) is a simple and reliable formulation of a hyperelastic model. It was derived from molecular chain statistics considerations in which vulcanized rubber is regarded as a three-dimensional network of long-chain molecules that are connected at a few points. It is described by the following expression:

$$\Psi(\mathbf{C}) = c_{10}(\bar{I}_1^C - 3) + \Psi_{vol}(J) \quad (5.9)$$

where $c_{10} = \frac{\mu}{2}$. The constant μ is the shear modulus of linear elasticity. Ψ_{vol} is the volumetric contribution presented in equation 5.5.

Regarding the pelvic girdle bones, they were considered as rigid structures. Limiting the bone deformations, this approach facilitates the convergence of the simulation. However, since the main difference between the two birthing positions simulated is the mobility of the sacrococcygeal joint, the sacrum and coccyx were considered as deformable structures. Thus, it was fundamental to consider the contribution of both cortical and trabecular tissues to bone strength. The cortical bone corresponds to the denser and stronger of the two types of bone tissue, so it can withstand compressive forces. On the other hand, the trabecular bone has more open spaces and supports shifts in weight distribution. The material properties of these tissues were obtained from the work of Wu et al. (2018) and are listed in table 5.3.

Table 5.3: Material properties of the sacrum and coccyx

	Young's Modulus [MPa]	Poisson Coeff.
Cortical bone	6140	0.3
Trabecular bone	1400	0.3

The sacroiliac joint is a synovial joint that, in females, facilitates the demands of pregnancy and parturition, since the ligaments involved enable the motion of this joint. Consequently, these movements can affect the pelvis dimensions. The pubic symphysis is a nonsynovial, slightly movable joint. In many species, including in humans, the cartilaginous pubic symphysis of the pregnant female is gradually replaced by fibrous connective tissue, forming flexible and elastic ligaments between the two pubic bones. The ligaments modeled in these joints are tension-only elements and the material properties were obtained from Lei et al. (2015) and are listed in table 5.4.

Table 5.4: Material properties and cross sectional area of the ligaments

Ligaments	Cross Sectional Area [mm ²]	Young's Modulus [MPa]	Poisson Coeff.
Sacroiliac	5.64	350	0.495
Sacrospinous	7.45	29	0.495
Sacrotuberous	8.04	33	0.495
Superior Pubic	3.33	19	0.495
Inferior Pubic	5.72	20	0.495

Ligaments are fibrous connective tissues that have to manage two opposite functions which are to ensure joint stability and joint mobility. Animal studies provide some insight into the mechanisms underlying the characteristics of ligaments in humans. For example, there is evidence which indicates the involvement of female sex hormones in modulating the knee joint laxity, which includes the medial collateral ligament, a complex apparatus that acts as the primary static stabilizer of the knee joint (Dehghan et al., 2016). Thus, and taking into account that there is little experimental data on the mechanical properties of the pubic ligaments, a Neo-Hookean constitutive model was applied to the 3D solid elements, used to simulate the pubic symphysis, the synovial part of the sacroiliac joints (see figure 5.11) and the sacrococcygeal joint, considering the material properties of the medial collateral ligament of the knee described in Orozco et al. (2018), similar to what was done in another study (Li et al., 2006): $c_{10} = 6.43 \text{ MPa}$ and $D_1 = 1.0 \times 10^{-4} \text{ MPa}^{-1}$. Since the stiffness introduced by these 3D elements is low, the overall stiffness of the joints is mainly provided by the pelvic ligaments, modeled with the truss elements.

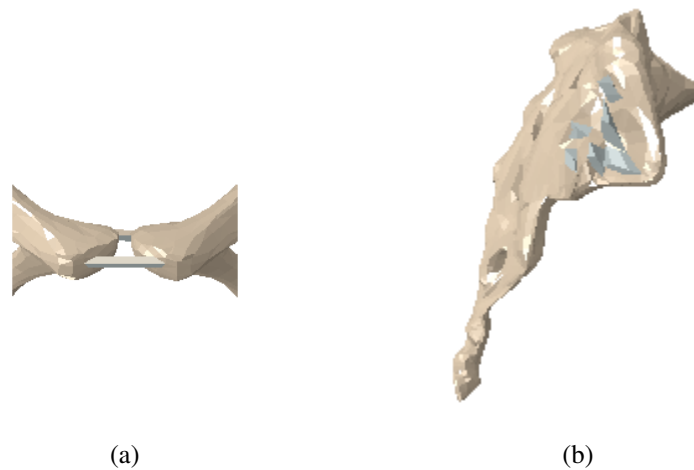


Figure 5.11: 3D solid elements used to simulate the interpubic disc of the pubic symphysis and the synovial part of the sacroiliac joints: (a) anterior view of pubic symphysis; (b) lateral view of sacrum

Concerning the fetus head, the material properties considered correspond to those of a material with high stiffness, such that the fetus can be considered rigid when compared with the pelvic floor, similarly to other numerical simulations of vaginal delivery (Oliveira et al., 2016). Taking into account that the main purpose of this work is to study the movement of the sacrum and coccyx and the widening of the pubic symphysis during a vaginal delivery, using this approach will reduce the fetus deformations and facilitate the convergence of the simulation.

5.2.3 Boundary Conditions

For the boundary conditions, a tie constraint was applied between the two supporting structures of the pelvic floor muscles (the lateral structures that include the arcus tendinous, obturator fascia, and the obturator internus) and the pubic bones. As a consequence, this constraints each of the nodes of the supporting structures (slave surface) to have the same motion as the point on the

pubic bones (master surface) to which it is closest. Furthermore, the nodes of the supporting structures that represent the different connections between the pelvic floor muscles and the sacrum, illustrated in black in figure 5.12, were considered fixed. Concerning the pelvic girdle bones, the sacrum nodes in the articular faces were fixed. A tie constraint was also applied between the sacrospinous and sacrotuberous ligaments and the fetal head.



Figure 5.12: Finite element model of the pelvic floor muscles in red with the identification of the fixed nodes in black

According to the cardinal movements, the vertical descent of the fetal head and its flexion/extension in vertex presentation and occipit anterior position were imposed by controlling the displacement and rotation of the reference point belonging to the model. Figure 5.13 illustrates the finite element model of the fetus head with the identification of the reference point.

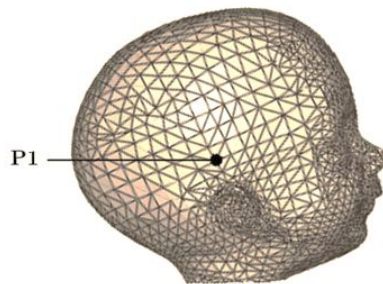


Figure 5.13: Finite element model of the fetus head with the identification of the reference point used to control its movement (P1)

5.3 Results and Discussion

Childbirth is a natural but complex process and there are several factors that need to be considered for proper management of delivery. In this work, numerical simulations assuming two different birthing positions (mob. coccyx model and non-mob coccyx model) were performed,

with the fetus in vertex presentation and occipit anterior position. The effects induced in the maternal pelvic girdle and in her pelvic floor muscles by the passage of the fetus head were analyzed.

As mentioned before, the fetus descent and head extension were controlled, but the remaining degrees of freedom were left free. Therefore, even though the occipito anterior position was simulated, the bones and pelvic floor imposed some constraints on the fetal head movements and, consequently, the predominant position was the left occipit anterior position, which has been adopted as the optimal fetal position (Webb et al., 2011).

5.3.1 Pubic Symphysis

During pregnancy and labor, the pubic symphysis can be more flexible and wider, aiming to facilitate the passage of the fetus through the birth canal. This physiological change was analyzed in the simulations performed. In figure 5.14, it is shown the widening of the pubic symphysis gap during the vertical descent of the fetus head.

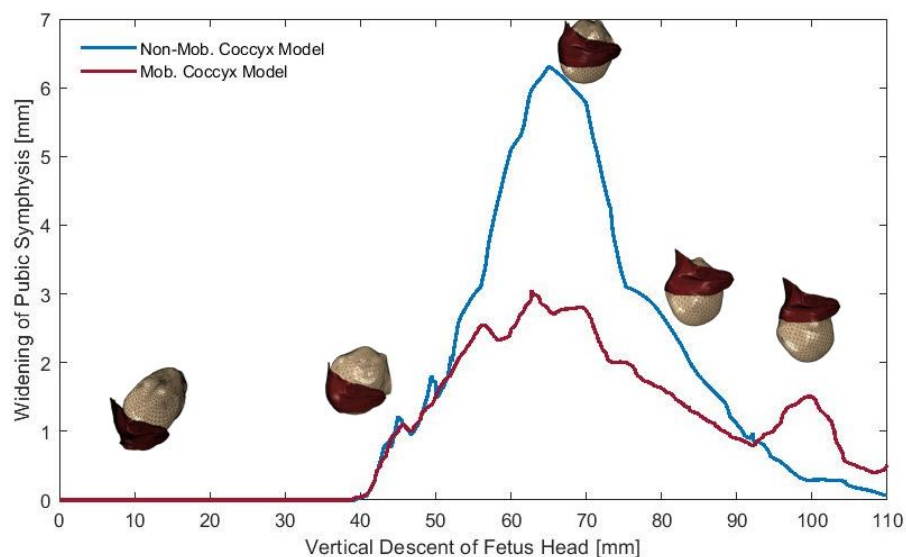


Figure 5.14: Widening of pubic symphysis during the vertical descent of the fetus head

The maximum value occurs at, approximately, a vertical descent of the fetus head of 65 mm, which corresponds to the moment when the fetus begins the head extension. Comparing the two models, the non-mob. coccyx model has a maximum widening of 6.3 mm, while the mob. coccyx model presents a maximum value of 3.2 mm. According to Jain et al. (2006) and Hwang (2015), a displacement of 2-3 mm of the pubic symphysis without discomfort is expected, but a displacement higher than 10 mm can also occur and, in this case, it is considered a pubic symphysis diastasis. Thus, in the selected positions, there is no rupture of this joint, despite the non-mob. coccyx model presents a higher widening. Regarding the mob. coccyx model, the widening verified after a 90 mm descent is related to the movement in the ventral, cranial direction of the coccyx, as seen in figure 5.16. This movement of the coccyx induces a decrease in the pelvic space available and,

as a consequence, it is necessary an increase of the pubic symphysis gap of the model to allow the passage of the fetal head.

The maximum principal stresses in the pubic ligaments were also obtained during the vertical descent of the fetus head (figure 5.15).

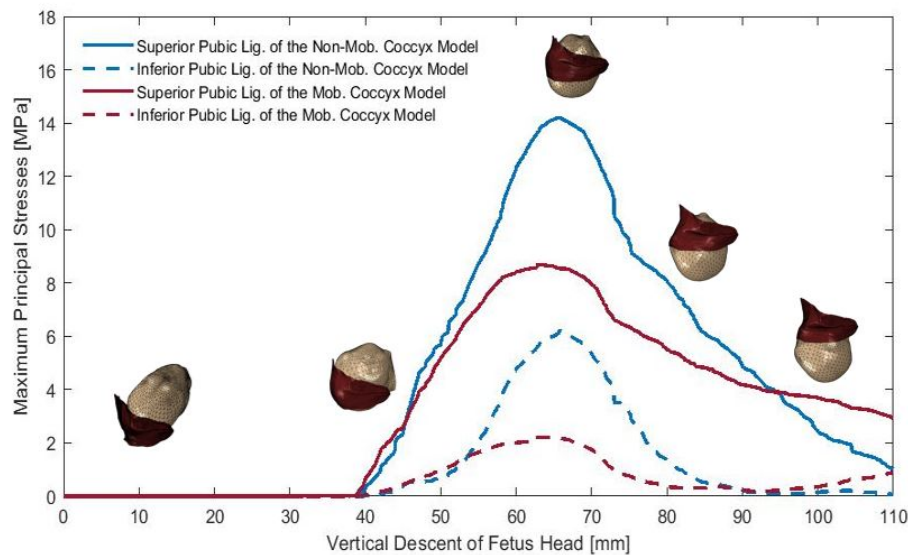


Figure 5.15: Maximum principal stresses in MPa in the superior and inferior pubic ligaments of the non-mob. coccyx model and mob. coccyx model during the vertical descent of the fetus head

Analyzing these results, it can be noted that the peak of stresses in the pubic ligaments occur at the same instance of the peak of the widening of the pubic symphysis. As expected, the maximum principal stresses measured in the non-mob. coccyx model are higher than in the mob. coccyx model. In the superior pubic ligaments, the maximum value obtained in the non-mob. coccyx model is 14.25 MPa and in the mob. coccyx model is 8.99 MPa. On the other hand, in the inferior pubic ligaments, the maximum value obtained in the non-mob. coccyx model is 6.29 MPa and in the mob. coccyx model is 2.88 MPa. This difference between the superior and inferior pubic ligaments is due to the fact that, as the pubic symphysis undergoes an approximately equal widening across all the joint, its narrowest points are in the most superior portion, as shown in figure 5.5. Furthermore, these values are consistent with the results from the widening of the pubic symphysis, since in the former model a higher widening of this joint occurs.

It is important to note that, during pregnancy, the levels of hormone relaxin increase, and ligamentous laxity occurs, which predisposes the widening of the pubic symphysis by altering the structure of collagen (Jain et al., 2006). However, the material properties considered for the superior and inferior pubic ligaments do not take into account this change in their characteristics, since no studies were found regarding the mechanical properties.

5.3.2 Sacrum and Coccyx

Concerning to sacrum and coccyx, a small amount of flexion and extension can occur at the sacrococcygeal joint. Flexion is produced by contraction of the levator ani muscles and the coccyx moves in a ventral, cranial direction. When the extension of coccyx occurs, it moves in a caudal, dorsal direction, according to Bø et al. (2001). In this way, the difference in distance from the tip of the coccyx to the reference line illustrated in figure 5.8 was calculated, as explained before, and the results obtained for the movement of coccyx during the vertical descent of the fetus head are shown in figure 5.16.

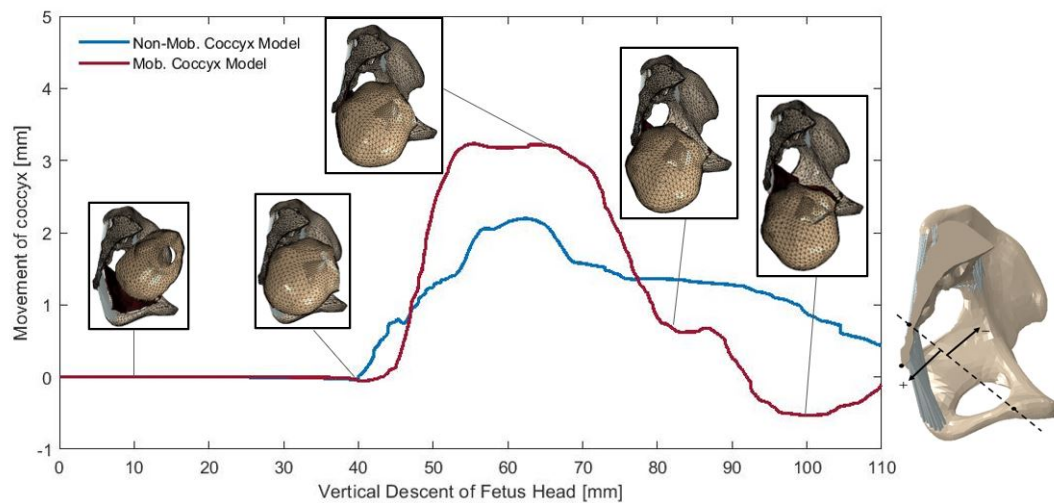


Figure 5.16: Movement of coccyx during the vertical descent of the fetus head

The peak of maximum movement of the tip of the coccyx occurs in both models at, approximately, the same instant of maximum widening of the pubic symphysis, i.e. 65 mm of vertical descent of fetus head. This instance corresponds to the moment when the fetus begins the head extension. In the mob. coccyx model, the maximum movement of the coccyx is 3.3 mm and, in the non-mob. coccyx model, this value is 2.2 mm. This displacement verified in the non-mob coccyx can be explained by the fact that, during the second stage of labor, it is required a successful negotiation of the maternal pelvis. Although the restricted movement of the coccyx allowed in this model, the fetal head presses this bone, causing a small movement that does not imply a high rotation of it, unlike what happens in the mob. coccyx model, as it is seen in figure 5.17.

The rotation of the tip of the coccyx was also evaluated and the results are shown in figure 5.17.

The peak of rotation occurs at, approximately, the same instance of the peak of the movement of this bone, as expected. Analyzing the maximum value obtained in both models, there is a very significant divergence between them. The non-mob. coccyx model has a rotation of 3.6° , while the mov. coccyx model has a rotation of 15.7° . During the passage of the fetal head, in the mob. coccyx model, a higher rotation and movement of the tip of the coccyx occurs, compared to the non-mob. coccyx, since the widening of the pubic symphysis of the former is much lower than the

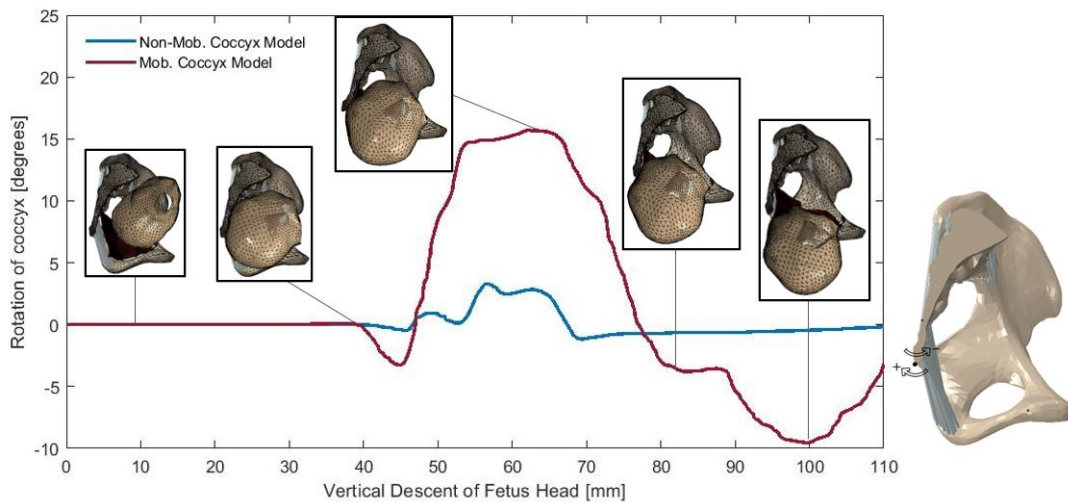


Figure 5.17: Rotation of coccyx during the vertical descent of the fetus head

latter. This is due to the fact that, in the non-mob. coccyx model, the movement of the coccyx is more restricted. Regarding the end of the simulation, which is when the pelvic bones tend to return to their original position, a flexion of the coccyx is observed. This movement can be explained by the fact that, in this joint, not all existing ligaments were modeled since the focus of this work is not the study of the ligaments themselves, but the movement of the coccyx.

According to a study on the movement of the coccyx during pelvic floor muscles contraction, it was found that the coccyx has an average movement of $8.1 \text{ mm} \pm 5.4 \text{ mm}$. During straining, this bone presents a mean movement of $3.7 \text{ mm} \pm 2.8 \text{ mm}$. The mean change from rest to contractions measured in degrees was $15.0^\circ \pm 10.2^\circ$, and from rest to straining $12.9^\circ \pm 10.9^\circ$ (Bø et al., 2001). Thus, it is possible to verify that the values obtained are in accordance with Bø et al. (2001) and, consequently, with the physiological limits of the sacrococcygeal joint. Note that if the movement of the fetus head imposes an excessive displacement of the tip of the coccyx, lesions in the sacrococcygeal ligaments or even coccyx fracture may occur (Hwang, 2015). Regarding fractures of the coccyx, they are, in the majority of the cases, associated with instrumented deliveries and the sitting position (Maigne et al., 2012).

To analyze the displacement on the x-axis that both the sacrum and coccyx suffered, a curve was defined in the sagittal plane of the sacrum and coccyx as shown in the figure 5.9. The results are presented in figure 5.18. For each of the two models, two curves were obtained during two different moments: the blue and red dashed curves were obtained when the vertical descent of the fetus head was 48 mm and the solid ones at the peak of maximum movement of the coccyx, which corresponds to a vertical descent of the fetus head of 65 mm. The black dashed line represents the beginning of the sacrococcygeal joint.

It can be observed that, in both instants, a higher displacement on the x-axis occurs when the normalized curve intersects the beginning of the sacrococcygeal joint, represented by a black dashed line. Thus, it is verified that the coccyx is the most affected bone, compared to the sacrum, by the movement of the fetus head. Regarding the displacement analyzed at the moment that

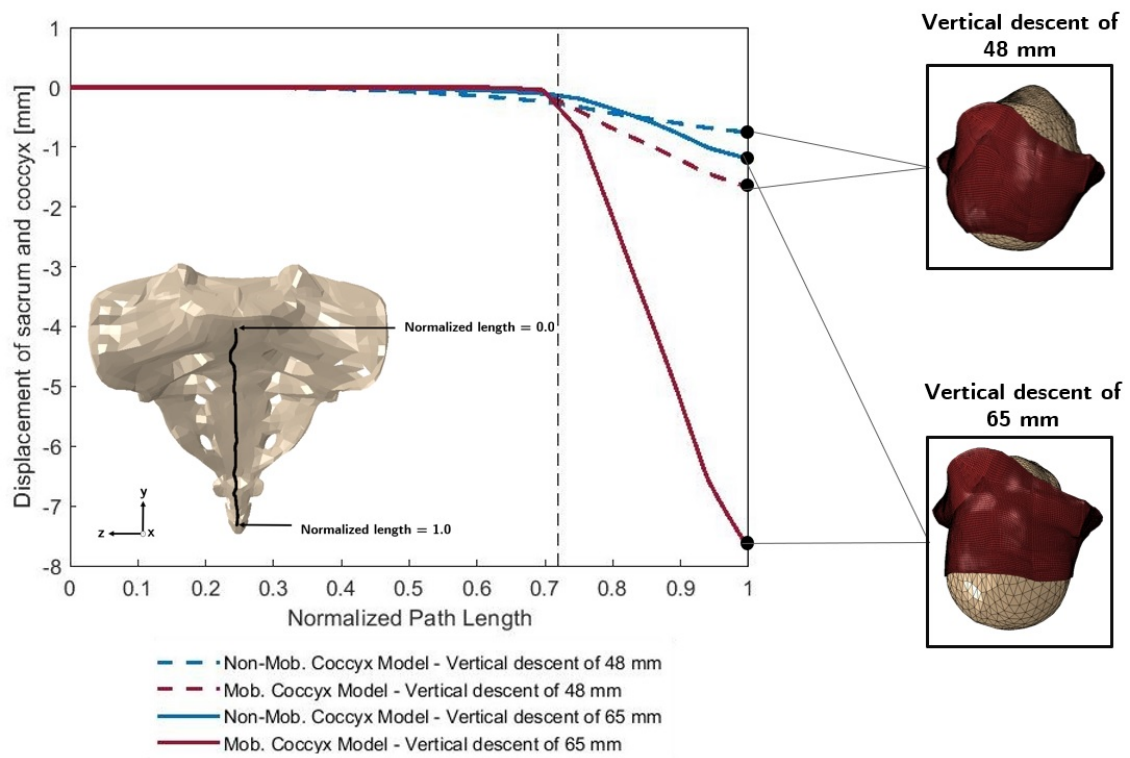


Figure 5.18: Displacement of sacrum and coccyx in x-axis along the normalized path at the sagittal plane of these bones in a vertical descent of the fetus head of 48 mm and 65 mm. The black dashed line corresponds to the beginning of the sacroccygeal joint

corresponds to the beginning of the movement of the coccyx, i.e. a vertical descent of the fetus head of 48 mm, as it can be seen in figure 5.16, lower values were obtained compared to the displacement observed at the peak of the movement of the coccyx, i.e. at a vertical descent of the fetus head of 65 mm. In this instance, a displacement of 7.6 mm occurs in the mob. coccyx model, which is higher than the displacement of 1.2 mm that occurs in the non-mob. coccyx model. These results are consistent with those obtained for the movement and rotation of coccyx, presented previously.

To study the impact on the sacrum and coccyx, the distribution of the maximum principal stresses on the cortical zone of these bones was analyzed in the peak coccyx movement instant. The results are shown in figure 5.19.

It is shown that higher maximum principal stresses are located on the most inferior part of the sacrum, sacroccygeal joint, and coccyx. Regarding the non-mob. coccyx model, it has a larger zone of high stresses, compared to the mob. coccyx model. This is consistent with the results of the displacement in the x-axis of these bones, since in the non-mob. coccyx model occurs a small displacement of the most inferior part of the sacrum. This is due to the fact that, in the non-mob. coccyx model, the coccyx has more restricted mobility, causing a greater impact on the cortical bone of sacrum and coccyx.

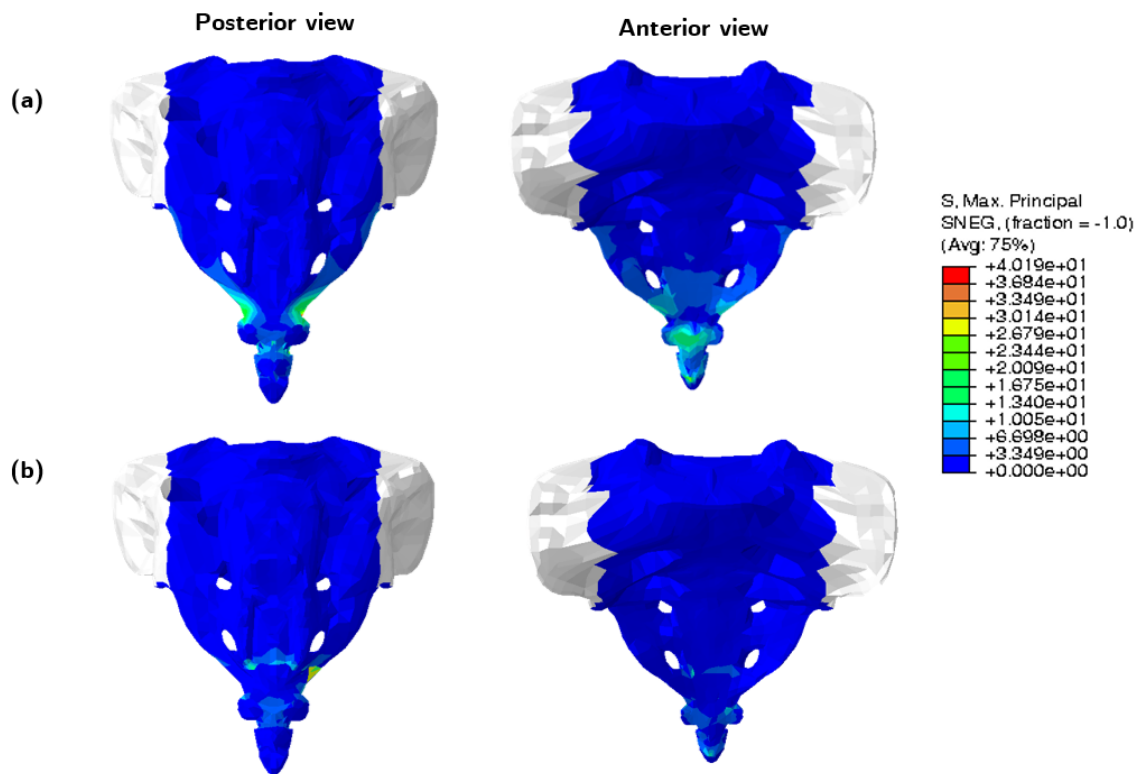


Figure 5.19: Distribution of the maximum principal stresses in MPa on the sacrum and coccyx, in the cortical bone tissue, in the (a) non-mob. coccyx model and (b) mob. coccyx model, at the moment of maximum movement of the coccyx

The biomechanics of pelvic fractures are not yet thoroughly understood because of its complex geometry and structure. Ricci et al. (2018) considered an ultimate tensile strength, i.e. the maximum stress that the cortical bone can withstand, that comprises values between 80 MPa and 120 MPa. Since the maximum stress value observed in this study is 40 MPa, it can be assumed that no significant injuries were caused. It is important to note that, during pregnancy, there are significant changes in maternal calcium and bone metabolism, since a large transfer of calcium to the fetus occurs. This can lead to changes in cortical and trabecular bone mass, structure, and dynamics (Sowers et al., 2000). However, these changes were not considered in the mechanical properties of the bones, since it is a topic still under investigation.

Globally, it is verified that different maternal positions cause changes in the available space for the passage of the fetal head. More specifically, positions in which the movement of the coccyx is more restricted, the widening of the pubic symphysis needs to be higher to allow for the space needed for the fetal head to pass. Furthermore, the obtained results suggest that the birthing positions that enable a higher movement of sacrum and coccyx, such as the majority of the vertical positions, coccyx can move more easily and, consequently, a lower widening of the pubic symphysis occurs. On the other hand, in horizontal positions, the force of the bed under these bones may close the pelvis. These results are consistent with the study developed by Reitter

et al. (2014), in which the impact of the different positions on pelvic dimensions were evaluated by comparing pregnant and non-pregnant women. It was verified that the changes in the maternal pelvis were more pronounced in pregnant women, suggesting a dynamic component in the female pelvis that may be more pronounced during parturition to facilitate birth. It was also observed that the vertical position, more specifically kneeling squat position, has higher diameters compared to the horizontal position (supine dorsal position), with the anteroposterior outlet presenting the most significant difference between the two positions. Note that the anteroposterior outlet corresponds to the distance from the tip of the coccyx to the low tip of the pubic symphysis. Furthermore, Desseauve et al. (2017) examined how birthing positions affect maternal, fetal and neonatal outcomes. Regarding the maternal outcomes, it was concluded that change to a more upright position for birthing is advantageous for the woman in the second stage of labor.

5.3.3 Pelvic Floor Muscles

Concerning the pelvic floor muscles, the maximum principal stresses were measured along the defined path at the most inferior portion of the pelvic floor muscles (figure 5.10) at the point of the simulation where its maximum occurs, as it is shown in figure 5.20.

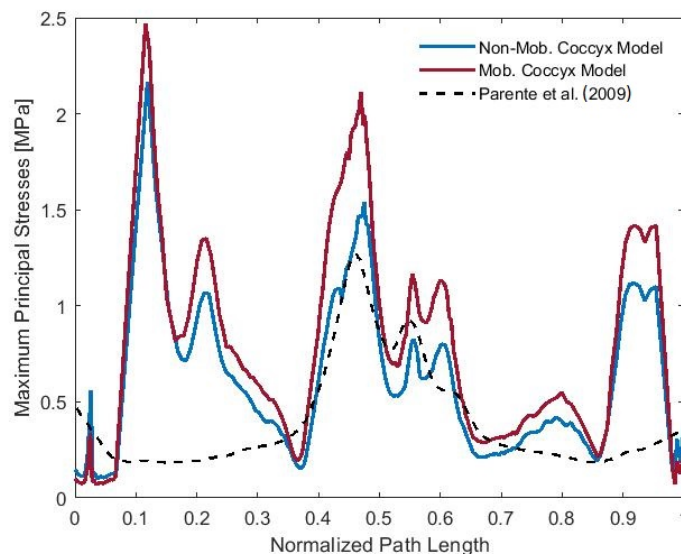


Figure 5.20: Maximum principal stresses in MPa calculated along the normalized path at the most inferior portion of the pelvic floor muscles (figure 5.10) at the peak stresses instant

To better understand the impact of the vertical descent of the fetus head in all model of the pelvic floor muscles, the distribution of the maximum principal stresses at the peak stresses instant was observed. The results are shown in figure 5.21.

In the non-mob. coccyx model, the instant analyzed corresponds to a vertical descent of the fetus head of 77 mm and, in the mob. coccyx model, to a vertical descent of 70 mm. In the mob. coccyx model, a higher pelvic space is available and, consequently, higher values of maximum principal stress were observed (approximately, 2.5 MPa) in the left area of the levator ani muscles,

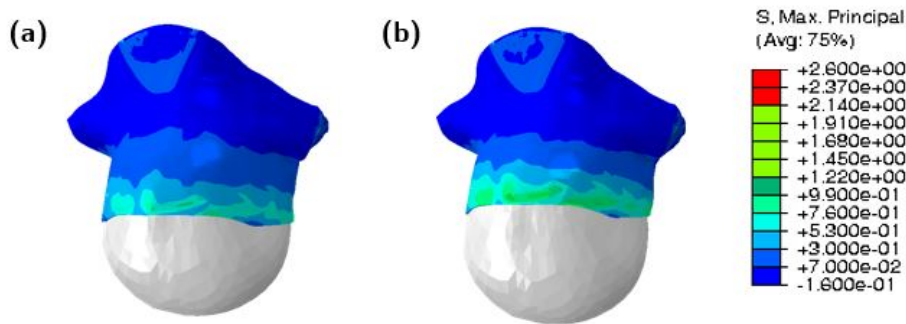


Figure 5.21: Distribution of the maximum principal stresses in MPa on the pelvic floor muscles at the peak stresses instant in the (a) non-mob. coccyx model and (b) mob. coccyx model

more specifically the pubococcygeal muscle. These differences in the instant analyzed and in the values obtained are due to small variations that may occur regarding the cardinal movements at the level of the fetal head, since there are some different in the space available in the mother's pelvis in both models.

Comparing these results with the obtained by [Parente et al. \(2009\)](#), it is observed that the peak of stresses occurs only in the most posterior area of the levator ani muscles. This can be explained by the fact that, in the present study, the predominant fetal position was the left occipit anterior position and, in the mentioned study, it was the occipit anterior position.

A stretch ratio was also calculated along the defined path at the most inferior portion of the pelvic floor muscles (figure 5.10) during the vertical descent of the fetus head. The results are shown in figure 5.22.

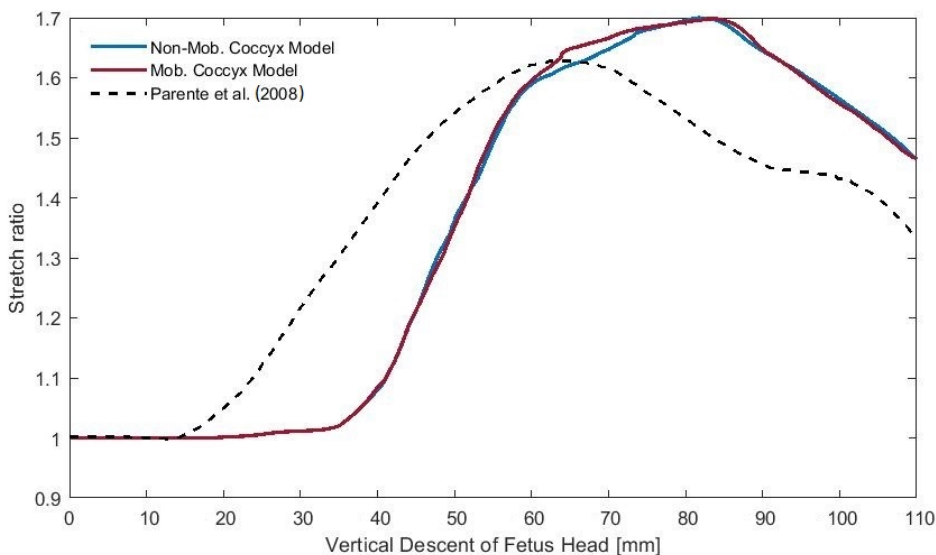


Figure 5.22: Stretch ratio calculated along the defined path at the most inferior portion of the pelvic floor muscles (figure 5.10) during the vertical descent of the fetus head

It can be noted that, for an initial length of 17.1 cm, the maximum stretch ratio value obtained

is 1.7, being similar in both models. [Parente et al. \(2008\)](#) also simulated the movements of the fetus during birth. Comparing the results, it is verified that the maximum stretch ratio occurs in different instances, due to the different fetal positions simulated and the restrictions imposed by the maternal pelvis, as explained before.

5.3.4 Fetus

The reaction forces in the medial-lateral direction exerted in the fetus head during its vertical descent were analyzed. In the model in which the movement of the coccyx is not restricted, i.e. the mob. coccyx model, a maximum reaction force of 175 N was obtained, while, in the other model, it was obtained a value of 239 N was obtained for the maximum reaction force in the medial-lateral direction. It was also verified that the peak instant of maximum value for the reaction forces is coincident with the moment of the vertical descent of the fetus head where the maximum principal stress occurs in both models: 70 mm in the non-mob. coccyx model and 77 mm in the mob. coccyx model.

[Oliveira et al. \(2016\)](#) performed numerical simulations of the vaginal delivery and the forces against fetal descent were obtained. Considering the model with the same constitutive model, a maximum value of 202 N was observed, which is similar to the results obtained in this study for the reaction forces in the medial-lateral direction exerted in the fetus head. The differences can be explained by the occipit anterior fetal position simulated in the mentioned study.

Chapter 6

Final Remarks and Future Work

6.1 Final Remarks

Vaginal delivery is a natural process that involves extensive physiologic changes in the mother and, consequently, several injuries can occur. Birthing positions serve as a non-medical intervention to facilitate labor, and different positions lead to different maternal and fetal outcomes. In this way, computational modeling has been used to replace *in vivo* animal studies, taking into account clinical, technical, and ethical reasons. These models can be used to simulate the mechanisms of labor and to better understand the biomechanics of different birthing positions. Accordingly, this may be a step further to understand how different maternal positions may influence the physiological outcomes of childbirth.

In this work, a finite element model simulates the fetal head movements during birth in vertex presentation and occipit anterior position, assuming two maternal positions: one that allows the movement of the coccyx and the other in which its movement is more restricted. This difference is based on the fact that, in the majority of the horizontal positions, such as supine and lithotomy positions, there is a bed under the sacrum and coccyx limiting its movement, unlike what happens in most vertical positions, such as kneeling and squatting positions. Thus, the space available for the passage of the fetus varies. Furthermore, the biomechanical model also takes into account the widening of the pubic symphysis that can occur during labor. Due to the constraints imposed by the bones and pelvic floor, the fetal head assumed a left occipit anterior position.

The numerical simulations performed showed that, in birthing positions in which the movement of the coccyx is restricted, a higher widening of the pubic symphysis occurs to allow the passage of the fetus head, without rupture. As a consequence, the cortical bone tissue of coccyx and the most inferior portion of sacrum suffer a higher impact. Knowing the ultimate tensile strength of this bone tissue, it can be assumed that no significant injuries occur. Analyzing the pelvic floor muscles, the left part of the levator ani muscles and the pubococcygeal muscle are the areas of greatest stress. Regarding the model that mimics the birthing positions that allow the movement of the coccyx, the widening of the pubic symphysis is lower and within the expected values. The movement and rotation measured in the tip of coccyx were higher, but also within the

physiological limits of the sacrococcygeal joint. The maximum stress value obtained for the pelvic floor muscles is higher because there are some variations in the movements of the fetus head since there is a higher space available to the passage of the fetus head in the model in which the coccyx is free to move. The left area of the levator ani muscles, more specifically the pubococcygeal muscle, are the most solicited muscles during delivery.

Therefore, it was verified that different birthing positions lead to changes in the maternal pelvic space, so certain positions can be adopted by the mother during the second stage of labor to reduce the risk of obstructed labor and the development of several dysfunctions. More specifically, positions in which the coccyx is free to move, a higher space is available for the passage of the fetal head. In this study, this birthing position appears to be more beneficial for the pelvic girdle bones of the mother.

Nevertheless, the problem studied is very complex and it is necessary to take into account the limitations and simplifications involved regarding the geometry of the biomechanical model and the mechanical properties attributed to the pelvic girdle bones, pelvic ligaments, and the fetal head. During pregnancy and labor, there are several hormonal changes in women that can influence the characteristics of bone tissues as well as ligaments; however, no studies were found on the mechanical properties of these structures in pregnant women.

6.2 Future Work

For future work, it would be important to perform experimental studies of pubic ligaments of pregnant women in order to include the effect of hormonal changes that occur during pregnancy.

It would also be interesting to simulate more specific birthing positions, i.e. to consider the different diameters of the woman's pelvis that each position implies. The influence of different pelvis types can also be a valuable modification to be studied.

In this work, the fetal head was considered a rigid structure, but it would be interesting to characterize the mechanical properties of the fetus and take them into account in the simulation. This modification to the model would allow the study of other variables such as the molding of the fetus head.

References

- Ahmad, A., Webb, S. S., Early, B., Sitch, A., Khan, K. and Macarthur, C. (2014), 'Association between fetal position at onset of labor and mode of delivery: A prospective cohort study', *Ultrasound in Obstetrics and Gynecology* **43**(2), 176–182.
- Aldabe, D., Ribeiro, D. C., Milosavljevic, S. and Bussey, M. D. (2012), 'Pregnancy-related pelvic girdle pain and its relationship with relaxin levels during pregnancy: A systematic review', *European Spine Journal* **21**(9), 1769–1776.
- Atwood, R. J. (1976), 'Parturitional Posture and Related Birth Behavior', *Acta Obstetrica et Gynecologica Scandinavica* **55**(57 S), 3–25.
- Bø, K., Lilleås, F., Talseth, T. and Hedland, H. (2001), 'Dynamic MRI of the pelvic floor muscles in an upright sitting position', *Neurourology and Urodynamics* **20**(2), 167–174.
- Bonet, J. and Wood, R. D. (2008), *Nonlinear Continuum Mechanics for Finite Element Analysis*, second edn.
- Bonet, J., Wood, R. D. and Gil, A. J. (2017), *Nonlinear Solid Mechanics For Finite Element Analysis: Statics*.
- Borg-Stein, J., Dugan, S. A. and Gruber, J. (2005), 'Musculoskeletal aspects of pregnancy', *American Journal of Physical Medicine and Rehabilitation* **84**(3), 180–192.
- Bower, A. F. (2010), *Applied Mechanics of Solids*, CRC Press Taylor & Francis Group.
- Dehghan, F., Soori, R., Dehghan, P., Gholami, K., Muniandy, S., Azarbayjani, M. A. and Yusof, A. (2016), 'Changes in knee laxity and relaxin receptor isoforms expression (RXFP1/RXFP2) in the knee throughout estrous cycle phases in rodents', *PLoS ONE* **11**(8), 1–14.
- Desseauve, D., Fradet, L., Lacouture, P. and Pierre, F. (2017), 'Position for labor and birth: State of knowledge and biomechanical perspectives', *European Journal of Obstetrics and Gynecology and Reproductive Biology* **208**, 46–54.
URL: <http://dx.doi.org/10.1016/j.ejogrb.2016.11.006>
- Donelson, S. S. and Minocha, A. (2002), *Pelvic floor dysfunction*, Vol. 5.
- Gabbe, Niebyl, Simpson, Landon, Galan, Jauniaux, Driscoll, Berghella and Grobman (2017), *Obstetrics: Normal and Problem Pregnancies*, Vol. 1, seventh edn, Elsevier.
- Grzelkowska-Kowalczyk, K. (2016), 'The Importance of Extracellular Matrix in Skeletal Muscle Development and Function', *Composition and Function of the Extracellular Matrix in the Human Body* pp. 3–24.

- Gupta, J. K. and Nikodem, C. (2000), 'Maternal posture in labour', *European Journal of Obstetrics and Gynecology and Reproductive Biology* **92**(2), 273–277.
- Hacker, N., Gambone, J. and Hobel, C. (2016), *Essentials of Obstetrics & Gynecology*, sixth edn, Elsevier.
- Hemmerich, A., Bandrowska, T. and Dumas, G. A. (2019), 'The effects of squatting while pregnant on pelvic dimensions: A computational simulation to understand childbirth', *Journal of Biomechanics* **87**, 64–74.
URL: <https://doi.org/10.1016/j.jbiomech.2019.02.017>
- Holzapfel, G. (2002), *Nonlinear Solid Mechanics: A Continuum Approach for Engineering Science*, Vol. 37.
- Huang, J., Zang, Y., Ren, L. H., Li, F. J. and Lu, H. (2019), 'A review and comparison of common maternal positions during the second-stage of labor', *International Journal of Nursing Sciences* **6**(4), 460–467.
URL: <https://doi.org/10.1016/j.ijnss.2019.06.007>
- Hwang, S. K. (2015), 'Musculoskeletal Health in Pregnancy and Postpartum', *Musculoskeletal Health in Pregnancy and Postpartum* pp. 171–179.
- Jain, S., Eedarapalli, P., Jamjute, P. and Sawdy, R. (2006), 'Symphysis pubis dysfunction: a practical approach to management', *The Obstetrician & Gynaecologist* **8**(3), 153–158.
- Janda, S., Van Der Helm, F. C. and De Blok, S. B. (2003), 'Measuring morphological parameters of the pelvic floor for finite element modelling purposes', *Journal of Biomechanics* **36**(6), 749–757.
- Kim, N. H. (2015), *Introduction to nonlinear finite element analysis*.
- Lei, J., Zhang, Y., Wu, G., Wang, Z. and Cai, X. (2015), 'The Influence of Pelvic Ramus Fracture on the Stability of Fixed Pelvic Complex Fracture', *Computational and Mathematical Methods in Medicine* **2015**.
- Li, Z., Alonso, J. E., Kim, J. E., Davidson, J. S., Etheridge, B. S. and Eberhardt, A. W. (2006), 'Three-dimensional finite element models of the human pubic symphysis with viscohyperelastic soft tissues', *Annals of Biomedical Engineering* **34**(9), 1452–1462.
- Lowdermilk, D. L. (2011), Labor and Birth Processes, in 'Maternity nursing', pp. 316–336.
- Macdonald, S., Magill-Cuerden, J. and Warwick, C. (2011), *Mayer's midwifery*, New York.
- Maigne, J. Y., Rusakiewicz, F. and Diouf, M. (2012), 'Postpartum coccydynia: A case series study of 57 women', *European Journal of Physical and Rehabilitation Medicine* **48**(3), 387–392.
- Martini, F. H., Timmons, M. J. and Tallitsch, R. B. (2012), *Human Anatomy*.
URL: www.amazon.com
- Martins, J. A., Pires, E. B., Salvado, R. and Dinis, P. B. (1998), 'A numerical model of passive and active behavior of skeletal muscles', *Computer Methods in Applied Mechanics and Engineering* **151**(3-4), 419–433.
- McGrath, M. (2004), 'Clinical considerations of sacroiliac joint anatomy: a review of function, motion and pain', *Journal of Osteopathic Medicine* **7**(1), 16–24.

- Michel, S. C., Rake, A., Treiber, K., Seifert, B., Chaoui, R., Huch, R., Marincek, B. and Kubik-Huch, R. A. (2002), 'MR obstetric pelvimetry: Effect of birthing position on pelvic bony dimensions', *American Journal of Roentgenology* **179**(4), 1063–1067.
- Moore, K. L., Dalley, A. F. and Agur, A. M. R. (2006), *Clinically oriented Anatomy: Abdomen*, Wolters Kluwer Health.
- Nieuwenhuijze, M., Jonge, A. D., Korstjens, I. and Lagro-Jansse, T. (2012), 'Factors influencing the fulfillment of women's preferences for birthing positions during second stage of labor', *Journal of Psychosomatic Obstetrics and Gynecology* **33**(1), 25–31.
- Oliveira, D. A., Parente, M. P., Calvo, B., Mascarenhas, T. and Natal Jorge, R. M. (2016), 'Numerical simulation of the damage evolution in the pelvic floor muscles during childbirth', *Journal of Biomechanics* **49**(4), 594–601.
URL: <http://dx.doi.org/10.1016/j.jbiomech.2016.01.014>
- Orozco, G. A., Tanska, P., Mononen, M. E., Halonen, K. S. and Korhonen, R. K. (2018), 'The effect of constitutive representations and structural constituents of ligaments on knee joint mechanics', *Scientific Reports* **8**(1), 1–15.
URL: <http://dx.doi.org/10.1038/s41598-018-20739-w>
- Parente, M. P., Natal Jorge, R. M., Mascarenhas, T., Fernandes, A. A. and Martins, J. A. (2008), 'Deformation of the pelvic floor muscles during a vaginal delivery', *International Urogynecology Journal* **19**(1), 65–71.
- Parente, M. P., Natal Jorge, R. M., Mascarenhas, T., Fernandes, A. A. and Martins, J. A. (2009), 'The influence of the material properties on the biomechanical behavior of the pelvic floor muscles during vaginal delivery', *Journal of Biomechanics* **42**(9), 1301–1306.
- Parente, M. P., Natal Jorge, R. M., Mascarenhas, T., Fernandes, A. A. and Silva-Filho, A. L. (2010), 'Computational modeling approach to study the effects of fetal head flexion during vaginal delivery', *American Journal of Obstetrics and Gynecology* **203**(3), 1–217.
URL: <http://dx.doi.org/10.1016/j.ajog.2010.03.038>
- Peña, E., Calvo, B., Martinez, M. A., Palanca, D. and Doblaré, M. (2006), 'Why Lateral Meniscectomy Is More Dangerous Than Medial Meniscectomy. A Finite Element Study.', *Journal of Orthopaedic Research* .
- Perry, A., Potter, P. and Ostendorf, W. (2014), *Clinical Nursing Skills & Techniques*, 8th edn.
- Posner, G. D., Dy, J., Black, A. and Jones, G. D. (2013), *Human Labor & Birth*.
- Reitter, A., Daviss, B. A., Bisits, A., Schollenberger, A., Vogl, T., Herrmann, E., Louwen, F. and Zangos, S. (2014), 'Does pregnancy and/or shifting positions create more room in a woman's pelvis?', *American Journal of Obstetrics and Gynecology* **211**(6), 1–662.
URL: <http://dx.doi.org/10.1016/j.ajog.2014.06.029>
- Ricci, P. L., Maas, S., Kelm, J. and Gerich, T. (2018), 'Finite element analysis of the pelvis including gait muscle forces: an investigation into the effect of rami fractures on load transmission', *Journal of Experimental Orthopaedics* **5**(1).
- Shorten, A., Donsante, J. and Shorten, B. (2002), 'Birth position, accoucheur, and perineal outcomes: Informing women about choices for vaginal birth', *Birth* **29**(1), 18–27.

- Simkin, P. (2002), 'Supportive care during labor: a guide for busy nurses.', *Journal of obstetric, gynecologic, and neonatal nursing* **31**(6), 721–732.
- Sipko, T., Grygier, D., Barczyk, K. and Elias, G. (2010), 'The Occurrence of Strain Symptoms in the Lumbosacral Region and Pelvis During Pregnancy and After Childbirth', *Journal of Manipulative and Physiological Therapeutics* **33**(5), 370–377.
URL: <http://dx.doi.org/10.1016/j.jmpt.2010.05.006>
- Sowers, M. F., Scholl, T., Harris, L. and Jannausch, M. (2000), 'Bone Loss in Adolescent and Adult Pregnant Women', *Obstetrics & Gynecology* **96**(2), 189–193.
- Standring, S., ed. (2016), *Gray's anatomy: the anatomical basis of clinical practice*.
- Webb, S. S., Plana, M. N., Zamora, J., Ahmad, A., Earley, B., MacArthur, C. and Khan, K. S. (2011), 'Abdominal palpation to determine fetal position at labor onset: A test accuracy study', *Acta Obstetrica et Gynecologica Scandinavica* **90**(11), 1259–1266.
- Woon, J. T. and Stringer, M. D. (2012), 'Clinical anatomy of the coccyx: A systematic review', *Clinical Anatomy* **25**(2), 158–167.
- World Health Organization (2019), *Trends in Maternal Mortality 2000 to 2017: estimates by WHO, UNICEF, UNFPA, World Bank Group and the United Nations Population Division*.
- Wu, T., Ren, X., Cui, Y., Cheng, X., Peng, S., Hou, Z. and Han, Y. (2018), 'Biomechanical study of three kinds of internal fixation for the treatment of sacroiliac joint disruption using biomechanical test and finite element analysis', *Journal of Orthopaedic Surgery and Research* **13**(1), 1–8.
- Zhao, Y., Li, J., Wang, D., Liu, Y., Tan, J. and Zhang, S. (2012), 'Comparison of stability of two kinds of sacro-iliac screws in the fixation of bilateral sacral fractures in a finite element model', *Injury* **43**(4), 490–494.
- Zileni, B. D., Glover, P., Jones, M., Teoh, K. K., Zileni, C. W. Z. and Muller, A. (2017), 'Malawi women's knowledge and use of labour and birthing positions: A cross-sectional descriptive survey', *Women and Birth* **30**(1), e1–e8.
URL: <http://dx.doi.org/10.1016/j.wombi.2016.06.003>

Appendix A

A.1 Article submitted to Computer Methods and Programs in Biomedicine Journal

Computer Methods and Programs in Biomedicine

Effect of the birthing position on its evolution from a biomechanical point of view

--Manuscript Draft--

Manuscript Number:	
Article Type:	Full Length Article
Section/Category:	Modelling & Simulation
Keywords:	Childbirth; Pubic Symphysis; Finite Element Method; Biomechanical Modeling
Corresponding Author:	Margarida Borges Pereira PORTUGAL
First Author:	Margarida Borges Pereira
Order of Authors:	Margarida Borges Pereira Dulce Oliveira Marco Parente Teresa Mascarenhas Renato Natal
Manuscript Region of Origin:	Europe
Abstract:	<p>Background and Objective</p> <p>During vaginal delivery, several positions can be adopted by the mother to be more comfortable and to help the labor process. The positions chosen are very influenced by factors such as monitoring and intervention during the second stage of labor. However, there is limited evidence to support the most ideal birthing position. This work aims at contributing to a better knowledge associated with the widening of the pubic symphysis and the biomechanics of vertical and horizontal birthing positions that can be adopted during the second stage of labor, as well as their resulting pathophysiological consequences.</p> <p>Methods</p> <p>A validated computational model composed by the pelvic floor muscles attached to the bones, and a fetus head was used to simulate vaginal deliveries. This model was modified to mimic two birthing positions: one that allows the free movement of the coccyx as in vertical positions and other in which this movement is more restricted as in horizontal positions. The widening of the pubic symphysis was also considered to facilitate the passage of the fetus head.</p> <p>Results</p> <p>The results obtained showed that in positions in which the movement of the coccyx is restricted, as in most horizontal positions, a widening of 6 mm of the pubic symphysis occurs. In contrast, in positions in which the coccyx is free to move, as in most vertical positions, a lower widening of the pubic symphysis occurs (3 mm), appearing to be more beneficial for the mother's pelvis, but slightly higher stresses were detected in the pelvic floor muscles.</p> <p>Conclusions</p> <p>Globally, the results obtained allow to conclude that different birthing positions lead to changes in the female pelvic space, so certain positions can be adopted by the mother during the second stage of labor to reduce the risk of obstructed labor and the development of several dysfunctions. More specifically, positions in which the coccyx is free to move, a higher space is available for the passage of the fetal head.</p>
Suggested Reviewers:	James Ashton-Miller

	College of Engineering, University of Michigan, USA jaam@umich.edu
	Christos E. Constantinou Stanford University School of Medicine, USA chris.constantinou@stanfordalumni.org
	Margot Damaser Cleveland Clinic Lerner Research Institute, USA damasem@ccf.org
	Steven Abramowitch University of Pittsburgh, USA sdast9@gmail.com
Opposed Reviewers:	

Dear Chief Editor of the journal Computer Methods and Programs in Biomedicine,

Please find in the attached files the contribution of the authors Margarida Borges, Dulce Oliveira, Marco Parente, Teresa Mascarenhas and Renato Natal Jorge, entitled "Effect of the birthing position on its evolution from a biomechanical point of view". We believe that this manuscript is appropriate for publication by Computer Methods and Programs in Biomedicine because it takes advantage of computing methods, such as computational modeling and simulation, to contribute to innovations and developments in the medical field, namely in the obstetrics field.

During labor, several birthing positions can be adopted, and, in recent years, they have shown potential benefits in promoting optimal maternal and neonatal outcomes, since maternal positions serve as the non-medical intervention to facilitate the progress of childbirth. However, the most ideal maternal position has been controversial since the few existing scientific evidence comes from clinical studies and the biomechanics of birth positioning are not yet fully understood. To the best of our knowledge, the adaptations that the maternal pelvis may undergo during the second stage of labor have not been considered in the studies that perform a biomechanical analysis using computational models of the musculoskeletal system of pregnant women. In this way, this work aims at contributing to a better knowledge associated with the widening of the pubic symphysis and the biomechanics of vertical and horizontal birthing positions that can be adopted during the second stage of labor, as well as their resulting pathophysiological consequences.

All the authors present in the manuscript have made substantial contributions to the production of the final manuscript, including the conception and design of the study, acquisition of data, analysis and interpretation of the obtained results, drafting the article and revising it. The final version submitted has been approved by all the authors present on the article.

The manuscript submitted for publication, including related data, figures and tables has not been previously published and is not under consideration elsewhere.

Sincerely yours,

Margarida Borges Pereira

Highlights

- Numerical simulations of vaginal deliveries assuming two birthing positions
- The finite element model includes: fetus head; pelvic bones, ligaments and muscles
- In most vertical positions, a higher movement and rotation of the coccyx occurs
- In most horizontal positions, a higher widening of the pubic symphysis occurs
- The left area of the levator ani muscles are the most solicited muscles

**Effect of the birthing position on its evolution from a
biomechanical point of view**

Margarida Borges^a, Dulce Oliveira^a, Marco Parente^a,
Teresa Mascarenhas^b, Renato Natal^a

^aINEGI-LAETA, Faculty of Engineering, University of
Porto
Campus FEUP, Rua Dr. Roberto Frias, 400, 4600-465
Porto, Portugal

^bCentro Hospitalar Universitário de São João, Faculty of
Medicine, University of Porto
Alameda Prof. Hernâni Monteiro, 4200-319 Porto,
Portugal

Corresponding author:

Margarida Borges

INEGI-LAETA, Faculty of Engineering, University of Porto
Campus FEUP, Rua Dr. Roberto Frias, 400, 4600-465
Porto, Portugal

Telephone: +351 229 578 710

Fax: +351 229 537 352

Email: mpereira@inegi.up.pt

ABSTRACT

Background and Objective:

During vaginal delivery, several positions can be adopted by the mother to be more comfortable and to help the labor process. The positions chosen are very influenced by factors such as monitoring and intervention during the second stage of labor. However, there is limited evidence to support the most ideal birthing position. This work aims at contributing to a better knowledge associated with the widening of the pubic symphysis and the biomechanics of vertical and horizontal birthing positions that can be adopted during the second stage of labor, as well as their resulting pathophysiological consequences.

Methods:

A validated computational model composed by the pelvic floor muscles attached to the bones, and a fetus head was used to simulate vaginal deliveries. This model was modified to mimic two birthing positions: one that allows the free movement of the coccyx as in vertical positions and other in which this movement is more restricted as in horizontal positions. The widening of the pubic symphysis was also considered to facilitate the passage of the fetus head.

Results:

The results obtained showed that in positions in which the movement of the coccyx is restricted, as in most horizontal positions, a widening of 6 mm of the pubic symphysis occurs. In contrast, in positions in which the coccyx is free to move, as in most vertical positions, a lower widening of the pubic symphysis occurs (3 mm), appearing to be more beneficial for the mother's pelvis, but slightly higher stresses were detected in the pelvic floor muscles.

Conclusions:

Globally, the results obtained allow to conclude that different birthing positions lead to changes in the female pelvic space, so certain positions can be adopted by the mother during the second stage of labor to reduce the risk of obstructed labor and the development of several dysfunctions. More specifically, positions in which the coccyx is free to move, a higher space is available for the passage of the fetal head.

Keywords: Childbirth, Pubic Symphysis, Finite Element Method, Biomechanical Modeling

INTRODUCTION

The mechanisms of labor and the likelihood of safe vaginal delivery depend largely on the bony architecture of the pelvis [1]. Maternal morbidity and mortality is unacceptably high and one of the main causes are biomechanical complications [2].

To facilitate the process of labor, ligament relaxation occurs during pregnancy and pubic symphysis can be more flexible and wider [3]. During the second stage of labor, several maternal postures can be adopted and the outcomes may vary [4]. Birthing positions can be classified into two main groups, depending on the angle made by the horizontal plane and the line linking the midpoints of the third and fifth lumbar vertebrae: when the angle is greater than 45° (or 30°) it is considered vertical, otherwise it is horizontal [5]. Regarding horizontal positions, such as supine and lithotomy positions, globally the coccyx movement is restricted due to the presence of the bed under it. In contrast, most of vertical positions, such as kneeling and squatting positions, allow the coccyx to move as the fetus descends.

In the past, women assumed a wide range of birthing positions and supine position was only used when labor lasted a long time or was very difficult and exhausting. More recently, there has been a growing awareness

among obstetricians and the supine position become popular, although its widespread use was not based on sound scientific evidence [6]. Therefore, it becomes important to understand the effects of different birthing positions. It is crucial to clarify the adaptation that the maternal pelvis may undergo by allowing the widening of the pubic symphysis. Knowing the risk and benefits of each position, pregnant women may decide on the birthing position adopted, which may help to prevent complications.

This work aims at contributing to a better knowledge associated with the widening of the pubic symphysis and the biomechanics of different positions. For this purpose, a finite element model of the mother and the fetus was modified to mimic two birthing positions: one that allows free movement of the coccyx and the other in which it is more restricted. This is because, in the majority of horizontal positions, the sacrum and coccyx movement is restricted, unlike in most vertical positions. Some pelvic joints were considered, allowing the widening of the pubic symphysis. The movements of the fetus during the second stage of labor in the vertex presentation and occipit anterior position were simulated.

MATERIALS AND METHODS

A three-dimensional (3D) finite element model validated for vaginal deliveries was used [7]. The mother's model includes the pelvic floor muscles and the supporting structures (arcus tendinous, obturator fascia, obturator internus and different connections between the muscles of the pelvic floor and the sacrum) that were modeled using hexahedral elements with hybrid formulation (C3D8H).

To account for the muscle behavior, the contributions of different parts of the tissue were considered, such as the contribution of: the extracellular matrix that endows the tissue strength and resilience (U_m); the fibers (U_f), both passive elastic part (U_{PE}) and active part (U_{SE}), responsible for muscle contraction; and the volumetric contribution to enforce the incompressibility condition (U_{vol}). A quasi-incompressible transversely isotropic hyperelastic model [8] already successfully applied [7] was used:

$$U = U_m(\bar{I}_1^C) + U_f(\bar{\lambda}_f, \alpha) + U_{vol}(J) \quad (1)$$

where

$$U_m = c \left[e^{b(\bar{I}_1^C - 3)} - 1 \right] \quad (2)$$

$$U_f = A \left[\overbrace{e^{a(\bar{\lambda}_f - 1)^2} - 1}^{U_{PE}} \right] + \overbrace{T_0^M \int_1^{\bar{\lambda}_f} f_{SE}(\lambda^M, \alpha) d\lambda^M}^{U_{SE}} \quad (3)$$

$$U_{vol} = \frac{1}{D_1} (J - 1)^2 \quad (4)$$

In these definitions, c , b , A , a , D_1 and T_0^M are constants, $\bar{I}_1^{\bar{C}}$ is the first invariant of the right Cauchy-Green strain tensor, \mathbf{C} , with the volume change eliminated:

$$\bar{I}_1^{\bar{C}} = tr(\bar{C}) = tr(\bar{F}^T \bar{F}) = J^{-2/3} tr(\mathbf{C}) \quad (5)$$

where \bar{F} is the deformation gradient with the volume change eliminated, J the volume change and $\bar{\lambda}_f$ the fiber stretch ratio in the direction \mathbf{N} of the undeformed fiber:

$$\bar{\lambda}_f = \sqrt{\mathbf{N}^T \bar{C} \mathbf{N}} = \sqrt{\bar{C} : (\mathbf{N} \otimes \mathbf{N})} \quad (6)$$



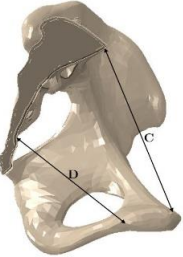
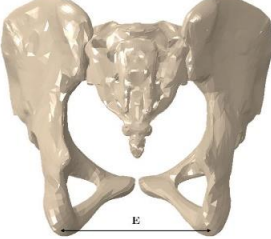
Regarding Equation (3), the following expression was used:

$$f_{SE} = \alpha \begin{cases} 1 - 4(\lambda^M - 1)^2 & \text{for } 0.5 < \lambda^M < 1.5 \\ 0 & \text{otherwise} \end{cases} \quad (7)$$

meaning that for $0.5 \geq \lambda^M \geq 1.5$ the muscle produces no energy. The level of activation is controlled by $\alpha \in [0,1]$. The constitutive parameters were retrieved from the literature [9]: $c = 0.00185$ MPa, $b = 1.173$, $A = 0.0280$ MPa, $a = 0.6215$, $D_1 = 1.0 \times 10^{-4}$ MPa⁻¹ and $T_0^M = 0.682$ MPa.

The mother's model also includes the pelvic girdle bones: the hip bones, sacrum and coccyx. The maternal pelvic diameters were modified according to Michel et al.[10] (Table 1) and the initial pubic symphysis gap was 4.05 mm [11].

Table 1 – Maternal pelvic diameters considered

Diameters [mm]		
	Transverse (A)	129
		Interspinous (B)
	Obstetric conjugate (C)	124
	Sagittal outlet (D)	115
	Intertuberous (E)	124

The pelvic girdle bones were modeled using rigid triangular shell elements with reduced integration (S3R). Limiting the bone deformations, this approach facilitates the convergence of the simulation. Since the sacrum and coccyx are important bones in the space available for the passage of the fetus, the cortical and trabecular bone tissues were modeled using FEMAP 2020.1 software and

the material properties (Table 2) were obtained from Wu et al.[12]. The former was modeled using triangular shell elements with reduced integration (S3R) with 2 mm of thickness [13] and the latter using tetrahedral elements with hybrid formulation (C3D4H).

Table 2 – Material properties of the sacrum and coccyx

	Young's Modulus	Poisson's
	[MPa]	Ratio
Cortical Bone	6140	0.3
Trabecular Bone	1400	0.3

In the pubic symphysis, the superior and inferior pubic ligaments were modeled as tension-only elements (linear truss elements (T3D2)). The sacroiliac, sacrospinous and sacrotuberous ligaments were also simulated using several linear truss elements (T3D2), based on anatomic data [14]. To give numerical stability to the simulation, linear beam elements (B31), using a low Young modulus, were superimposed to the truss elements mesh of the sacrospinous and sacrotuberous ligaments, providing a residual bending stiffness. The material properties applied were obtained from Lei et al.[15] and are listed in Table 3.

Table 3 – Material properties and cross-sectional area of the ligaments

Ligaments	Cross-Sectional Area [mm ²]	Young's Modulus [MPa]	Poisson's Ratio
Sacroiliac	5.64	350	0.495
Sacrospinous	7.45	29	0.495
Sacrotuberous	8.04	33	0.495
Superior Pubic	3.33	19	0.495
Inferior Pubic	5.72	20	0.495

The biomechanical model of the mother is shown in Figure 1.

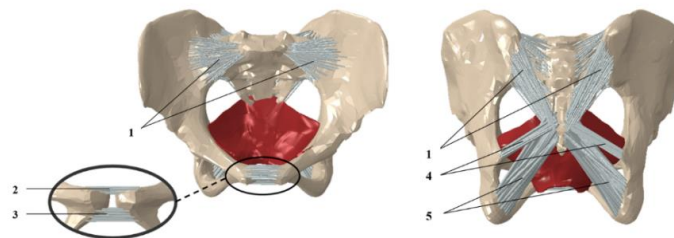


Figure 1 - Finite element model of the mother with the modeled ligaments: 1, sacroiliac ligaments; 2, superior pubic ligament; 3, inferior pubic ligament; 4, sacrospinous ligament; 5, sacrotuberous ligament.

In this work, two birthing positions were mimicked: in the mobile coccyx model (mob. coccyx model), the coccyx is mobile and, in the non-mobile coccyx model (non-mob.

coccyx model), its movement is more restricted. The sacrococcygeal joint was considered in the mob. coccyx model, as it is illustrated in Figure 2.

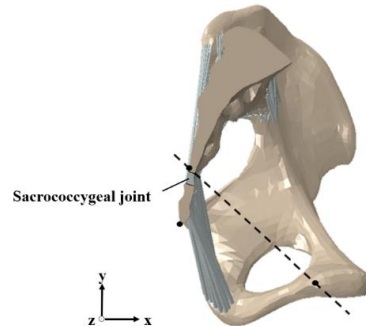


Figure 2 – Finite element model of the pelvic girdle bones with the sacrococcygeal joint. Illustration of the reference line from the inferior border of the pubic symphysis to the inferior border of the sacrum.

To ensure a correct simulation of the motion of the pelvis joints and to provide some stability to the simulation, 3D solid elements were added in the joints area. In the sacroiliac joint, a group of wedge elements with hybrid formulation (C3D6H) were added to mimic the synovial part of this joint. In the pubic symphysis, another group of 3D solid elements was added to mimic the interpubic disc. A Neo-Hookean constitutive model was applied to these elements and to the sacrococcygeal joint elements[16]:

$$U(\mathbf{C}) = c_{10}(\bar{I}_1^C - 3) + U_{vol}(J) \quad (8)$$

where c_{10} is a material constant. Due to little experimental data on the pelvic ligaments, the material properties of the medial collateral ligament of the knee [17] were considered, similar to what was done in Li et al.[18]: $c_{10}=6.43 \text{ MPa}$ and $D_1= 1.0 \times 10^{-4} \text{ MPa}^{-1}$. The stiffness introduced by these elements is low, so the overall stiffness of the joints is mainly provided by the pelvic ligaments.

Regarding the fetal model, the head was modeled using tetrahedral elements (C3D4) [19]. The material properties considered correspond to those of a material with high stiffness, such that it can be considered rigid when compared with the pelvic floor to reduce the fetus deformations and facilitate the convergence of the simulation [20].

For the boundary conditions, a tie constraint was applied between the two supporting structures of the pelvic floor muscles (the arcus tendinous, obturator fascia, and the obturator internus) and the pubic bones. This constrains the supporting structures to have the same motion as the pubic bones. The nodes of the supporting structures that represent the different connections between the pelvic floor muscles and the sacrum were considered fixed. The sacrum nodes in the articular faces were fixed. A tie constraint was also applied between the sacrospinous and

sacrospinous ligaments and the fetal head. According to the cardinal movements, the vertical descent of the fetal head and its flexion/extension were imposed by controlling the displacement and rotation of the reference point belonging to the model [7].

In this way, the second stage of a birth in vertex presentation and occipit anterior position was simulated using Abaqus software 2018.

RESULTS

During numerical simulations, the fetus descent and head extension were controlled, but the remaining degrees of freedom were left free. Even though an occipit anterior position was simulated, the bones and pelvic floor imposed some constraints and the predominant position was the left occipit anterior.

Regarding the pubic symphysis, its widening was analyzed (Figure 3) based on the distance between the narrowest points of the symphyseal gap. The maximum value occurs at, approximately, a vertical descent of the fetus head of 65 mm, which corresponds to the moment when the fetus begins the head extension. The non-mob. coccyx model has a maximum widening of 6.3 mm, while the mob. coccyx model presents a maximum value of 3.2 mm.

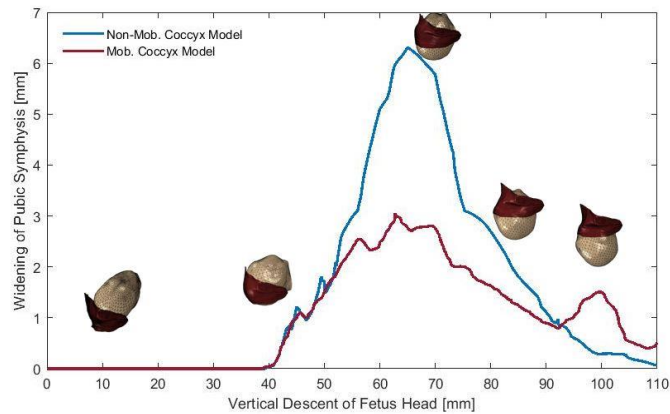


Figure 3 - Widening of pubic symphysis during the vertical descent of the fetus head.

The maximum principal stresses in the pubic ligaments were also obtained (Figure 4). The peak of stresses in these ligaments occur at the same instance of the maximum widening of the pubic symphysis and the stresses measured in the non-mob. coccyx model are higher than in the mob. coccyx model. Regarding the superior pubic ligaments, the maximum value in the non-mob. coccyx model is 14.25 MPa and in the mob. coccyx model is 8.99 MPa. In the inferior pubic ligaments, the maximum value obtained in the non-mob. coccyx model is 6.29 MPa and in the mob. coccyx model is 2.88 MPa.

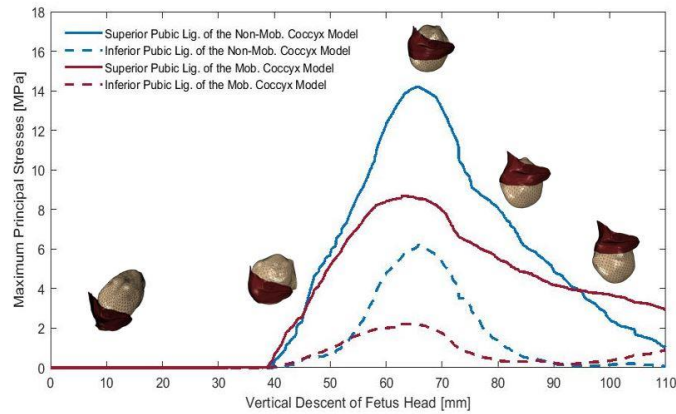


Figure 4 - Maximum principal stresses in MPa in the superior and inferior pubic ligaments of the non-mob. coccyx model and mob. coccyx model during the vertical descent of the fetus head.

At the sacrococcygeal joint, a small amount of flexion and extension of the coccyx can occur. Flexion is produced by contraction of the levator ani muscles and the coccyx moves in a ventral, cranial direction; when extension occurs, the coccyx moves in a caudal, dorsal direction [21]. Figure 5 shows the difference in distance from the tip of the coccyx to the reference line also illustrated in Figure 2.

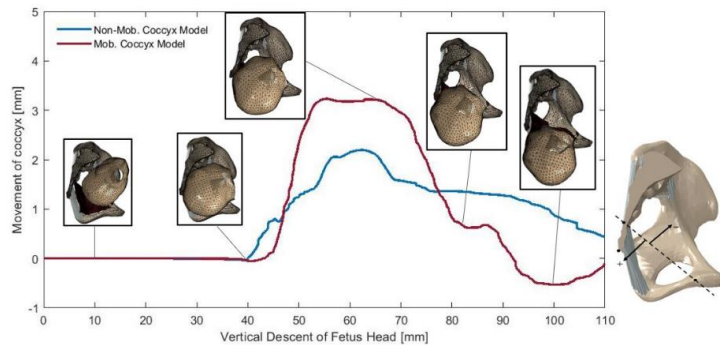


Figure 5 - Movement of coccyx during the vertical descent of the fetus head.

The rotation of the coccyx was also obtained (Figure 6).

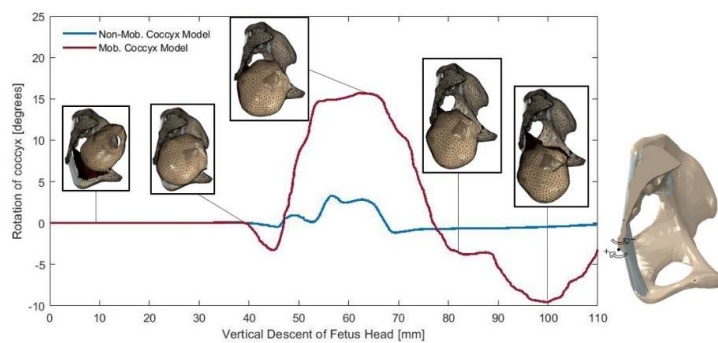


Figure 6 - Rotation of coccyx during the vertical descent of the fetus head.

The peak of maximum movement and rotation of the coccyx occurs at, approximately, the same instant of maximum widening of the pubic symphysis. In the mob. coccyx model, the maximum movement of the coccyx is 3.3 mm and, in the non-mob. coccyx model, is 2.2 mm. Analyzing the maximum rotation obtained, there is a very

significant divergence between them: the non-mob. coccyx model has a rotation of 3.6° , while the mob. coccyx model has a movement of 15.7° .

To analyze the displacement on the x-axis that the sacrum and coccyx suffered, a curve was defined in the sagittal plane of these bones (Figure 7). For each model, two curves were obtained during two different moments: the blue and red dashed curves were obtained when the vertical descent of the fetus head was 48 mm and the solid curves at the peak of maximum movement of the coccyx, i.e. a vertical descent of the fetus head of 65 mm. The black dashed line represents the beginning of the sacrococcygeal joint. Regarding the beginning of the movement of the coccyx (vertical descent of 48 mm), lower displacement values were obtained compared to what was observed at the peak of the movement of the coccyx (vertical descent of the fetus head of 65 mm), in which a displacement of 7.6 mm occurs in the mob. coccyx model, while in the other model occurs a displacement of 1.2 mm.

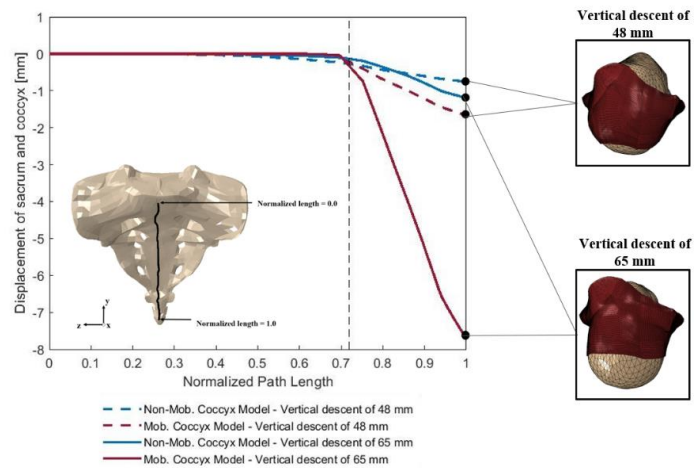


Figure 7 - Displacement of sacrum and coccyx in x-axis along the normalized path at the sagittal plane of these bones in a vertical descent of the fetus head of 48 mm and 65 mm. The black dashed line corresponds to the beginning of the sacrococcygeal joint.

The distribution of the maximum principal stresses on the cortical zone of these bones was also analyzed in the peak coccyx movement instant. The higher stresses are located on the most inferior part of the sacrum, sacrococcygeal joint, and coccyx, being 40 MPa the maximum value obtained. In the non-mob. coccyx model, a larger zone of high stresses was observed, compared to the mob. coccyx model.

Concerning the pelvic floor muscles, the maximum principal stresses were measured along the defined path at the most inferior portion of these muscles when its maximum occurs (Figure 8). In the non-mob. coccyx

model, the instant analyzed corresponds to a vertical descent of the fetus head of 70 mm and, in the mob. coccyx model, to a vertical descent of 77 mm. These differences are due to small variations that may occur regarding the cardinal movements at the level of the fetal head, since there are some different in the space available in the mother's pelvis in both models. To better understand the impact of the vertical descent of the fetus head in all model of the pelvic floor muscles, the distribution of the maximum principal stresses at the peak stresses instant was also observed. In the mob. coccyx model, higher stress values were observed in the left area of the levator ani, namely in the pubococcygeal muscles.

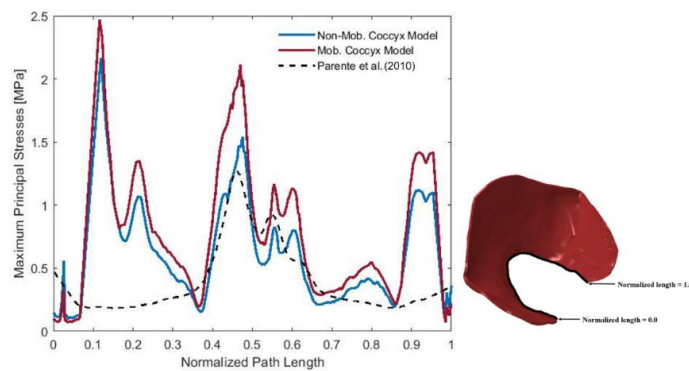


Figure 8 - Maximum principal stresses calculated at the peak stresses instant along the normalized path in the lower portion of the pelvic floor muscles, identifying the initial (normalized length = 0.0) and final (normalized length = 1.0) position.

A stretch ratio, defined as the ratio between the current tissue length to the original tissue length, was also calculated along the defined path at the most inferior portion of the pelvic floor muscles. For an initial length of 17.1 cm, the maximum value obtained is 1.7 in both models.

The reaction forces in the medial-lateral direction exerted in the fetus head during its vertical descent were also analyzed. In the mob. coccyx model, a maximum reaction force of 175 N was obtained, while, in the other model, it was obtained a value of 239 N. The peak instant of maximum value for the reaction forces is coincident with the moment of the vertical descent of the fetus head where the maximum principal stress occurs in both models.

DISCUSSION

In this work, a finite element model simulates the fetal head movements during birth in vertex presentation and occipit anterior position, assuming two birthing positions: one that allows the movement of the coccyx and other in which its movement is more restricted. Due to the constraints imposed by the bones and pelvic floor, the fetal head assumed a left occipit anterior position, which has been adopted as the optimal fetal position [22].

During labor, a displacement of 2-3 mm of the pubic symphysis without discomfort is expected, but, when a displacement higher than 10 mm occurs, it is considered a pubic symphysis diastasis [3]. Thus, in the selected positions, there is no rupture of this joint, despite the non-mob. coccyx model presents a higher widening, causing higher stresses in the pubic ligaments of this model. Regarding the mob. coccyx model, the widening of the pubic symphysis verified after a 90 mm descent is related to the movement in the ventral, cranial direction of the coccyx, as seen in Figure 5. This movement induces a decrease in the pelvic space available to allow the passage of the fetal head and, therefore, it is necessary an increase of the pubic symphysis gap. Note that, during pregnancy, ligamentous laxity occurs, predisposing the widening of the pubic symphysis [11]. However, this change was not take into account since no studies were found regarding the mechanical properties.

During the passage of the fetal head, in the mob. coccyx model, a higher movement and rotation of the coccyx occurs since the widening of the pubic symphysis of the former is much lower than the latter. Regarding the end of the simulation, the pelvic bones tend to return to their original position and a flexion of the coccyx is observed, because, in this joint, not all existing ligaments were

modeled since the focus of this work is not the study of the ligaments themselves.

According to a study on the movement of the coccyx during pelvic floor muscles contraction, it was found that the coccyx has an average movement of 8.1 ± 5.4 mm, which measured in degrees is $15.0 \pm 10.2^\circ$. During straining, this bone presents a mean movement of 3.7 ± 2.8 mm and $12.9 \pm 10.9^\circ$ [21]. The values obtained are in accordance with these and, consequently, within the physiological limits of the sacrococcygeal joint.

In Figure 7, it can be observed that a higher displacement on the x-axis occurs when the normalized curve intersects the beginning of the sacrococcygeal joint. It is verified that the coccyx is the most affected bone by the movement of the fetus head. The small movement verified in the non-mob coccyx is due to the successful negotiation of the maternal pelvis that is required. Due to the restricted mobility of the coccyx, a greater impact on the cortical bone of the sacrum and coccyx is observed. Although the biomechanics of pelvic fractures are not yet thoroughly understood, the ultimate tensile strength comprises values between 80 and 120 MPa [23]. Since the maximum stress value observed in this study is 40 MPa, it can be assumed that no serious injuries occur. Note that, during pregnancy, there are several changes in maternal calcium and bone

metabolism [24], but these changes were not considered since it is a topic under investigation.

These results suggest that in the birthing positions that enable a higher movement of the sacrum and coccyx, such as the majority of the vertical positions, coccyx can move more easily and a lower widening of the pubic symphysis occurs. In horizontal positions, the force of the bed under these bones may close the pelvis, causing a higher widening of the pubic symphysis. These results are consistent with Reitter et al.[25] that verified that the changes in the maternal pelvis are more pronounced in pregnant women to facilitate birth. It was observed that the vertical position has higher diameters compared to the horizontal position, with the distance from the tip of the coccyx to the low tip of the pubic symphysis presenting the most significant difference between the two positions. Desseauve et al.[5] also concluded that change to a more upright position for birthing is advantageous for the woman in the second stage of labor.

The stresses obtained in the pelvic floor muscles can be compared with other study [9], in which the peak of stresses occurred only in the most posterior area of the levator ani muscles. This can be explained by the different fetal positions simulated. Regarding the stretch ratio, Parente et al.[7] examined the maximum value obtained. It

is verified that the maximum stretch ratio occurs in different instances, due to the restrictions imposed by the maternal pelvis and the different fetal positions simulated.

In Oliveira et al.[20], numerical simulations of the vaginal delivery were performed and a maximum value of 202 N for the reaction force was observed, which is similar to results obtained in this study.

To conclude, different birthing positions lead to changes in the maternal pelvic space, so certain positions can be adopted by the mother during the second stage of labor to reduce the risk of obstructed labor and the development of several dysfunctions. More specifically, positions in which the coccyx is free to move, like most of the vertical positions, have a higher space available for the passage of the fetal head, appearing to be more beneficial for the pelvic girdle bones of the mother. The left area of the levator ani muscles, particularly of the pubococcygeal muscle, is the most solicited.

Nevertheless, the problem studied is very complex and it is necessary to consider some limitations and simplifications involved. For future work, it would be important to perform experimental studies of pubic ligaments of pregnant women and to simulate more specific birthing positions.

ACKNOWLEDGMENTS

This research was supported by Portuguese FCT under research project UIDB/50022/2020 and by the project NORTE-01-0145-FEDER-030062 (SIM4SafeBirth) cofinanced by NORTE2020, through FEDER.

REFERENCES

- [1] S. Rustamova, M. Predanic, M. Summersille, W.R. Cohen, Changes in symphysis pubis width during labor, *Journal of Perinatal Medicine*. 37 (2009) 370–373. <https://doi.org/10.1515/JPM.2009.051>.
- [2] A. Hemmerich, T. Bandrowska, G.A. Dumas, The effects of squatting while pregnant on pelvic dimensions: A computational simulation to understand childbirth, *Journal of Biomechanics*. 87 (2019) 64–74. <https://doi.org/10.1016/j.jbiomech.2019.02.017>.
- [3] S.K. Hwang, Musculoskeletal Health in Pregnancy and Postpartum, *Musculoskeletal Health in Pregnancy and Postpartum*. (2015) 171–179. <https://doi.org/10.1007/978-3-319-14319-4>.
- [4] J. Huang, Y. Zang, L.H. Ren, F.J. Li, H. Lu, A review and comparison of common maternal positions during the second-stage of labor,

International Journal of Nursing Sciences. 6 (2019)
460–467.

<https://doi.org/10.1016/j.ijnss.2019.06.007>.

- [5] D. Desseauve, L. Fradet, P. Lacouture, F. Pierre, Position for labor and birth: State of knowledge and biomechanical perspectives, *European Journal of Obstetrics and Gynecology and Reproductive Biology*. 208 (2017) 46–54.
<https://doi.org/10.1016/j.ejogrb.2016.11.006>.
- [6] J.K. Gupta, C. Nikodem, Maternal posture in labour, *European Journal of Obstetrics and Gynecology and Reproductive Biology*. 92 (2000) 273–277. [https://doi.org/10.1016/S0301-2115\(99\)00272-9](https://doi.org/10.1016/S0301-2115(99)00272-9).
- [7] M.P.L. Parente, R.M. Natal Jorge, T. Mascarenhas, A.A. Fernandes, J.A.C. Martins, Deformation of the pelvic floor muscles during a vaginal delivery, *International Urogynecology Journal*. 19 (2008) 65–71.
<https://doi.org/10.1007/s00192-007-0388-7>.
- [8] J.A.C. Martins, E.B. Pires, R. Salvado, P.B. Dinis, A numerical model of passive and active behavior of skeletal muscles, *Computer Methods in Applied*

- Mechanics and Engineering. 151 (1998) 419–433.
[https://doi.org/10.1016/S0045-7825\(97\)00162-X](https://doi.org/10.1016/S0045-7825(97)00162-X).
- [9] M.P.L. Parente, R.M. Natal Jorge, T. Mascarenhas, A.L. Silva-Filho, The influence of pelvic muscle activation during vaginal delivery, *Obstetrics and Gynecology*. 115 (2010) 804–808.
<https://doi.org/10.1097/AOG.0b013e3181d534cd>.
- [10] S.C.A. Michel, A. Rake, K. Treiber, B. Seifert, R. Chaoui, R. Huch, B. Marincek, R.A. Kubik-Huch, MR obstetric pelvimetry: Effect of birthing position on pelvic bony dimensions, *American Journal of Roentgenology*. 179 (2002) 1063–1067.
<https://doi.org/10.2214/ajr.179.4.1791063>.
- [11] S. Jain, P. Eedarapalli, P. Jamjute, R. Sawdy, Symphysis pubis dysfunction: a practical approach to management, *The Obstetrician & Gynaecologist*. 8 (2006) 153–158.
<https://doi.org/10.1576/toag.8.3.153.27250>.
- [12] T. Wu, X. Ren, Y. Cui, X. Cheng, S. Peng, Z. Hou, Y. Han, Biomechanical study of three kinds of internal fixation for the treatment of sacroiliac joint disruption using biomechanical test and finite element analysis, *Journal of Orthopaedic Surgery*

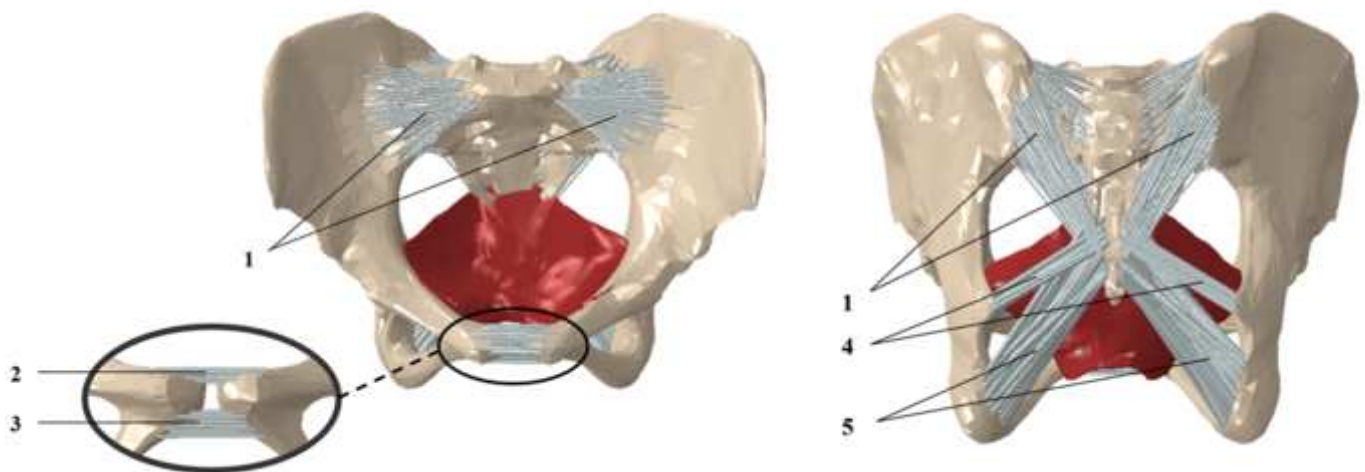
- and Research. 13 (2018) 1–8.
<https://doi.org/10.1186/s13018-018-0858-2>.
- [13] Y. Zhao, J. Li, D. Wang, Y. Liu, J. Tan, S. Zhang, Comparison of stability of two kinds of sacro-iliac screws in the fixation of bilateral sacral fractures in a finite element model, *Injury*. 43 (2012) 490–494.
<https://doi.org/10.1016/j.injury.2011.12.023>.
- [14] S. Standring, ed., *Gray's anatomy: the anatomical basis of clinical practice*, 2016.
- [15] J. Lei, Y. Zhang, G. Wu, Z. Wang, X. Cai, The Influence of Pelvic Ramus Fracture on the Stability of Fixed Pelvic Complex Fracture, *Computational and Mathematical Methods in Medicine*. 2015 (2015). <https://doi.org/10.1155/2015/790575>.
- [16] N.H. Kim, *Introduction to nonlinear finite element analysis*, 2015. <https://doi.org/10.1007/978-1-4419-1746-1>.
- [17] G.A. Orozco, P. Tanska, M.E. Mononen, K.S. Halonen, R.K. Korhonen, The effect of constitutive representations and structural constituents of ligaments on knee joint mechanics, *Scientific Reports*. 8 (2018) 1–15.
<https://doi.org/10.1038/s41598-018-20739-w>.

- [18] Z. Li, J.E. Alonso, J.E. Kim, J.S. Davidson, B.S. Etheridge, A.W. Eberhardt, Three-dimensional finite element models of the human pubic symphysis with viscohyperelastic soft tissues, *Annals of Biomedical Engineering*. 34 (2006) 1452–1462. <https://doi.org/10.1007/s10439-006-9145-1>.
- [19] M.P.L. Parente, R.M. Natal Jorge, T. Mascarenhas, A.A. Fernandes, A.L. Silva-Filho, Computational modeling approach to study the effects of fetal head flexion during vaginal delivery, *American Journal of Obstetrics and Gynecology*. 203 (2010) 217.e1-217.e6. <https://doi.org/10.1016/j.ajog.2010.03.038>.
- [20] D.A. Oliveira, M.P.L. Parente, B. Calvo, T. Mascarenhas, R.M. Natal Jorge, Numerical simulation of the damage evolution in the pelvic floor muscles during childbirth, *Journal of Biomechanics*. 49 (2016) 594–601. <https://doi.org/10.1016/j.jbiomech.2016.01.014>.
- [21] K. Bø, F. Lilleås, T. Talseth, H. Hedland, Dynamic MRI of the pelvic floor muscles in an upright sitting position, *Neurourology and Urodynamics*. 20 (2001) 167–174. [https://doi.org/10.1002/1520-6777\(2001\)20:2<167::AID-NAU19>3.0.CO;2-4](https://doi.org/10.1002/1520-6777(2001)20:2<167::AID-NAU19>3.0.CO;2-4).

- [22] S.S. Webb, M.N. Plana, J. Zamora, A. Ahmad, B. Earley, C. MacArthur, K.S. Khan, Abdominal palpation to determine fetal position at labor onset: A test accuracy study, *Acta Obstetrica et Gynecologica Scandinavica*. 90 (2011) 1259–1266. <https://doi.org/10.1111/j.1600-0412.2011.01226.x>.
- [23] P.L. Ricci, S. Maas, J. Kelm, T. Gerich, Finite element analysis of the pelvis including gait muscle forces: an investigation into the effect of rami fractures on load transmission, *Journal of Experimental Orthopaedics*. 5 (2018). <https://doi.org/10.1186/s40634-018-0151-7>.
- [24] M.F. Sowers, T. Scholl, L. Harris, M. Jannausch, Bone Loss in Adolescent and Adult Pregnant Women, *Obstetrics & Gynecology*. 96 (2000) 189–193. <https://doi.org/10.1097/00006250-200008000-00007>.
- [25] A. Reitter, B.A. Daviss, A. Bisits, A. Schollenberger, T. Vogl, E. Herrmann, F. Louwen, S. Zangos, Does pregnancy and/or shifting positions create more room in a woman's pelvis?, *American Journal of Obstetrics and Gynecology*. 211 (2014) 662.e1-662.e9. <https://doi.org/10.1016/j.ajog.2014.06.029>.

Figure1

[Click here to access/download;Figure;figure1.tiff](#)



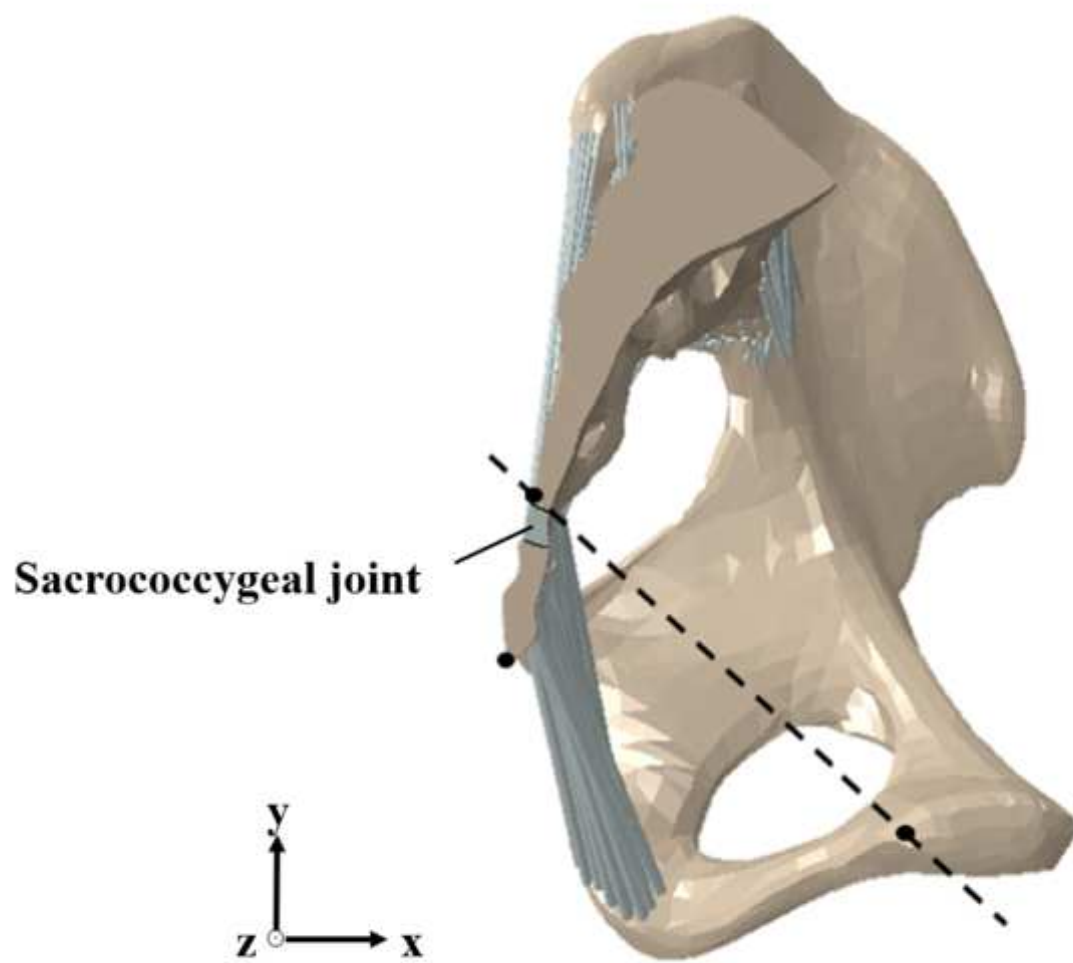


Figure3

[Click here to access/download;Figure;figure3.tiff](#)

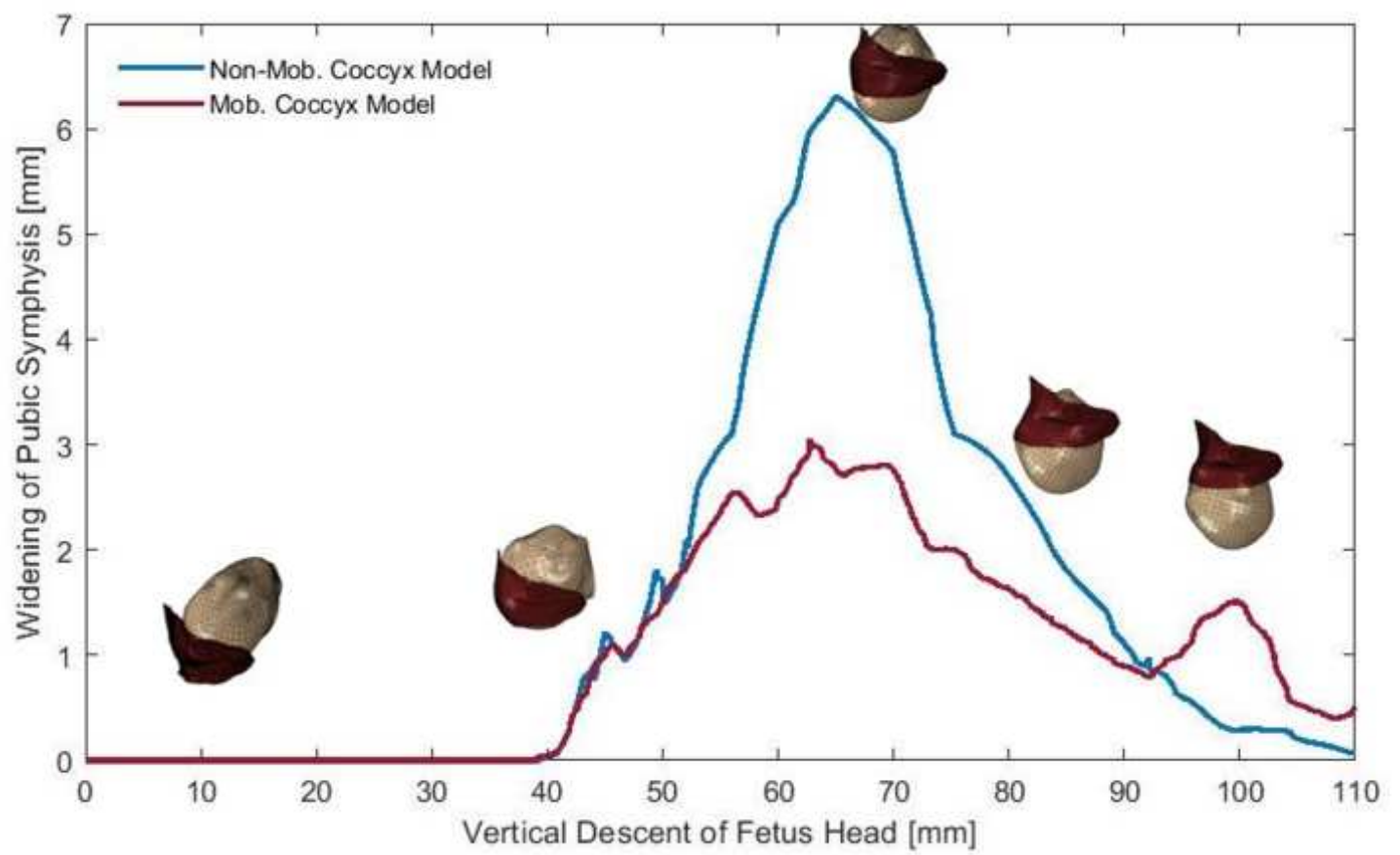


Figure4

[Click here to access/download;Figure;figure4.tiff](#)

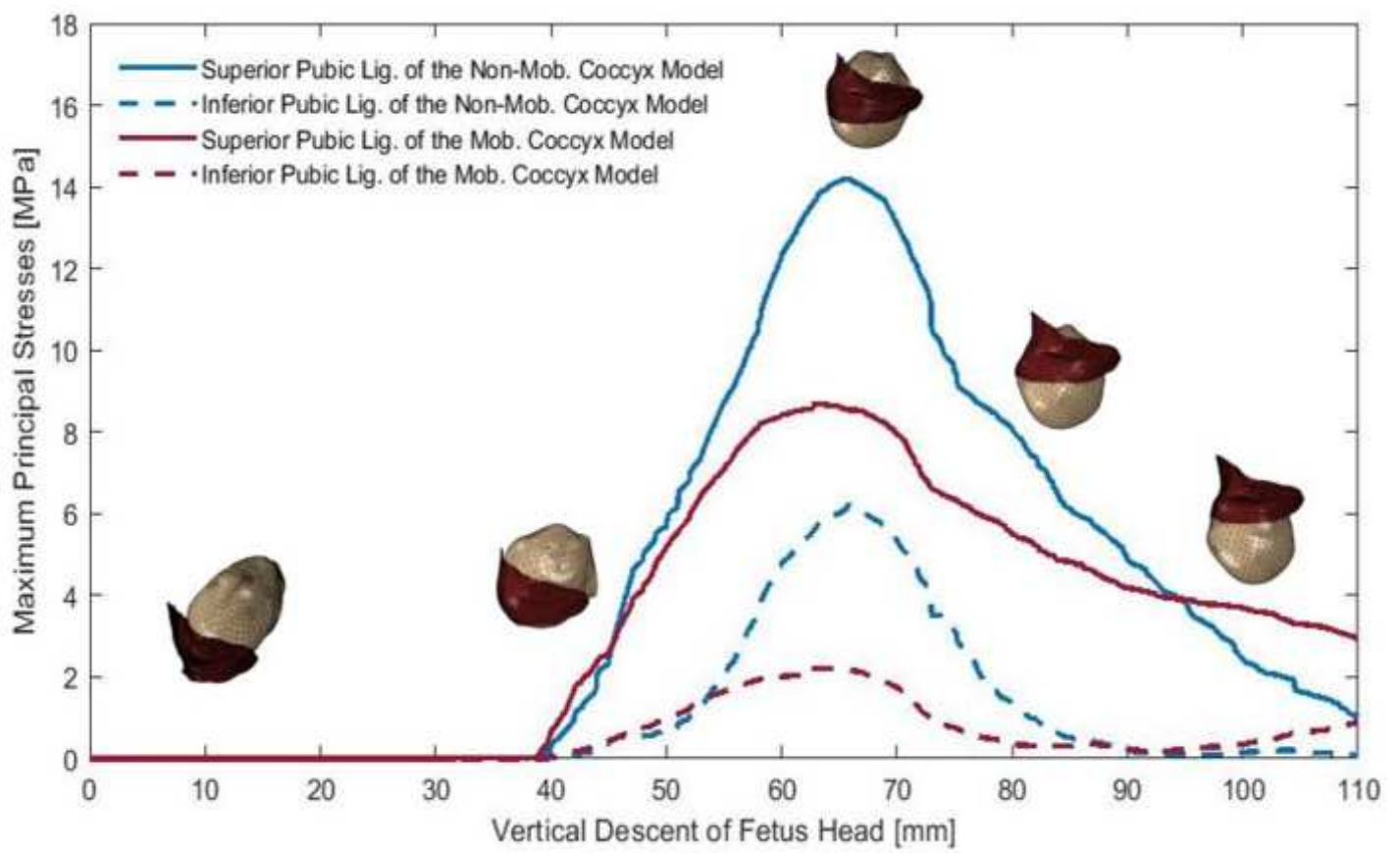


Figure5

[Click here to access/download;Figure;figure5.tiff](#)

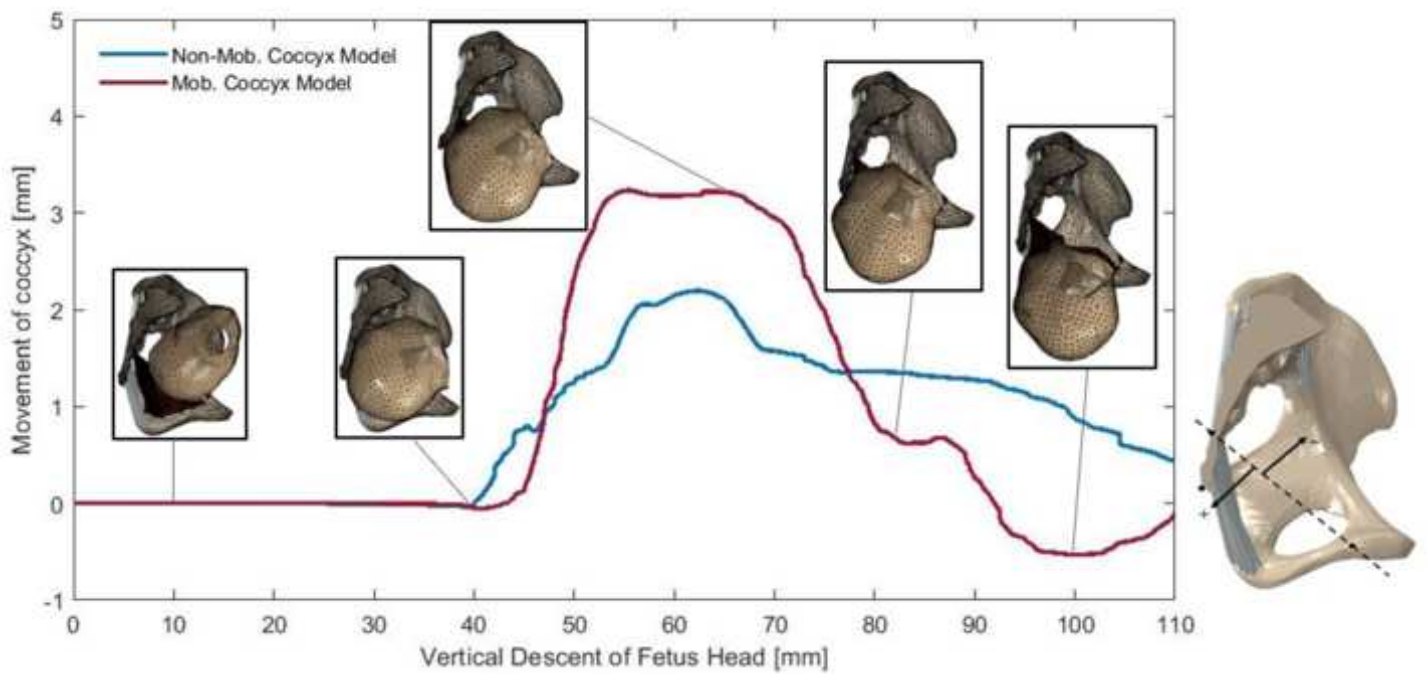


Figure6

[Click here to access/download;Figure;figure6.tiff](#)

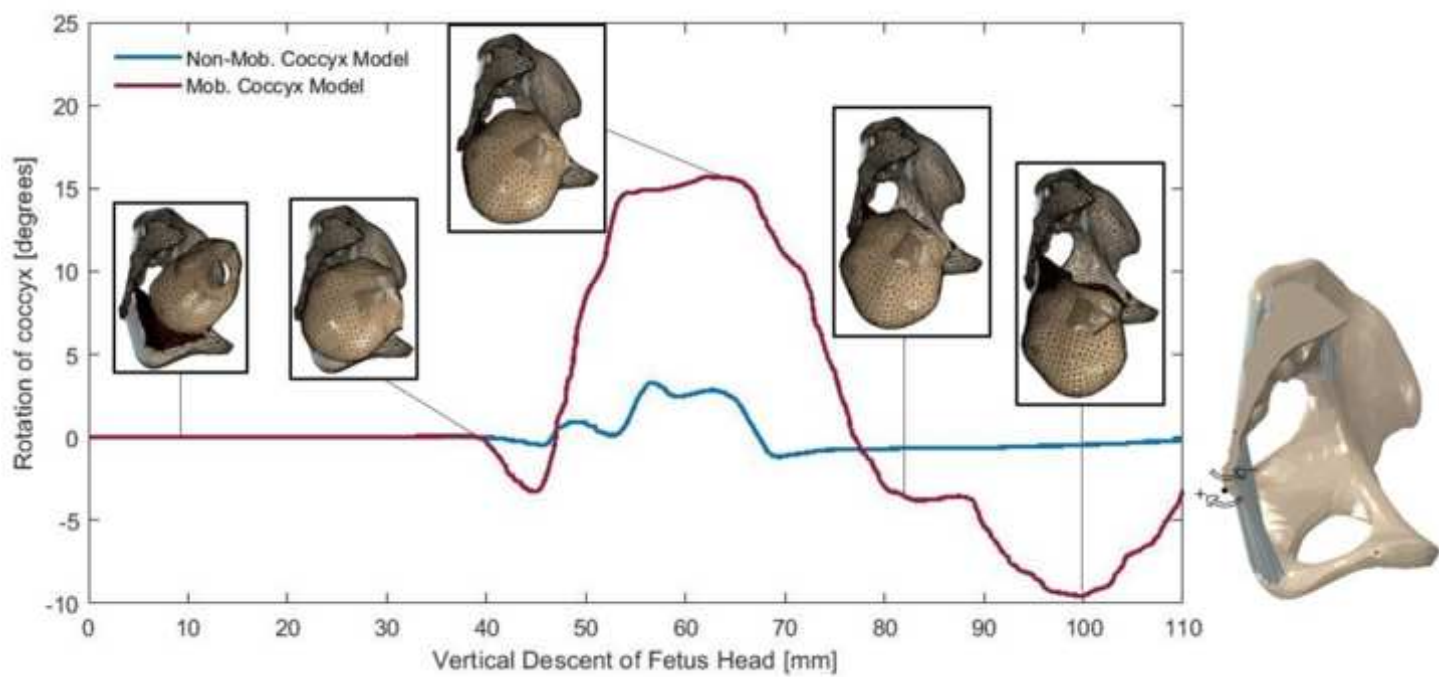


Figure7

[Click here to access/download;Figure;figure7.tiff](#)

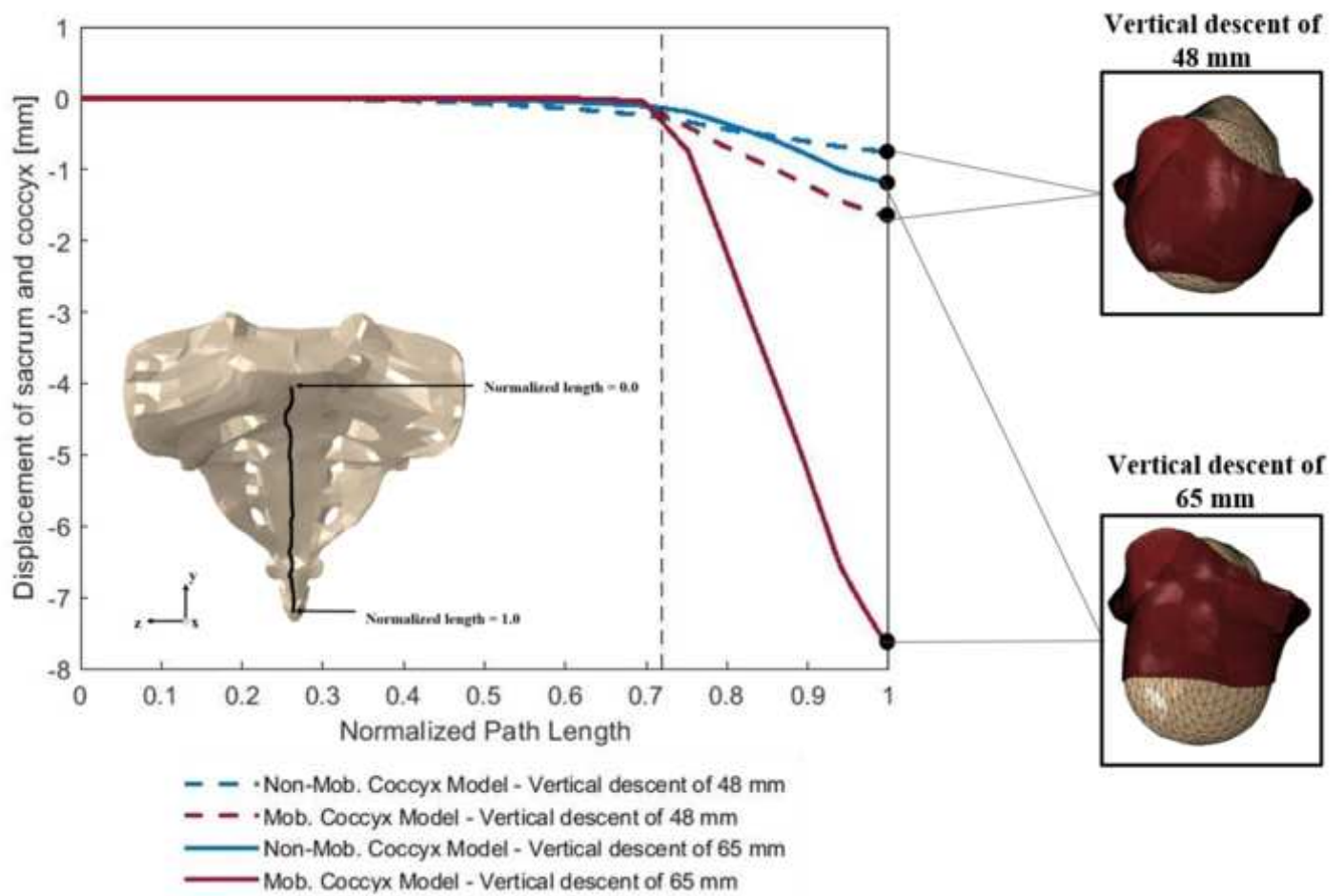


Figure8

[Click here to access/download;Figure;figure8.tiff](#)

